Image Reconstruction

Marc Kachelrieß

German Cancer Research Center (DKFZ)
Heidelberg, Germany
www.dkfz.de/ct

DEUTSCHES
KREBSFORSCHUNGSZENTRUM
IN DER HELMHOLTZ-GEMEINSCHAFT

Contents

- Analytical Image Reconstruction (90 min)
  - Filtered backprojection
  - Gridding
  - Applications in CT, MR, PET, SPECT, …
- Iterative image Reconstruction (90 min)
  - Kaczmarz, PWLS
  - Statistical reconstruction
  - Applications in CT, MR, PET, SPECT, …

Not Contained

- Preprocessing
- Postprocessing
- Artifact correction
- …

Part 2

Iterative Image Reconstruction

$$x^2 = y$$

Model

$$x = \sqrt{y}$$

Solution

Filtered Backprojection (FBP)

Measurement: $p(\vartheta,\xi) = \int dx dy\, f(x,y)\delta(x\cos\vartheta + y\sin\vartheta - \xi)$

Fourier transform:

$$\int d\xi\, p(\vartheta,\xi)e^{-2\pi i\xi u} = \int dx dy\, f(x,y)e^{-2\pi i u(x\cos\vartheta + y\sin\vartheta)}$$

This is the central slice theorem: $P(\vartheta,u) = F(u\cos\vartheta, u\sin\vartheta)$

Inversion: $f(x,y) = \int_0^\pi d\vartheta \int_{-\infty}^{\infty} du\, |u| P(\vartheta,u)e^{2\pi i u(x\cos\vartheta + y\sin\vartheta)}$

$$= \int_0^\pi d\vartheta\, p(\vartheta,\xi) * k(\xi)\Big|_{\xi = x\cos\vartheta + y\sin\vartheta}$$

„I hate to think!
I reconstruct iterative.“

Freek Beekman, Fully3D Meeting, Lindau, Germany, 2007

2D Parallel Beam Reconstruction

Analytical tomographic reconstruction

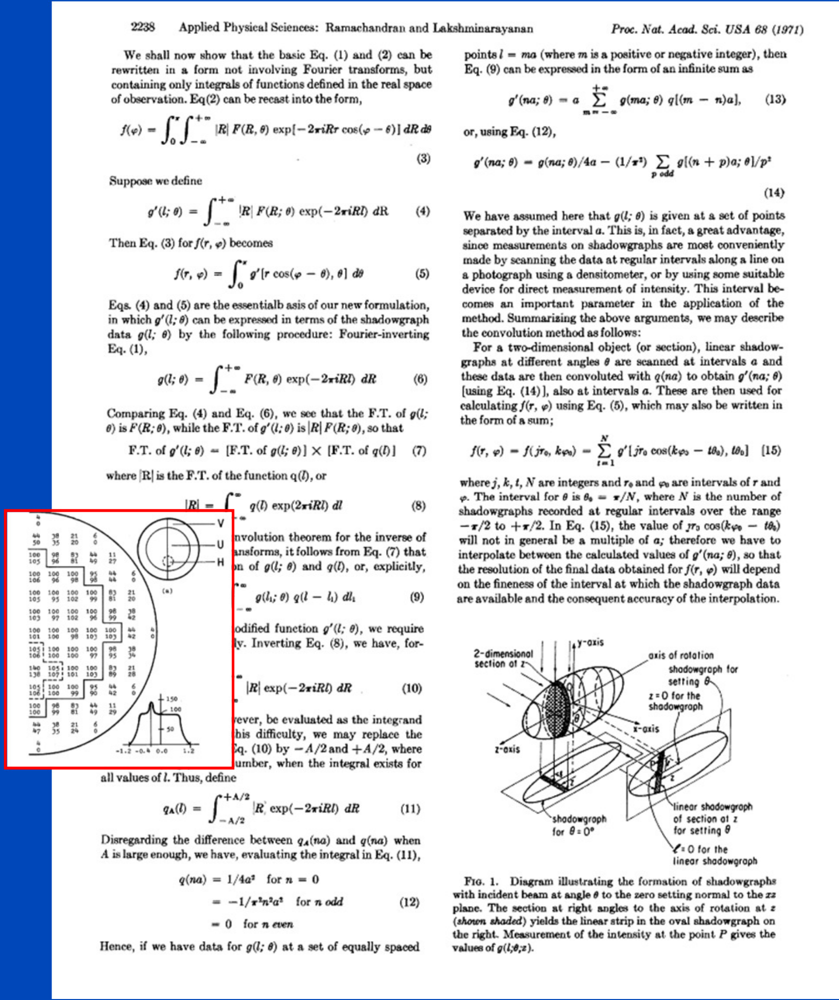

We shall now show that the basic Eq. (1) and (2) can be rewritten in a form not involving Fourier transforms, but containing only integrals of functions defined in the real space of observation. Eq(2) can be recast into the form,

$$f(\varphi) = \int_0^{\pi}\int_{-\infty}^{+\infty} |R|\, F(R,\theta)\, \exp[-2\pi i R r \cos(\varphi-\theta)]\, dR\, d\theta \tag{3}$$

Suppose we define

$$g'(l;\theta) = \int_{-\infty}^{+\infty} |R|\, F(R;\theta)\, \exp(-2\pi i R l)\, dR \tag{4}$$

Then Eq. (3) for $f(r, \varphi)$ becomes

$$f(r,\varphi) = \int_0^{\pi} g'[r\cos(\varphi-\theta), \theta]\, d\theta \tag{5}$$

Eqs. (4) and (5) are the essentialb asis of our new formulation, in which $g'(l;\theta)$ can be expressed in terms of the shadowgraph data $g(l;\theta)$ by the following procedure: Fourier-inverting Eq. (1),

$$g(l;\theta) = \int_{-\infty}^{+\infty} F(R,\theta)\, \exp(-2\pi i R l)\, dR \tag{6}$$

Comparing Eq. (4) and Eq. (6), we see that the F.T. of $g(l;\theta)$ is $F(R;\theta)$, while the F.T. of $g'(l;\theta)$ is $|R|\, F(R;\theta)$, so that

$$\text{F.T. of } g'(l;\theta) = [\text{F.T. of } g(l;\theta)] \times [\text{F.T. of } q(l)] \tag{7}$$

where $|R|$ is the F.T. of the function $q(l)$, or

$$|R| = \int_{-\infty}^{\infty} q(l)\, \exp(2\pi i R l)\, dl \tag{8}$$

...nvolution theorem for the inverse of ...ansforms, it follows from Eq. (7) that ...n of $g(l;\theta)$ and $q(l)$, or, explicitly,

$$\ldots \int_{-\infty}^{\infty} g(l_1;\theta)\, q(l-l_1)\, dl_1 \tag{9}$$

...odified function $g'(l;\theta)$, we require ...y. Inverting Eq. (8), we have, for-

$$\ldots |R| \exp(-2\pi i R l)\, dR \tag{10}$$

...ever, be evaluated as the integrand ...his difficulty, we may replace the ...q. (10) by $-A/2$ and $+A/2$, where ...umber, when the integral exists for all values of l. Thus, define

$$q_A(l) = \int_{-A/2}^{+A/2} |R|\, \exp(-2\pi i R l)\, dR \tag{11}$$

Disregarding the difference between $q_A(na)$ and $q(na)$ when A is large enough, we have, evaluating the integral in Eq. (11),

$$\begin{aligned} q(na) &= 1/4a^2 \quad \text{for } n = 0 \\ &= -1/\pi^2 n^2 a^2 \quad \text{for } n \text{ odd} \\ &= 0 \quad \text{for } n \text{ even} \end{aligned} \tag{12}$$

Hence, if we have data for $g(l;\theta)$ at a set of equally spaced points $l = ma$ (where m is a positive or negative integer), then Eq. (9) can be expressed in the form of an infinite sum as

$$g'(na;\theta) = a \sum_{m=-\infty}^{+\infty} g(ma;\theta)\, q[(m-n)a], \tag{13}$$

or, using Eq. (12),

$$g'(na;\theta) = g(na;\theta)/4a - (1/\pi^2) \sum_{p\ \text{odd}} g[(n+p)a;\theta]/p^2 \tag{14}$$

We have assumed here that $g(l;\theta)$ is given at a set of points separated by the interval a. This is, in fact, a great advantage, since measurements on shadowgraphs are most conveniently made by scanning the data at regular intervals along a line on a photograph using a densitometer, or by using some suitable device for direct measurement of intensity. This interval becomes an important parameter in the application of the method. Summarizing the above arguments, we may describe the convolution method as follows:

For a two-dimensional object (or section), linear shadowgraphs at different angles θ are scanned at intervals a and these data are then convoluted with $q(na)$ to obtain $g'(na;\theta)$ [using Eq. (14)], also at intervals a. These are then used for calculating $f(r,\varphi)$ using Eq. (5), which may also be written in the form of a sum;

$$f(r,\varphi) = f(jr_0, k\varphi_0) = \sum_{t=1}^{N} g'[jr_0\cos(k\varphi_0 - t\theta_0), t\theta_0] \tag{15}$$

where j, k, t, N are integers and r_0 and φ_0 are intervals of r and φ. The interval for θ is $\theta_0 = \pi/N$, where N is the number of shadowgraphs recorded at regular intervals over the range $-\pi/2$ to $+\pi/2$. In Eq. (15), the value of $jr_0\cos(k\varphi_0 - t\theta_0)$ will not in general be a multiple of a; therefore we have to interpolate between the calculated values of $g'(na;\theta)$, so that the resolution of the final data obtained for $f(r,\varphi)$ will depend on the fineness of the interval at which the shadowgraph data are available and the consequent accuracy of the interpolation.

FIG. 1. Diagram illustrating the formation of shadowgraphs with incident beam at angle θ to the zero setting normal to the xz plane. The section at right angles to the axis of rotation at z (*shown shaded*) yields the linear strip in the oval shadowgraph on the right. Measurement of the intensity at the point P gives the values of $g(l;\theta;z)$.

Iterative tomographic reconstruction

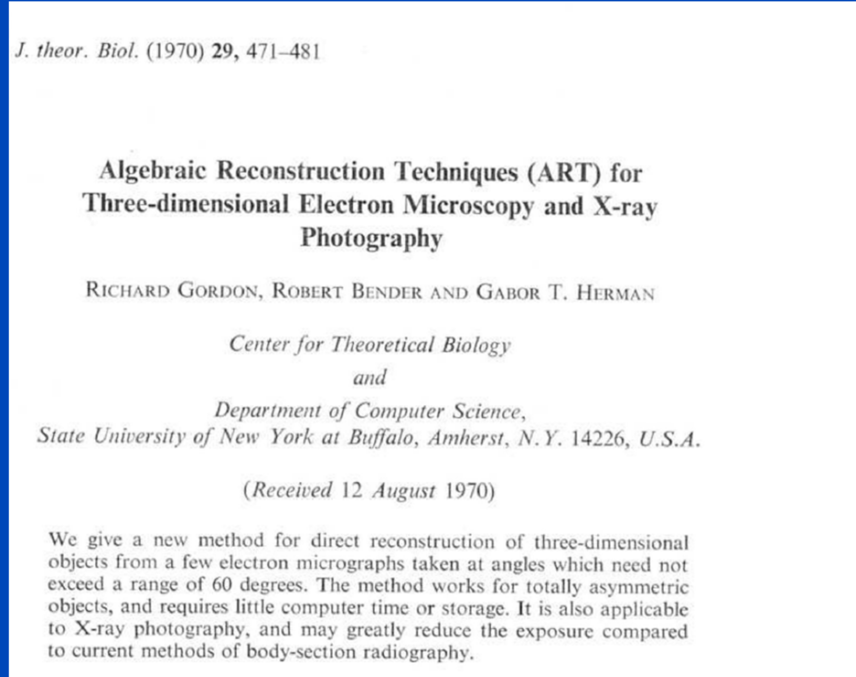

J. theor. Biol. (1970) **29**, 471–481

Algebraic Reconstruction Techniques (ART) for Three-dimensional Electron Microscopy and X-ray Photography

RICHARD GORDON, ROBERT BENDER AND GABOR T. HERMAN

Center for Theoretical Biology

and

Department of Computer Science, State University of New York at Buffalo, Amherst, N.Y. 14226, U.S.A.

(*Received* 12 *August* 1970)

We give a new method for direct reconstruction of three-dimensional objects from a few electron micrographs taken at angles which need not exceed a range of 60 degrees. The method works for totally asymmetric objects, and requires little computer time or storage. It is also applicable to X-ray photography, and may greatly reduce the exposure compared to current methods of body-section radiography.

$$f_{\nu+1} = f_\nu + \mathsf{R}_\nu^{\mathrm{T}} \frac{p_\nu - \mathsf{R}_\nu f_\nu}{\mathsf{R}_\nu^2 1}$$

Spiral Cone Beam CT Reconstruction

Analytical tomographic reconstruction

However, since it has turned out that the differences between these options are negligible we will only present the definitions and rebinning equations for the FL method, which is the most simple one.

Although all following considerations only use elementary geometry, the multitude of different coordinate systems and the complexity of the ray geometries for a given focus position α and detectors u and v together with the tilted planes under consideration complicate the situation. Thus before starting to discuss the FL reconstruction method we will do some preparations first.

A. Coordinate systems

The global ξ-η-ζ system is given by rotating the x-y-z axes by $\vartheta+\alpha_R$ about the z-axis. The base vectors are

$$\xi(\vartheta)=\begin{pmatrix}\cos(\alpha_R+\vartheta)\\ \sin(\alpha_R+\vartheta)\\ 0\end{pmatrix},\quad \eta(\vartheta)=\begin{pmatrix}-\sin(\alpha_R+\vartheta)\\ \cos(\alpha_R+\vartheta)\\ 0\end{pmatrix},$$

$$\zeta(\vartheta)=\begin{pmatrix}0\\ 0\\ 1\end{pmatrix}=\mathbf{z}.$$

We define the local (i.e., corresponding to a given reconstruction position α_R) tilted coordinate system with base $(\mathbf{x}',\mathbf{y}',\mathbf{z}')$ to have *both* the x'- and the y'-axis lying in R. The y'-axis shall coincide with the central ray at projection $\alpha=\alpha_R$. Thus we have

$$\mathbf{x}'=\begin{pmatrix}\cos\alpha_R\cos\gamma\\ \sin\alpha_R\cos\gamma\\ \sin\gamma\end{pmatrix},\quad \mathbf{y}'=\begin{pmatrix}-\sin\alpha_R\\ \cos\alpha_R\\ 0\end{pmatrix},$$

$$\mathbf{z}'=\begin{pmatrix}-\cos\alpha_R\sin\gamma\\ -\sin\alpha_R\sin\gamma\\ \cos\gamma\end{pmatrix}.$$

Rotating this system by ϑ' about the z'-axis yields the local parallel geometry ξ'-η'-ζ' system with the base vectors

$$\begin{pmatrix}\cos\alpha_R\cos\vartheta'\cos\gamma-\sin\alpha_R\sin\vartheta'\\ \ldots\cos\alpha_R\sin\vartheta'\\ \ldots\gamma\end{pmatrix},$$

$$\begin{pmatrix}\ldots-\sin\alpha_R\cos\vartheta'\\ \ldots+\cos\alpha_R\cos\vartheta'\\ \ldots\sin\gamma\end{pmatrix},$$

…espect to the world coor- …center of the above given …e primed origin $\mathbf{o}'$. All …stems reduce to their cor- …ns (unprimed identifiers)

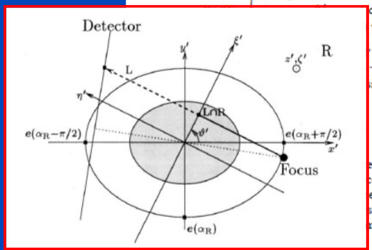

It will turn out that the transformation between local ray parameters (ϑ',ξ') and global ray parameters (ϑ,ξ) is quite important. It is given from the longitudinal projection (along z) of a ray from local to world coordinates. To be more precise: For a given ray with the parameters (ϑ',ξ') we are looking for the parameters (ϑ,ξ) that the corresponding line would yield after having been projected into the plane $z=0$. Mathematically this yields the term

$$P(\mathbf{o}'+\xi'\xi'(\vartheta')+\mathrm{R}\,\boldsymbol{\eta}'(\vartheta'))=\xi\xi(\vartheta)+\mathrm{R}\,\boldsymbol{\eta}(\vartheta),$$

with the projection operator

$$P=\begin{pmatrix}1&0&0\\ 0&1&0\\ 0&0&0\end{pmatrix}.$$

This allows us to derive the desired transformation rules. We will just state the results:

$$\cos\vartheta=\frac{\cos\vartheta'}{\sqrt{\cos^2\vartheta'+\cos^2\gamma\sin^2\vartheta'}},$$

$$\sin\vartheta=\frac{\sin\vartheta'\cos\gamma}{\sqrt{\cos^2\vartheta'+\cos^2\gamma\sin^2\vartheta'}},\tag{9}$$

$$\xi=\frac{\xi'\cos\gamma}{\sqrt{\cos^2\vartheta'+\cos^2\gamma\sin^2\vartheta'}}.$$

To calculate the primed parameters as a function of the unprimed ones we need the inverse transform of Eq. (9):

$$\cos\vartheta'=\frac{\cos\vartheta\cos\gamma}{\sqrt{\sin^2\vartheta+\cos^2\gamma\cos^2\vartheta}},$$

$$\sin\vartheta'=\frac{\sin\vartheta}{\sqrt{\sin^2\vartheta+\cos^2\gamma\cos^2\vartheta}},\tag{10}$$

$$\xi'=\frac{\xi}{\sqrt{\sin^2\vartheta+\cos^2\gamma\cos^2\vartheta}}.$$

For convenience, Fig. 5 gives a view onto the reconstruction plane R and the primed coordinates. Further we want to give a useful relationship that directly becomes evident from Eqs. (9) and (10):

$$\sqrt{\cos^2\vartheta'+\cos^2\gamma\sin^2\vartheta'}\sqrt{\sin^2\vartheta+\cos^2\gamma\cos^2\vartheta}=\cos\gamma.$$

B. Projections onto the detector plane

It will be necessary to know the projection of a given point $\mathbf{r}$ from the focus location $\mathbf{s}(\alpha)$ onto the detector. The calculation is uninstructive, we will simply state the result in detector coordinates u and v:

$$u=\rho(-x\cos\alpha-y\sin\alpha),$$
$$v=\rho\left(d\frac{\alpha}{2\pi}-z\right)\tag{11}$$

with

Iterative tomographic reconstruction

J. theor. Biol. (1970) **29**, 471–481

Algebraic Reconstruction Techniques (ART) for Three-dimensional Electron Microscopy and X-ray Photography

RICHARD GORDON, ROBERT BENDER AND GABOR T. HERMAN

Center for Theoretical Biology
and
Department of Computer Science,
State University of New York at Buffalo, Amherst, N.Y. 14226, U.S.A.

(*Received* 12 *August* 1970)

We give a new method for direct reconstruction of three-dimensional objects from a few electron micrographs taken at angles which need not exceed a range of 60 degrees. The method works for totally asymmetric objects, and requires little computer time or storage. It is also applicable to X-ray photography, and may greatly reduce the exposure compared to current methods of body-section radiography.

$$f_{\nu+1}=f_\nu+\mathrm{R}_\nu^{\mathrm{T}}\,\frac{p_\nu-\mathrm{R}_\nu f_\nu}{\mathrm{R}_\nu^2 1}$$

Short Scan Cone Beam Reconstruction

Analytical tomographic reconstruction

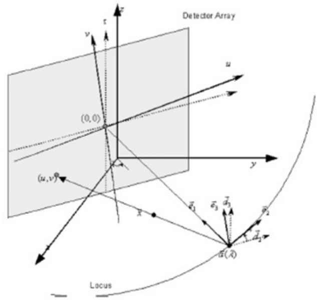

FIG. 1. Cone-beam geometry with equally spatial cone-beam data. (u,v) forms a local detection coordinate system with its horizontal axis parallel to the vector tangential to the spiral locus; (ω, τ) forms an alternative detection system with its horizontal axis parallel to the x-y plane.

$$\vec{e}_1=(-\cos\lambda,-\sin\lambda,0), \quad (2)$$

$$\vec{e}_2=\vec{a}'(\lambda)/\|\vec{a}'(\lambda)\|=(-\sin\lambda\cos\xi,\cos\lambda\cos\xi,\sin\xi), \quad (3)$$

(4)

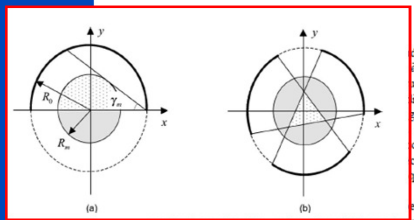

... VOI reconstruction algorithm in two steps: (1) cone-beam data to fan-beam data conversion via a cosine correction,[7] and (2) fan-beam reconstruction using a Noo ROI reconstruction formula.[1] First, cone-beam data are approximately converted to fan-beam data via cosine correction:[7]

$$g_c^{(m)}(\lambda,u,v)=g^{(m)}(\lambda,u,v)\frac{\sqrt{D^2+u^2}}{\sqrt{D^2+u^2+v^2}}. \quad (5)$$

Then, we can apply the super-short-scan fan-beam formula (37) in Ref. 1 for 3-D VOI reconstruction:

$$f(\vec{x})=\frac{1}{2\pi}\int_\Lambda d\lambda\left[\frac{\sqrt{D^2+(\tilde{u})^2}}{D\|\vec{x}-\vec{a}(\lambda)\|}\times w(\lambda,\tilde{u})g_F^{(m)}(\lambda,\tilde{u},\tilde{v})\right]_{\tilde{u}=\tilde{u}^*(\lambda,\vec{x}),\tilde{v}=\tilde{v}^*(\lambda,\vec{x})}, \quad (6)$$

$$\tilde{u}^*(\lambda,\vec{x})=\frac{D[\vec{x}-\vec{a}(\lambda)]\cdot\vec{e}_2}{[\vec{x}-\vec{a}(\lambda)]\cdot\vec{e}_1}, \quad (7)$$

$$\tilde{v}^*(\lambda,\vec{x})=\frac{D[\vec{x}-\vec{a}(\lambda)]\cdot\vec{e}_3}{[\vec{x}-\vec{a}(\lambda)]\cdot\vec{e}_1}, \quad (8)$$

$$w(\lambda,\tilde{u})=\frac{\eta(\lambda)}{\eta(\lambda)+\eta(\lambda+\pi-2\tan^{-1}(\tilde{u}/D))}, \quad (9)$$

$$g_F^{(m)}(\lambda,\tilde{u},\tilde{v})=\int_{-u_m}^{u_m}du\,h_H(\tilde{u}-u)\frac{D}{\sqrt{D^2+u^2}}\left(\frac{\partial}{\partial\lambda}+\frac{\partial u}{\partial\lambda}\frac{\partial}{\partial u}+\frac{\partial v}{\partial\lambda}\frac{\partial}{\partial v}\right)g_c^{(m)}(\lambda,u,\tilde{v}), \quad (10)$$

$$\frac{\partial u}{\partial\lambda}=D\cos\xi+\frac{u^2}{D\cos\xi}-\frac{u}{D}\tan\xi(u\sin\xi+v\cos\xi), \quad (11)$$

$$\frac{\partial v}{\partial\lambda}=-D\sin\xi+\frac{uv}{D\cos\xi}-\frac{v}{D}\tan\xi(u\sin\xi+v\cos\xi), \quad (12)$$

where $\tilde{u}^*(\lambda,\vec{x})$ and $\tilde{v}^*(\lambda,\vec{x})$ are the coordinates of $\vec{x}$ projected on the detector plane, $w(\lambda,\tilde{u})$ is the weight function as Noo *et al.* defined in Ref. 1, $g_F^{(m)}(\lambda,\tilde{u},\tilde{v})$ is a natural extension of formula (38) in Ref. 1, and u_m is the half length of the detector plane. The definition of $\eta(\lambda)$ in (9) will be specified in Sec. III. Detailed derivations of (11) and (12) are in the Appendix. Function $h_H(\cdot)$ in (10) represents the Hilbert transform kernel defined as

$$h_H(u)=-\int_{-\infty}^{\infty}d\sigma\,i\,\mathrm{sgn}(\sigma)e^{i2\pi\sigma u}=\frac{1}{\pi u}. \quad (13)$$

Note that on the mid-plane in the case of circular scanning,[1]

$$\frac{\sqrt{D^2+\tilde{u}^2}}{D\|\vec{x}-\vec{a}(\lambda)\|}=\frac{1}{R_0+\vec{x}\cdot\vec{e}_1}. \quad (14)$$

Hence, we approximately have

$$f(\vec{x})=\frac{1}{2\pi}\int_\Lambda d\lambda\frac{1}{R_0+\vec{x}\cdot\vec{e}_1}\times[w(\lambda,\tilde{u})g_F^{(m)}(\lambda,\tilde{u},\tilde{v})]_{\tilde{u}=\tilde{u}^*(\lambda,\vec{x}),\tilde{v}=\tilde{v}^*(\lambda,\vec{x})}. \quad (15)$$

There is a substantial flexibility with constructing a local detection coordinate system. Some researchers, such as Kachelriess *et al.*,[9] prefer using $\vec{d}_1=\vec{e}_1$, $\vec{d}_2=(-\sin\lambda,\cos\lambda,0)$ and $\vec{d}_3=(0,0,1)$ to define a natural detection system (ω,τ) shown as in Fig. 1. In this local system, the reconstruction can be performed using the same formulas as (5)–(10) except that

Iterative tomographic reconstruction

J. theor. Biol. (1970) 29, 471–481

Algebraic Reconstruction Techniques (ART) for Three-dimensional Electron Microscopy and X-ray Photography

RICHARD GORDON, ROBERT BENDER AND GABOR T. HERMAN

Center for Theoretical Biology
and
Department of Computer Science,
State University of New York at Buffalo, Amherst, N.Y. 14226, U.S.A.

(*Received* 12 *August* 1970)

We give a new method for direct reconstruction of three-dimensional objects from a few electron micrographs taken at angles which need not exceed a range of 60 degrees. The method works for totally asymmetric objects, and requires little computer time or storage. It is also applicable to X-ray photography, and may greatly reduce the exposure compared to current methods of body-section radiography.

$$f_{\nu+1}=f_\nu+\mathsf{R}_\nu^{\mathrm{T}}\frac{p_\nu-\mathsf{R}_\nu f_\nu}{\mathsf{R}_\nu^2 1}$$

dkfz.

Exact Spiral Reconstruction

Analytical tomographic reconstruction

2014 ALEXANDER KATSEVICH

endpoints of the PI segment containing x. We will call $I_{PI}(x) := [s_b(x), s_t(x)]$ the PI parametric interval. The part of the spiral corresponding to $I_{PI}(x)$ will be denoted $C_{PI}(x)$. Also, inside the PI there exists $\check{s} = \check{s}(x)$ such that the plane through $y(\check{s})$ and parallel to $\dot{y}(\check{s}), \ddot{y}(\check{s})$, contains x.

Fix $x \in U$. It is clear that any plane through x intersects $C_{PI}(x)$ at least at one point. Introduce the following sets:

$$
\begin{aligned}
Crit(x) &= \{\xi \in \mathbb{R}^3 \setminus 0 : \Pi(x,\xi) \text{ contains } y(s_b(x)), y(s_t(x)) \text{ or} \\
&\qquad \Pi(x,\xi) \text{ is tangent to } C_{PI}(x)\} \cup \{0\}, \\
\Xi_1(x) &= \{\xi \in \mathbb{R}^3 : \xi \notin Crit(x) \text{ and } \Pi(x,\xi) \cap C_{PI}(x) \text{ contains one point}\}, \\
\Xi_3(x) &= \mathbb{R}^3 \setminus \{\Xi_1(x) \cup Crit(x)\}.
\end{aligned} \tag{2.5}
$$

By construction, the sets $Crit(x), \Xi_{1,3}(x)$ are pairwise disjoint, their union is all of $\mathbb{R}^3$, $Crit(x)$ is closed and has Lebesgue measure zero, and $\Xi_{1,3}(x)$ are open.

Denote

$$
e_1(s,x) := \frac{[\beta(s,x) \times \dot{y}(s)] \times \beta(s,x)}{|[\beta(s,x) \times \dot{y}(s)] \times \beta(s,x)|}. \tag{2.6}
$$

By construction, $e_1(s,x)$ is a unit vector in the plane through $y(s)$ and is spanned by $\beta(s,x), \dot{y}(s)$. Moreover, $e_1(s,x)$ is perpendicular to $\beta(s,x)$. For convenience, here and in the rest of the paper, we think of vectors $\beta(s,x), e_1(s,x), e_2(s,x)$ (to be defined below) and their linear combinations as if they are attached to $y(s)$.

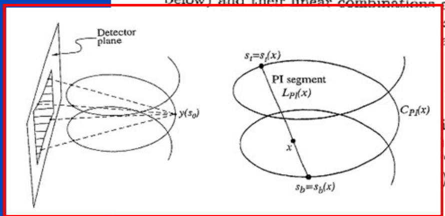

$x)\}$, find $s_{tan} \in I_{PI}(x), s_{tan} \neq s$, such that the …angent to $C_{PI}(x)$ at $y(s_{tan})$. This is equivalent

$y(s))] \cdot \dot{y}(s_{tan}) = 0, \; s_{tan} \neq s.$

…ion $s_{tan} \in I_{PI}(x)$ to (2.7) is shown below (see …. Also, we will show below (see (2.35) and the …$^\infty$ with respect to s on $(s_b(x), s_t(x)) \setminus \{\check{s}(x)\}$ …)] by setting

$$
s_{tan}(s,x) = \begin{cases} s_t(x), & s = s_b(x), \\ \check{s}(x), & s = \check{s}(x), \\ s_b(x), & s = s_t(x). \end{cases} \tag{2.8}
$$

Once $s_{tan} = s_{tan}(s,x)$ has been found, denote similarly to (2.6)

$$
\begin{aligned}
e_2(s,x) &:= \frac{[\beta(s,x) \times \Theta] \times \beta(s,x)}{|[\beta(s,x) \times \Theta] \times \beta(s,x)|}, \\
\Theta &= \begin{cases} \operatorname{sgn}(s - s_{tan}(s,x))\beta(s_{tan},x), & s \in (s_b(x), s_t(x)) \setminus \{\check{s}(x)\}, \\ \dot{y}(s_{tan}), & s \in \{s_b(x), \check{s}(x), s_t(x)\}. \end{cases}
\end{aligned} \tag{2.9}
$$

By construction, $e_2(s,x)$ is a unit vector in the plane through $x, y(s)$ and is a tangent to $C_{PI}(x)$ at $y(s_{tan})$. In addition, $e_2(s,x)$ is perpendicular to $\beta(s,x)$. Using (2.8) and the inequalities $s_{tan}(s,x) > \check{s}(x)$ if $s < \check{s}(x)$, $s_{tan}(s,x) < \check{s}(x)$ if $s > \check{s}(x)$ (see (2.39) below), we conclude that $e_2(s,x)$ is continuous with respect to s on $[s_b(x), s_t(x)]$.

Iterative tomographic reconstruction

J. theor. Biol. (1970) **29**, 471–481

Algebraic Reconstruction Techniques (ART) for Three-dimensional Electron Microscopy and X-ray Photography

RICHARD GORDON, ROBERT BENDER AND GABOR T. HERMAN

Center for Theoretical Biology
and
Department of Computer Science,
State University of New York at Buffalo, Amherst, N.Y. 14226, U.S.A.

(*Received* 12 *August* 1970)

We give a new method for direct reconstruction of three-dimensional objects from a few electron micrographs taken at angles which need not exceed a range of 60 degrees. The method works for totally asymmetric objects, and requires little computer time or storage. It is also applicable to X-ray photography, and may greatly reduce the exposure compared to current methods of body-section radiography.

$$
f_{\nu+1} = f_\nu + \mathsf{R}_\nu^{\mathrm{T}} \frac{p_\nu - \mathsf{R}_\nu f_\nu}{\mathsf{R}_\nu^2 1}
$$

Exact Cone Beam Reconstruction

Analytical tomographic reconstruction

The final ingredient is an auxiliary cutoff function. Let $\eta(\alpha) \in C^\infty(S^2)$ be even (i.e., $\eta(\alpha) = \eta(-\alpha)$) and equal zero in a neighborhood of

$$\Omega(x) := \left(\bigcup_{k,s\in I_{reg}(x)} \alpha_k(s,x)\right) \cup \mathrm{Crit}(x). \quad (2.5)$$

Clearly, $\eta(\alpha)$ depends on x. Since the role of η is only temporary, the dependence of η on x is omitted for simplicity.

Now, when all the ingredients are available, we derive the inversion formula. Define

$$(\mathcal{B}_\eta f)(x) := -\frac{1}{8\pi^2}\int_{S^2}\sum_j \frac{n(s_j,x,\alpha)}{\alpha\cdot\dot{y}(s_j)} \times \frac{\partial}{\partial s}\left\{\int_{\alpha^\perp}\nabla_{\Theta,\alpha}D_f(y(s),\Theta)d\Theta\right\}\Big|_{s=s_j}\eta(\alpha)d\alpha. \quad (2.6)$$

Here, $\nabla_{\Theta,\alpha}D_f(y(s),\Theta)$ denotes the derivative of D_f with respect to Θ along α:

$$(\nabla_{\Theta,\alpha}D_f)(y(s),\Theta) = \frac{\partial}{\partial t}D_f\left(y(s),\sqrt{1-t^2}\Theta+t\alpha\right)\Big|_{t=0}, \quad \Theta\in\alpha^\perp. \quad (2.7)$$

Using Grangeat's formula and the change of variables $p\to s$ defined by $p =$

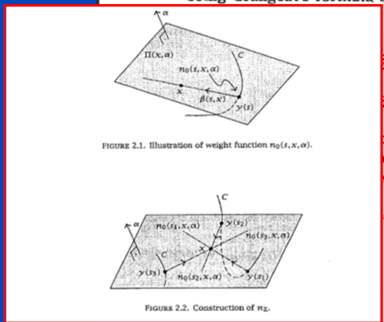

FIGURE 2.1. Illustration of weight function $n_0(s,x,\alpha)$.

FIGURE 2.2. Construction of n_Σ.

$$\frac{\partial}{\partial s}\left\{\int_{\alpha^\perp}\nabla_{\Theta,\alpha}D_f(y(s),\Theta)d\Theta\right\}\Big|_{s=s_j} \quad (2.8)$$

$$\hat{f}(\alpha,p)|_{p=\alpha\cdot y(s_j)=\alpha\cdot x},$$

don transform of f. Equations (2.6) and (2.8) make
ounded away from zero on suppη. From (2.8) and
e get

$$= \frac{1}{(2\pi)^3}\int_{\mathbb{R}^3}\eta\left(\frac{\xi}{|\xi|}\right)\tilde{f}(\xi)e^{-i\xi\cdot x}d\xi. \quad (2.9)$$

$$\int_{\alpha^\perp}\nabla_{\Theta,\alpha}\frac{\partial}{\partial q}D_f(y(q),\Theta)|_{q=s}d\Theta. \quad (2.10)$$

The reason for replacing $\partial/\partial s$ by $(\partial/\partial q)(\cdot)|_{q=s}$ is that in what follows, parametrization of Θ depend on s. The derivative $(\partial/\partial q)(\cdot)|_{q=s}$ emphasizes the fact that we first differentiate $D_f(y(s),\Theta)$ with respect to s, and then integrate the result with respect to Θ.

Using (2.10), rewrite (2.6) as follows:

$$(\mathcal{B}_\eta f)(x) = -\frac{1}{8\pi^2}\int_{S^2}\sum_j\frac{n(s_j,x,\alpha)}{\alpha\cdot\dot{y}(s_j)}g(s_j,\alpha)\eta(\alpha)d\alpha. \quad (2.11)$$

Iterative tomographic reconstruction

J. theor. Biol. (1970) **29**, 471–481

Algebraic Reconstruction Techniques (ART) for Three-dimensional Electron Microscopy and X-ray Photography

RICHARD GORDON, ROBERT BENDER AND GABOR T. HERMAN

Center for Theoretical Biology

and

Department of Computer Science,
State University of New York at Buffalo, Amherst, N.Y. 14226, U.S.A.

(*Received* 12 *August* 1970)

We give a new method for direct reconstruction of three-dimensional objects from a few electron micrographs taken at angles which need not exceed a range of 60 degrees. The method works for totally asymmetric objects, and requires little computer time or storage. It is also applicable to X-ray photography, and may greatly reduce the exposure compared to current methods of body-section radiography.

$$f_{\nu+1} = f_\nu + \mathrm{R}_\nu^{\mathrm{T}}\frac{p_\nu - \mathrm{R}_\nu f_\nu}{\mathrm{R}_\nu^2 1}$$

Reconstruction from Truncated Data

Analytical tomographic reconstruction

The fan-beam DBP formula is derived in the same way as the fan-beam FBP is usually presented: a change of coordinates (equation (25)) is invoked in the parallel FBP formula. A vital property which allows the final FBP formulation in fan-beam mode is the fact that the ramp filter is homogeneous of degree −2. Fortunately, we can describe the derivative using a filtering kernel $\delta'(r)$,

$$p'(\phi, r) = \frac{\partial}{\partial r} p(\phi, r) = \int_{-\infty}^{\infty} p(\phi, r')\delta'(r - r')\,\mathrm{d}r' \qquad (27)$$

and the filtering kernel is homogeneous of degree −2: $\delta'(\lambda r) = \delta'(r)/\lambda^2$ for $\lambda > 0$.

We must begin by writing the parallel DBP formula for a 2π scan,

$$b_0(x) = \int_0^{\pi} p'(\phi, x\cdot\alpha)\,\mathrm{d}\phi = \frac{1}{2}\int_0^{2\pi} p'(\phi, x\cdot\alpha)\,\mathrm{sgn}(\sin\phi)\,\mathrm{d}\phi \qquad (28)$$

and use (27) to match the form of the conventional FBP,

$$b_0(x) = \frac{1}{2}\int_0^{2\pi}\int_{-\infty}^{\infty} p(\phi, r')\delta'(x\cdot\alpha - r')\,\mathrm{sgn}(\sin\phi)\,\mathrm{d}r'\,\mathrm{d}\phi. \qquad (29)$$

Now the change of variables (equation (25)) is carried out, and the usual manipulations (see, e.g., Kak and Slaney (1987)) to arrive at the fan-beam formula

$$b_0(x) = \frac{1}{2}\int_0^{2\pi}\frac{R_0 D}{T^2}\int_{-\infty}^{\infty}\frac{D}{\sqrt{D^2+u^2}}\bar{p}(\xi, u)\delta'(u^* - u)\,\mathrm{sgn}\left(\sin\left(\xi + \arctan\frac{u}{D}\right)\right)\mathrm{d}u\,\mathrm{d}\xi$$

$$= \frac{1}{2}\int_0^{2\pi}\frac{R_0 D}{T^2}\frac{\mathrm{d}}{\mathrm{d}u}\left\{\frac{D}{\sqrt{D^2+u^2}}\bar{p}(\xi, u)\,\mathrm{sgn}\left(\sin\left(\xi + \arctan\frac{u}{D}\right)\right)\right\}\Bigg|_{u=u^*}\mathrm{d}\xi \qquad (30)$$

where

$$- x_2\cos\xi \qquad (31)$$

...sured perpendicularly from the detector ...$\xi, \cos\xi)$, and u^* is the value of u on the ...he direction of the u-axis is $(\cos\xi, \sin\xi)$

$$\ldots\sin\xi - x_2\cos\xi). \qquad (32)$$

... path of equations (28) to (30), departing

$$\ldots - \theta))\,\mathrm{d}\phi \qquad (33)$$

$$\ldots\left(\xi + \arctan\frac{u}{D} - \theta\right)\right)\Bigg\}\Bigg|_{u=u^*}\mathrm{d}\xi \qquad (34)$$

where T and u^* are given in equations (31) and (32).

In practice, equation (34) is difficult to implement accurately due to the discontinuity caused by the signum function in the argument of the derivative. By applying the product rule, the derivative of the discontinuity can be avoided. We show in the appendix that equation (34) leads to the following form which is more suitable for implementation,

$$b_\theta(x) = \frac{1}{2}\int_0^{2\pi}\frac{R_0 D}{T^2}\,\mathrm{sgn}\left(\sin\left(\xi + \arctan\frac{u^*}{D} - \theta\right)\right)\frac{\mathrm{d}}{\mathrm{d}u}\left\{\frac{D}{\sqrt{D^2+u^2}}\bar{p}(\xi, u)\right\}\Bigg|_{u=u^*}\mathrm{d}\xi$$

$$+ \frac{\bar{p}(\xi_1, u_1^*)}{\|x - v_1\|} - \frac{\bar{p}(\xi_2, u_2^*)}{\|x - v_2\|} \qquad (35)$$

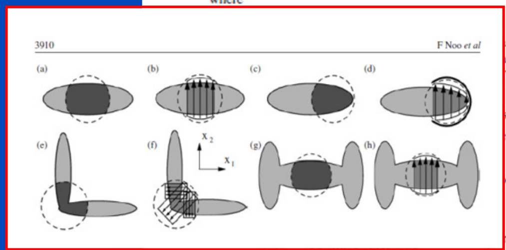

Iterative tomographic reconstruction

J. theor. Biol. (1970) **29**, 471–481

Algebraic Reconstruction Techniques (ART) for Three-dimensional Electron Microscopy and X-ray Photography

RICHARD GORDON, ROBERT BENDER AND GABOR T. HERMAN

Center for Theoretical Biology

and

Department of Computer Science, State University of New York at Buffalo, Amherst, N.Y. 14226, U.S.A.

(*Received 12 August* 1970)

We give a new method for direct reconstruction of three-dimensional objects from a few electron micrographs taken at angles which need not exceed a range of 60 degrees. The method works for totally asymmetric objects, and requires little computer time or storage. It is also applicable to X-ray photography, and may greatly reduce the exposure compared to current methods of body-section radiography.

$$f_{\nu+1} = f_\nu + \mathrm{R}_\nu^{\mathrm{T}}\,\frac{p_\nu - \mathrm{R}_\nu f_\nu}{\mathrm{R}_\nu^2 1}$$

Image Reconstruction within ROIs

Analytical tomographic reconstruction

$$f(\vec{r})=f_c(x_c,s_a,s_b),\qquad g(\vec{r})=g_c(x_c,s_a,s_b),\qquad (21)$$

where $\vec{r}$ and x_c are related through Eq. (3). In terms of $P(u_d,v_d,s)$ the backprojection image on a chord line specified by s_a and s_b is

$$g_c(x_c,s_a,s_b)=\int_{s_a}^{s_b} \mathrm{d}s \frac{\mathrm{sgn}[-\hat{\beta}\cdot\hat{e}_w(s)]}{|\vec{r}(x_c)-\vec{r}_0(s)|}\frac{\partial}{\partial s}P(u_d,v_d,s)\Big|_{\hat{\beta}}. \qquad (22)$$

The signum factor in the integral derives from the extension of the data function in Eq. (17). For $\vec{r}$ on the chord line, the kernel $K(\vec{r},\vec{r}')$ in Eq. (15) can be rewritten as

$$K(\vec{r},\vec{r}')=\frac{1}{2\pi j}\int_{\mathbb{R}} \mathrm{d}\nu_c\,\mathrm{sgn}(\nu_c)\exp[2\pi j\nu_c(x_c-x_c')]\delta(y_c')\delta(z_c') = \frac{1}{2\pi^2(x_c-x_c')}\delta(y_c')\delta(z_c'), \qquad (23)$$

where $\vec{r}'\in\mathbb{R}^3$, and ν_c denotes the spatial frequency with respect to x_c.

Applying Eq. (23) to Eq. (14) yields

$$f_c(x_c,s_a,s_b)=\frac{1}{2\pi^2}\int_{\mathbb{R}} \frac{\mathrm{d}x_c'}{x_c-x_c'}g_c(x_c',s_a,s_b), \qquad (24)$$

where $x_c\in\mathbb{R}$. Therefore, the image $f_c(x_c,s_a,s_b)$ on the chord line is the Hilbert transform, along the chord line,

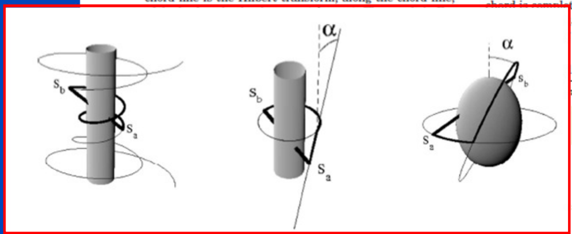

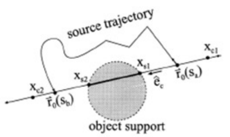

Fig. 3. Diagram illustrating the support segment ($x_c\in[x_{s1},x_{s2}]$) and backprojection segment ($x_c\in[x_{c1},x_{c2}]$).

$$g_c(x_c,s_a,s_b)=2\int_{\mathbb{R}} \frac{\mathrm{d}x_c'}{x_c'-x_c}f_c(x_c',s_a,s_b) = 2\int_{x_{c1}}^{x_{c2}}\frac{\mathrm{d}x_c'}{x_c'-x_c}f_c(x_c',s_a,s_b), \qquad (25)$$

where $x_c\in\mathbb{R}$, and parameters x_{c1} and x_{c2} satisfy $x_{c1}\in(-\infty,x_{s1}]$ and $x_{c2}\in[x_{s2},\infty)$, respectively. We refer to $[x_{c1},x_{c2}]$ as the backprojection segment. We obtained the last part of Eq. (25) by observing that $f_c(x_c,s_a,s_b)=0$ for $x_c\notin[x_{s1},x_{s2}]$.

The result in Eq. (25) represents a Hilbert transform on a finite interval, and its inversion can be obtained as[22–24]

$$f_c(x_c,s_a,s_b)=\frac{1}{2\pi^2}\frac{1}{\sqrt{(x_{c2}-x_c)(x_c-x_{c1})}}\times\left[\int_{x_{c1}}^{x_{c2}}\frac{\mathrm{d}x_c'}{x_c-x_c'}\sqrt{(x_{c2}-x_c')(x_c'-x_{c1})}\times g_c(x_c',s_a,s_b)+C\right], \qquad (26)$$

where $x_c\in[x_{c1},x_{c2}]$, the relationship between x_c and $\vec{r}$ is determined by Eq. (3), and the constant C is given by

$$C=2\pi\int_{x_{c1}}^{x_{c2}} f_c(x_c,s_a,s_b)\mathrm{d}x_c = 2\pi D(\vec{r}_0(s_a),\hat{e}_c). \qquad (27)$$

Because the second term in Eq. (26) is only a constant that can be readily obtained directly from data, the computation load required for reconstructing the image on a ...ely determined by that for computing the ... (26). ... the form of the first term, Eq. (26) can be

$$\ldots\frac{1}{\ldots^2\sqrt{(x_{c2}-x_c)(x_c-x_{c1})}}\left[\int_{\mathbb{R}} \frac{\mathrm{d}x_c'}{x_c-x_c'} g_\Pi(x_c',s_a,s_b)+2\pi D(\vec{r}_0(s_a),\hat{e}_c)\right], \qquad (28)$$

$$\ldots=\Pi_c(x_c')\sqrt{(x_{c2}-x_c')(x_c'-x_{c1})}\,g_c(x_c',s_a,s_b), \qquad (29)$$

and $\Pi_c(x_c')=1$ if $x_c'\in[x_{c1},x_{c2}]$ and 0 if $x_c'\notin[x_{c1},x_{c2}]$. Unlike the first term (i.e., the Hilbert transform over a finite interval) in Eq. (26) that does not appear to represent explicitly a shift-invariant filtration on the x_c' axis, Eq. (28) indicates explicitly a shift-invariant filtering (i.e., the Hilbert transform) over the entire x_c' axis. Such a change may have practical significance because the Hilbert transform can now be calculated efficiently by use of the fast-Fourier-transform (FFT) technique.

It can be observed in Eq. (29) that the image on the chord can be obtained exactly from knowledge of the backprojection image on a support segment, specified by

Iterative tomographic reconstruction

J. theor. Biol. (1970) **29**, 471–481

Algebraic Reconstruction Techniques (ART) for Three-dimensional Electron Microscopy and X-ray Photography

Richard Gordon, Robert Bender and Gabor T. Herman

Center for Theoretical Biology
and
Department of Computer Science,
State University of New York at Buffalo, Amherst, N.Y. 14226, U.S.A.

(*Received* 12 *August* 1970)

We give a new method for direct reconstruction of three-dimensional objects from a few electron micrographs taken at angles which need not exceed a range of 60 degrees. The method works for totally asymmetric objects, and requires little computer time or storage. It is also applicable to X-ray photography, and may greatly reduce the exposure compared to current methods of body-section radiography.

$$f_{\nu+1} = f_\nu + \mathrm{R}_\nu^{\mathrm{T}}\frac{p_\nu - \mathrm{R}_\nu f_\nu}{\mathrm{R}_\nu^2 1}$$

Image Reconstruction within ROIs

Analytical tomographic reconstruction

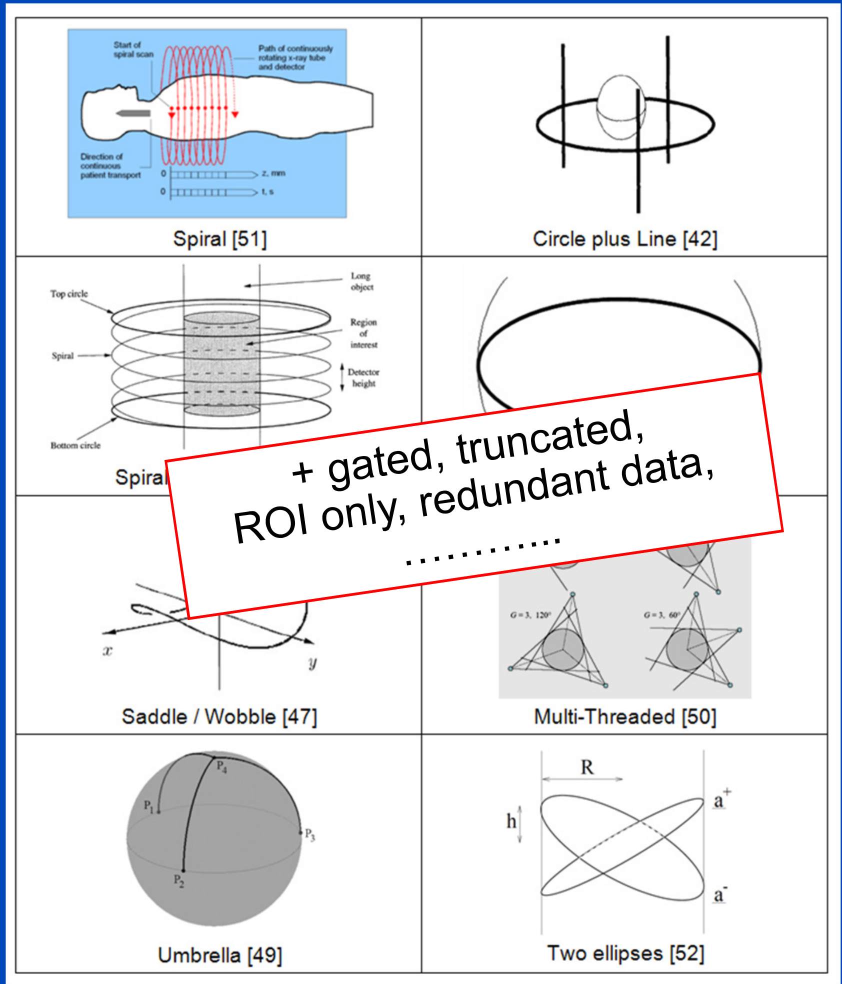

Iterative tomographic reconstruction

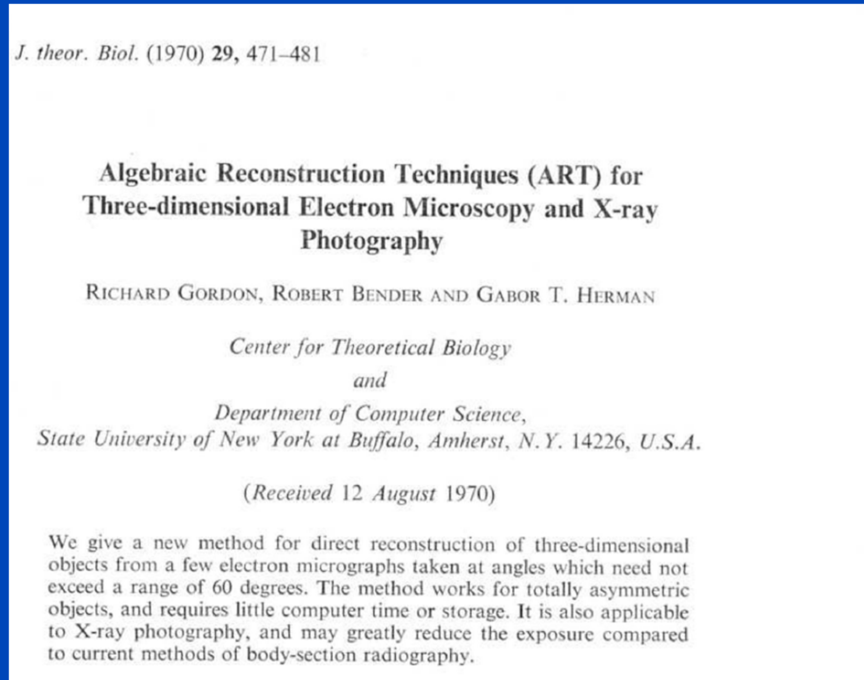
J. theor. Biol. (1970) **29**, 471–481

Algebraic Reconstruction Techniques (ART) for Three-dimensional Electron Microscopy and X-ray Photography

RICHARD GORDON, ROBERT BENDER AND GABOR T. HERMAN

Center for Theoretical Biology

and

Department of Computer Science, State University of New York at Buffalo, Amherst, N.Y. 14226, U.S.A.

(*Received* 12 *August* 1970)

We give a new method for direct reconstruction of three-dimensional objects from a few electron micrographs taken at angles which need not exceed a range of 60 degrees. The method works for totally asymmetric objects, and requires little computer time or storage. It is also applicable to X-ray photography, and may greatly reduce the exposure compared to current methods of body-section radiography.

$$f_{\nu+1} = f_\nu + \mathrm{R}_\nu^{\mathrm{T}} \frac{p_\nu - \mathrm{R}_\nu f_\nu}{\mathrm{R}_\nu^2 1}$$

dkfz.

$$x^2 = y$$

Model

$$\cancel{x = \sqrt{y}}$$

$$(x_n + \Delta x_n)^2 = y$$

$$x_n^2 + 2x_n \Delta x_n + \cancel{\Delta x_n^2} = y$$

$$x_n^2 + 2x_n \Delta x_n \approx y$$

$$\Delta x_n = \tfrac{1}{2}(y - x_n^2)/x_n$$

$$x_{n+1} = x_n + \Delta x_n$$

Update equation

Influence of Update Equation and Model

$0.5\,(3 - x_n^2)/x_n$	$0.4\,(3 - x_n^2)/x_n$	$0.5\,(3 - x_n^{2.1})/x_n$
$x_0 = 1.$	$x_0 = 1.$	$x_0 = 1.$
$x_1 = 2.$	$x_1 = 1.8$	$x_1 = 2.$
$x_2 = 1.75$	$x_2 = 1.74667$	$x_2 = 1.67823$
$x_3 = 1.73214$	$x_3 = 1.73502$	$x_3 = 1.68833$
$x_4 = 1.73205$	$x_4 = 1.73265$	$x_4 = 1.68723$
$x_5 = 1.73205$	$x_5 = 1.73217$	$x_5 = 1.68734$
$x_6 = 1.73205$	$x_6 = 1.73207$	$x_6 = 1.68733$
$x_7 = 1.73205$	$x_7 = 1.73206$	$x_7 = 1.68733$
$x_8 = 1.73205$	$x_8 = 1.73205$	$x_8 = 1.68733$

$$x^2 = 3, \quad x_0 = 1, \quad x_{n+1} = x_n + \Delta x_n$$

dkfz.

CT System Matrix

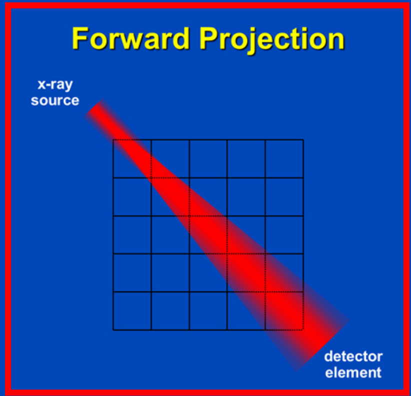

$$\underbrace{\boldsymbol{R}}_{\text{Radon or x-ray transform}} \cdot \underbrace{\boldsymbol{f}}_{\text{image to be reconstructed}} = \underbrace{\boldsymbol{p}}_{\text{measured rawdata}}$$

$$\boldsymbol{R} = \begin{pmatrix} r_{11} & r_{12} & \cdots & r_{1M} \\ r_{21} & r_{22} & \cdots & r_{2M} \\ \vdots & \vdots & \ddots & \vdots \\ r_{N1} & r_{N2} & \cdots & r_{NM} \end{pmatrix}, \quad \boldsymbol{f} = \begin{pmatrix} f_1 \\ f_2 \\ \vdots \\ f_M \end{pmatrix}, \quad \boldsymbol{p} = \begin{pmatrix} p_1 \\ p_2 \\ \vdots \\ p_N \end{pmatrix}$$

Kaczmarz's Method

$$\underbrace{\boldsymbol{R}}_{N \times M} \cdot \underbrace{\boldsymbol{f}}_{M \times 1} = \underbrace{\boldsymbol{p}}_{N \times 1}$$

$$\boldsymbol{R} = \begin{pmatrix} \boldsymbol{r}_1 \\ \boldsymbol{r}_2 \\ \vdots \\ \boldsymbol{r}_N \end{pmatrix}, \quad |\boldsymbol{r}_n| = 1$$

$$\boldsymbol{r}_n \cdot \boldsymbol{f} = p_n$$

Kaczmarz‘s Method (2)

- Successively solve $\boldsymbol{r}_n \cdot \boldsymbol{f} = p_n$
- To do so, project onto the hyperplanes

$$\boldsymbol{r}_n \cdot \big(\boldsymbol{f} + \lambda \boldsymbol{r}_n\big) = p_n$$

$$\lambda = p_n - \boldsymbol{r}_n \cdot \boldsymbol{f}$$

$$\boldsymbol{f}_{\text{new}} = \boldsymbol{f} + \lambda \boldsymbol{r}_n$$

$$\boldsymbol{f}_{\text{new}} = \boldsymbol{f} + \boldsymbol{r}_n \big(p_n - \boldsymbol{r}_n \cdot \boldsymbol{f}\big)$$

- Repeat until some convergence criterion is reached

$$\boldsymbol{f}_{\nu+1} = \boldsymbol{f}_\nu + \boldsymbol{r}_n \big(p_n - \boldsymbol{r}_n \cdot \boldsymbol{f}_\nu\big)$$

Kaczmarz's Method (3)

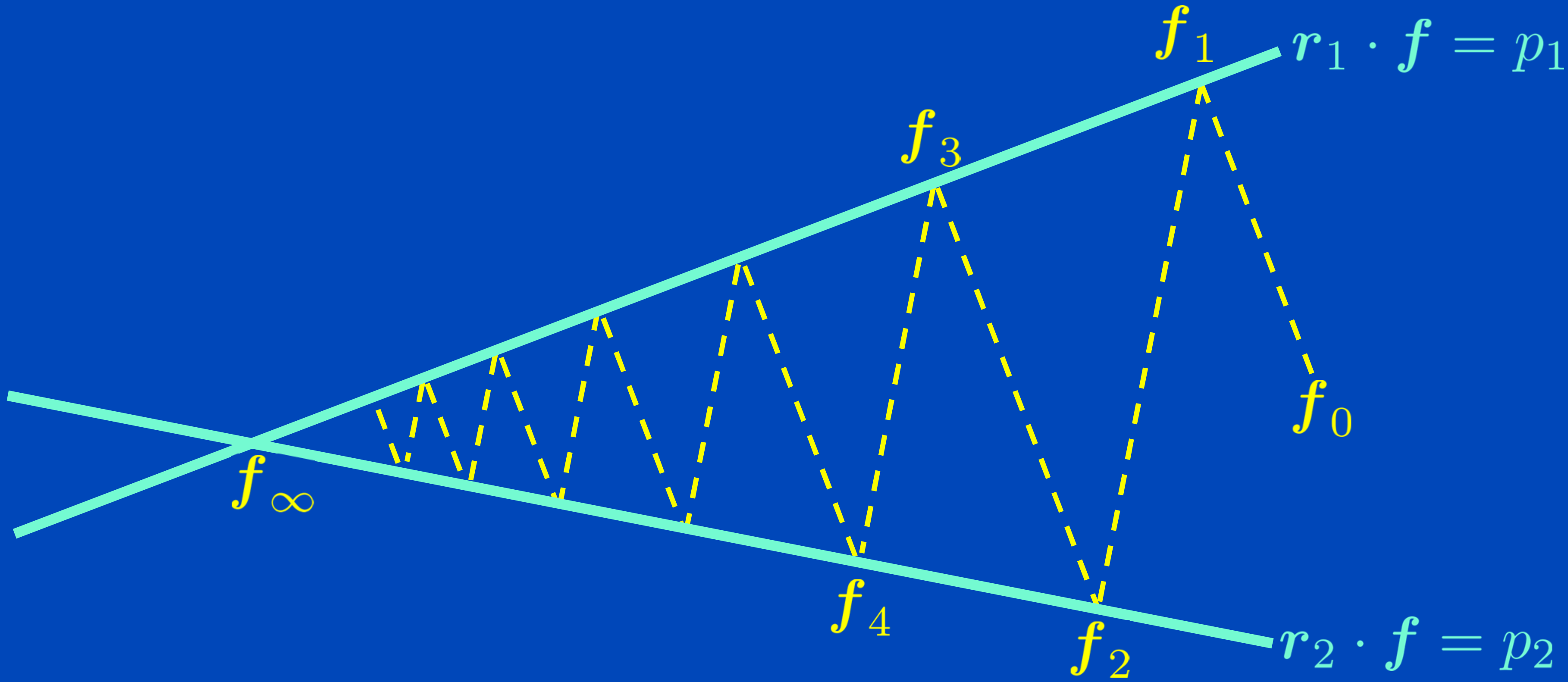

$$\boldsymbol{f}_{\nu+1} = \boldsymbol{f}_\nu + \boldsymbol{r}_n \big(p_n - \boldsymbol{r}_n \cdot \boldsymbol{f}_\nu\big)$$

Kaczmarz in Image Reconstruction: Algebraic Reconstruction Technique (ART)

$$\boldsymbol{f}_{\nu+1} = \boldsymbol{f}_\nu + \boldsymbol{r}_n\big(p_n - \boldsymbol{r}_n \cdot \boldsymbol{f}_\nu\big)$$

$$\boxed{\boldsymbol{f}_{\nu+1} = \boldsymbol{f}_\nu + \boldsymbol{R}^{\mathrm{T}} \cdot \frac{\boldsymbol{p} - \boldsymbol{R} \cdot \boldsymbol{f}_\nu}{\boldsymbol{R}^2 \cdot \mathbf{1}}}$$

Kaczmarz‘s Method = ART

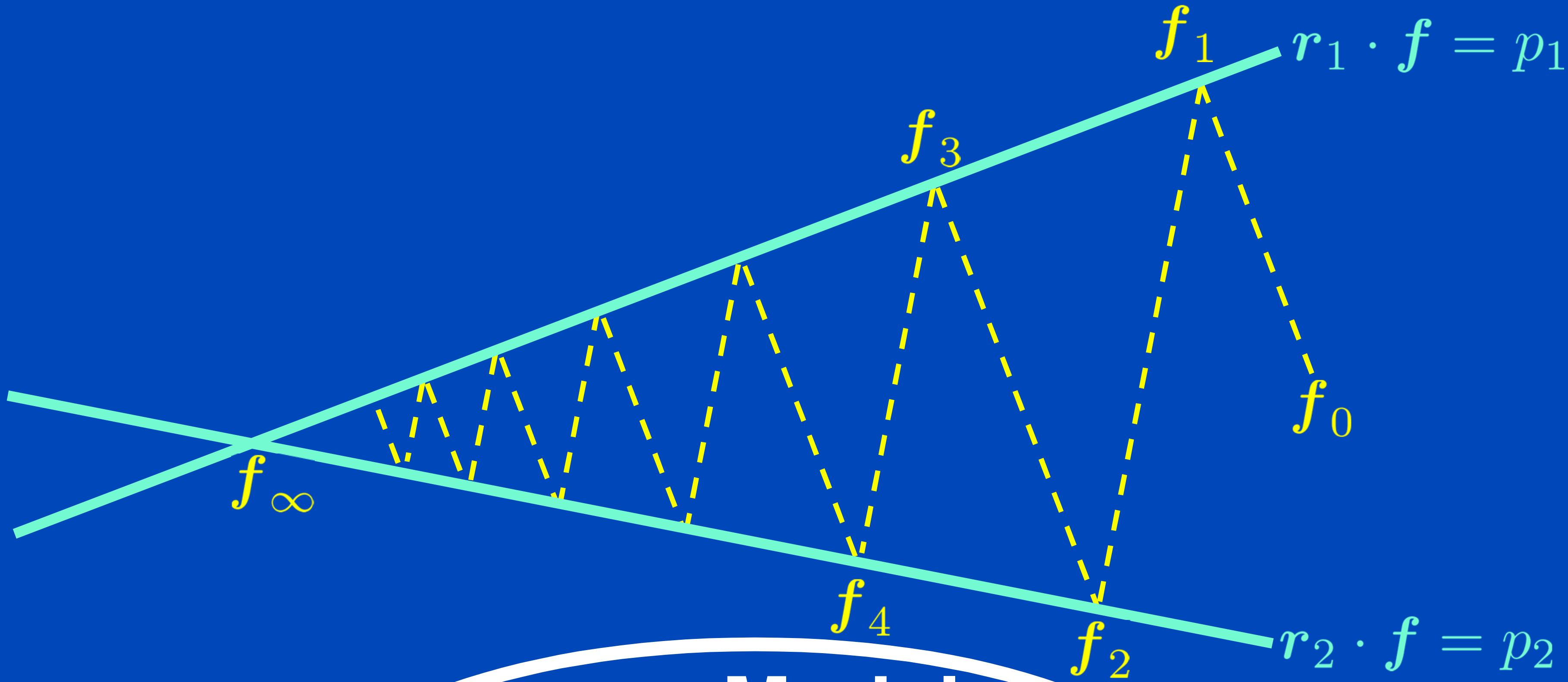

Model

$$\boldsymbol{f}_{\nu+1} = \boldsymbol{f}_\nu + \boldsymbol{R}^{\mathrm{T}} \cdot \frac{\boldsymbol{p} - \boldsymbol{R} \cdot \boldsymbol{f}_\nu}{\boldsymbol{R}^2 \cdot \boldsymbol{1}}$$

Update equation

Kaczmarz‘s Method = ART

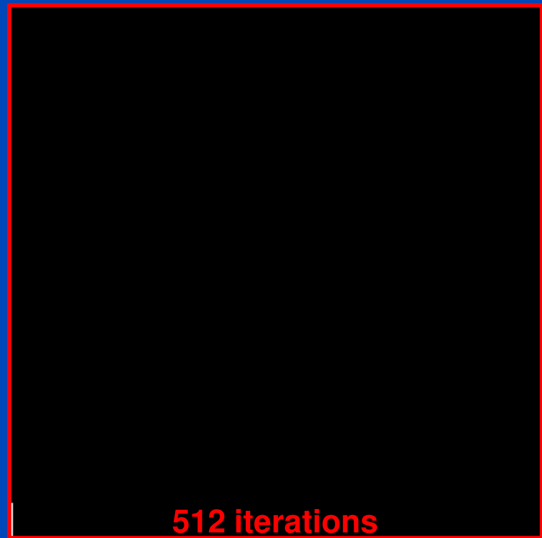

$$\boldsymbol{f}_{\nu+1} = \boldsymbol{f}_{\nu} + \boldsymbol{R}^{\mathrm{T}} \cdot \frac{\boldsymbol{p} - \boldsymbol{R} \cdot \boldsymbol{f}_{\nu}}{\boldsymbol{R}^2 \cdot \mathbf{1}}$$

apply inverse model

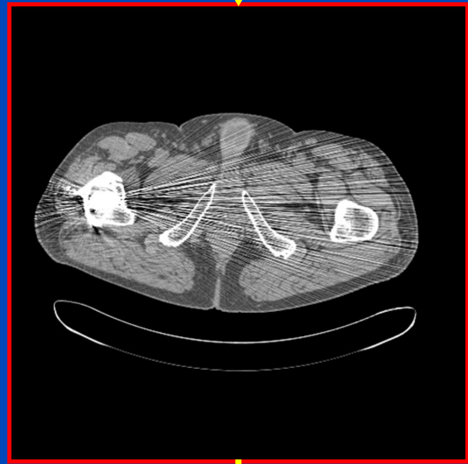

apply forward model

$$\boldsymbol{f}_{\nu+1} = \boldsymbol{f}_{\nu} + \boldsymbol{R}^{\mathrm{T}} \cdot \frac{\boldsymbol{p} - \boldsymbol{R} \cdot \boldsymbol{f}_{\nu}}{\boldsymbol{R}^{2} \cdot \boldsymbol{1}}$$

Direct vs. Filtered Backprojection

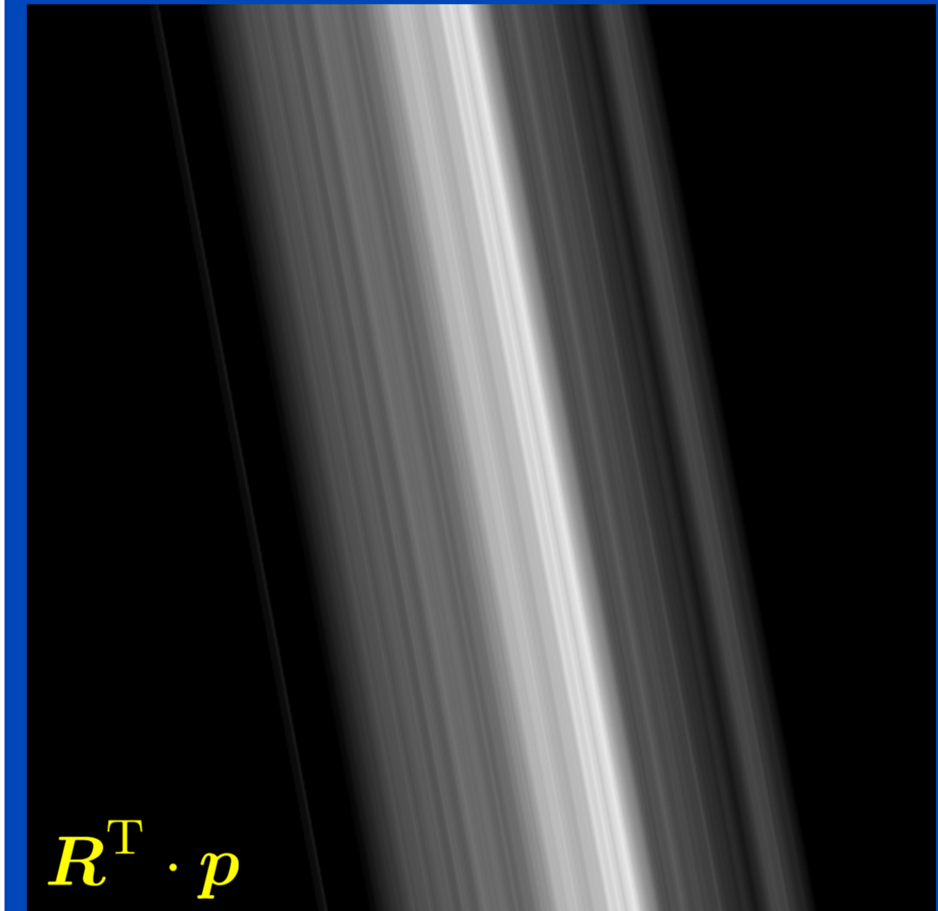

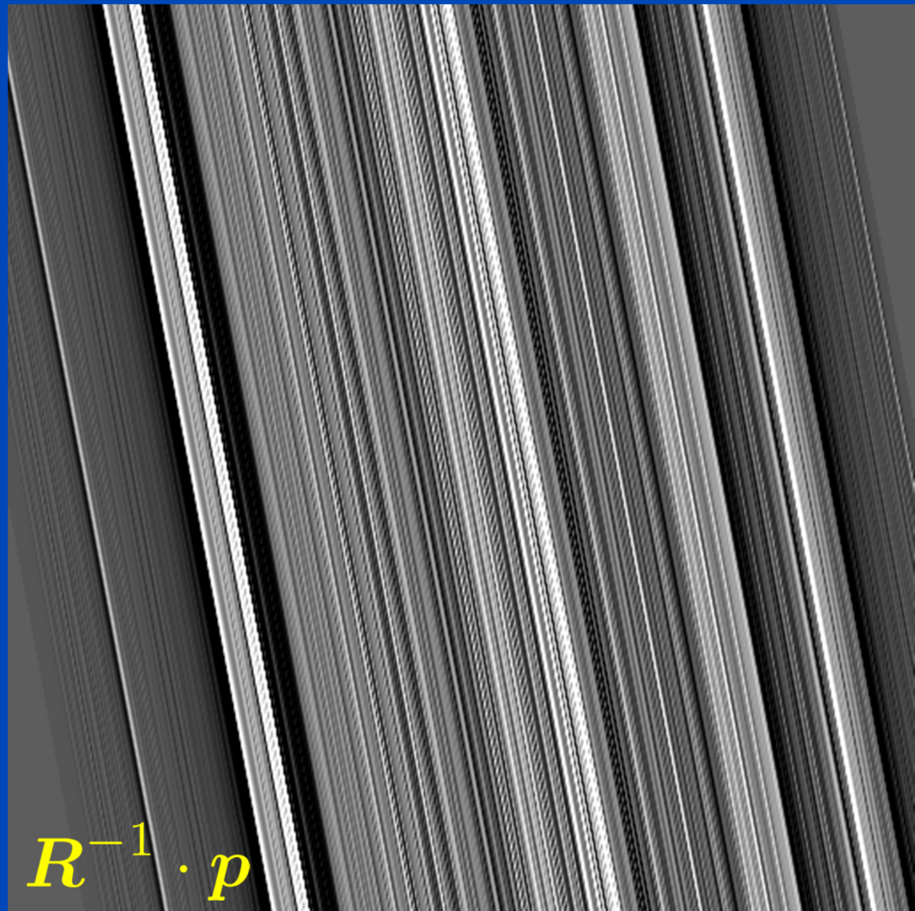

Flavours of Iterative Reconstruction

- **ART** $$\boldsymbol{f}_{\nu+1} = \boldsymbol{f}_\nu + \boldsymbol{R}^{\mathrm{T}} \cdot \frac{\boldsymbol{p} - \boldsymbol{R} \cdot \boldsymbol{f}_\nu}{\boldsymbol{R}^2 \cdot \boldsymbol{1}}$$
- **SART** $$\boldsymbol{f}_{\nu+1} = \boldsymbol{f}_\nu + \frac{1}{\boldsymbol{R}^{\mathrm{T}} \cdot \boldsymbol{1}} \boldsymbol{R}^{\mathrm{T}} \cdot \frac{\boldsymbol{p} - \boldsymbol{R} \cdot \boldsymbol{f}_\nu}{\boldsymbol{R} \cdot \boldsymbol{1}}$$
- **MLEM** $$\boldsymbol{f}_{\nu+1} = \boldsymbol{f}_\nu \frac{\boldsymbol{R}^{\mathrm{T}} \cdot \left(e^{-\boldsymbol{R} \cdot \boldsymbol{f}_\nu}\right)}{\boldsymbol{R}^{\mathrm{T}} \cdot \left(e^{-\boldsymbol{p}}\right)}$$
- **OSC** $$\boldsymbol{f}_{\nu+1} = \boldsymbol{f}_\nu + \boldsymbol{f}_\nu \frac{\boldsymbol{R}^{\mathrm{T}} \cdot \left(e^{-\boldsymbol{R} \cdot \boldsymbol{f}_\nu} - e^{-\boldsymbol{p}}\right)}{\boldsymbol{R}^{\mathrm{T}} \cdot \left(e^{-\boldsymbol{R} \cdot \boldsymbol{f}_\nu} \boldsymbol{R} \cdot \boldsymbol{f}_\nu\right)}$$
- **and hundreds more …**

Cost Functions

- **General expression:** $\boldsymbol{f} = \arg\min_{\boldsymbol{f}} C(\boldsymbol{f})$

- **Examples:**

$$C(\boldsymbol{f}) = \left(\boldsymbol{R} \cdot \boldsymbol{f} - \boldsymbol{p}\right)^2$$

$$C(\boldsymbol{f}) = \left(\boldsymbol{W} \cdot (\boldsymbol{R} \cdot \boldsymbol{f} - \boldsymbol{p})\right)^2$$

$$C(\boldsymbol{f}) = \left(\boldsymbol{W} \cdot (\boldsymbol{R} \cdot \boldsymbol{f} - \boldsymbol{p})\right)^2 + \beta P(\boldsymbol{f})$$

statistical properties and **preconditioning**

additional penalties

Linear PWLS

PWLS $$C(\boldsymbol{f}) = (\boldsymbol{R}\cdot\boldsymbol{f}-\boldsymbol{p})^{\mathrm{T}}\cdot\boldsymbol{W}\cdot(\boldsymbol{R}\cdot\boldsymbol{f}-\boldsymbol{p})+\beta\boldsymbol{f}^{\mathrm{T}}\cdot\boldsymbol{Q}\cdot\boldsymbol{f}$$

Gradient $$\boldsymbol{\nabla}C(\boldsymbol{f}) \propto \boldsymbol{R}^{\mathrm{T}}\cdot\boldsymbol{W}\cdot(\boldsymbol{R}\cdot\boldsymbol{f}-\boldsymbol{p})+\beta\boldsymbol{Q}\cdot\boldsymbol{f}$$

Gradient update $$f_{\nu+1} = f_\nu - \alpha_\nu\boldsymbol{\nabla}C(\boldsymbol{f}_\nu)$$

At convergence $$\boldsymbol{\nabla}C(\boldsymbol{f}_\infty) = 0$$

Fixed point $$\boldsymbol{f}_\infty = (\boldsymbol{R}^{\mathrm{T}}\cdot\boldsymbol{W}\cdot\boldsymbol{R}+\beta\boldsymbol{Q})^{-1}\cdot\boldsymbol{R}^{\mathrm{T}}\cdot\boldsymbol{W}\cdot\boldsymbol{p}$$

Assume there exists $\hat{f}$ such that $R\cdot\hat{f}=p$. Then everything reduces to a shift variant image filter:

$$\boldsymbol{f}_\infty = (\boldsymbol{R}^{\mathrm{T}}\cdot\boldsymbol{W}\cdot\boldsymbol{R}+\beta\boldsymbol{Q})^{-1}\cdot\boldsymbol{R}^{\mathrm{T}}\cdot\boldsymbol{W}\cdot\boldsymbol{R}\cdot\hat{\boldsymbol{f}}$$

In case of shift invariance we can convert to Fourier domain:

$$\mathsf{F}\boldsymbol{f}_\infty = \frac{1}{1+\beta\frac{\mathsf{F}\boldsymbol{Q}}{\mathsf{F}\boldsymbol{R}^{\mathrm{T}}\cdot\boldsymbol{W}\cdot\boldsymbol{R}}}\mathsf{F}\hat{\boldsymbol{f}}$$

high-pass

low-pass

dkfz.

Non-Linear PWLS

PWLS $C(\boldsymbol{f}) = (\boldsymbol{R}\cdot\boldsymbol{f}-\boldsymbol{p})^{\mathrm{T}}\cdot\boldsymbol{W}\cdot(\boldsymbol{R}\cdot\boldsymbol{f}-\boldsymbol{p})+\beta P(\boldsymbol{f})$

Gradient $\boldsymbol{\nabla}C(\boldsymbol{f}) \propto \boldsymbol{R}^{\mathrm{T}}\cdot\boldsymbol{W}\cdot(\boldsymbol{R}\cdot\boldsymbol{f}-\boldsymbol{p})+\beta\boldsymbol{\nabla}P(\boldsymbol{f})$ $\approx \boldsymbol{Q}(\boldsymbol{f})\cdot\boldsymbol{f}$

Gradient update $\boldsymbol{f}_{\nu+1} = \boldsymbol{f}_\nu - \alpha_\nu\boldsymbol{\nabla}C(\boldsymbol{f}_\nu)$

At convergence $\boldsymbol{\nabla}C(\boldsymbol{f}_\infty) = 0$

Fixed point $\boldsymbol{f}_\infty = (\boldsymbol{R}^{\mathrm{T}}\cdot\boldsymbol{W}\cdot\boldsymbol{R}+\beta\boldsymbol{Q}(\boldsymbol{f}_\infty))^{-1}\cdot\boldsymbol{R}^{\mathrm{T}}\cdot\boldsymbol{W}\cdot\boldsymbol{p}$

Assume there exists $\hat{f}$ such that $R\cdot\hat{f}=p$. Then everything reduces to a shift variant image filter:

$$\boldsymbol{f}_\infty = (\boldsymbol{R}^{\mathrm{T}}\cdot\boldsymbol{W}\cdot\boldsymbol{R}+\beta\boldsymbol{Q}(\boldsymbol{f}_\infty))^{-1}\cdot\boldsymbol{R}^{\mathrm{T}}\cdot\boldsymbol{W}\cdot\boldsymbol{R}\cdot\hat{\boldsymbol{f}}$$

Iterative Reconstruction: Parameters

- Image/object representation
  - Pixel centers
  - Pixel area
  - Blobs
  - Sampling density (pixel size, pixel locations, …)

$$f(x,y)=\sum_m f_m b(x-x_m, y-y_m)$$

- Forward model (forward projection)
  - Joseph-type, Bresenham-type, distance-driven-type, …
  - Needle beam (infinitely thin ray), many needle beams per ray, …
  - Beam shape (varying beam cross-section, angular blurring, …)
  - Physical effects (beam hardening, scatter, motion, detector sensitivity, non-linear partial volume effect, …)
- Objective function, update equation
  - Statistical model (Gaussian, Poisson, shifted Poisson, …)
  - Regularisation (edge-preserving, …)
  - Artifact reduction

$$C(\boldsymbol{f})=\left(\boldsymbol{R}\cdot\boldsymbol{f}-\boldsymbol{p}\right)^2$$

- Inverse model (backprojection)
  - Transpose of forward model
  - Pixel-driven backprojection
  - Filtered backprojection
  - …

Image Representation

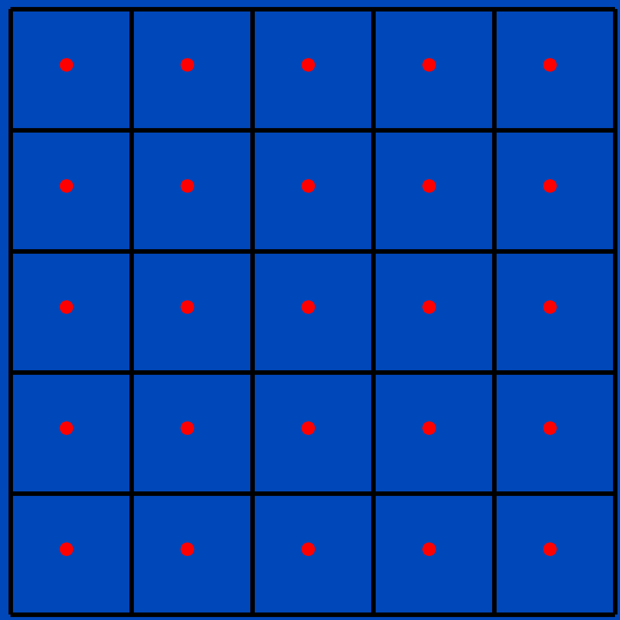

$$b(x,y) = \bullet$$

Image Representation

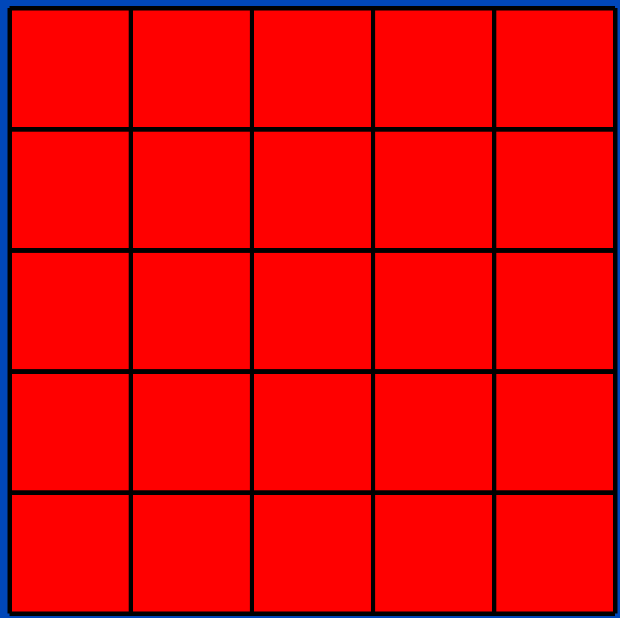

$b(x, y) =$ 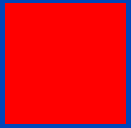

Image Representation

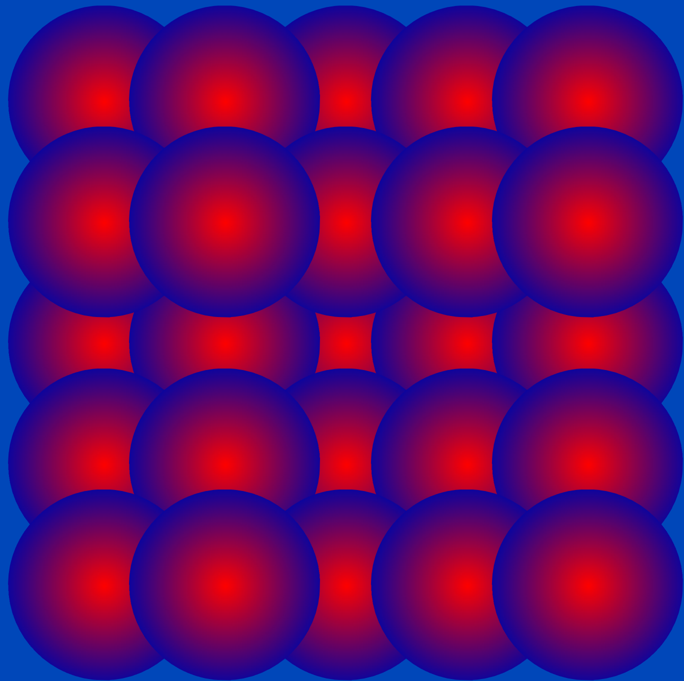

$b(x, y) =$ 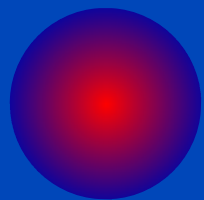

Forward Model: Beam Shape

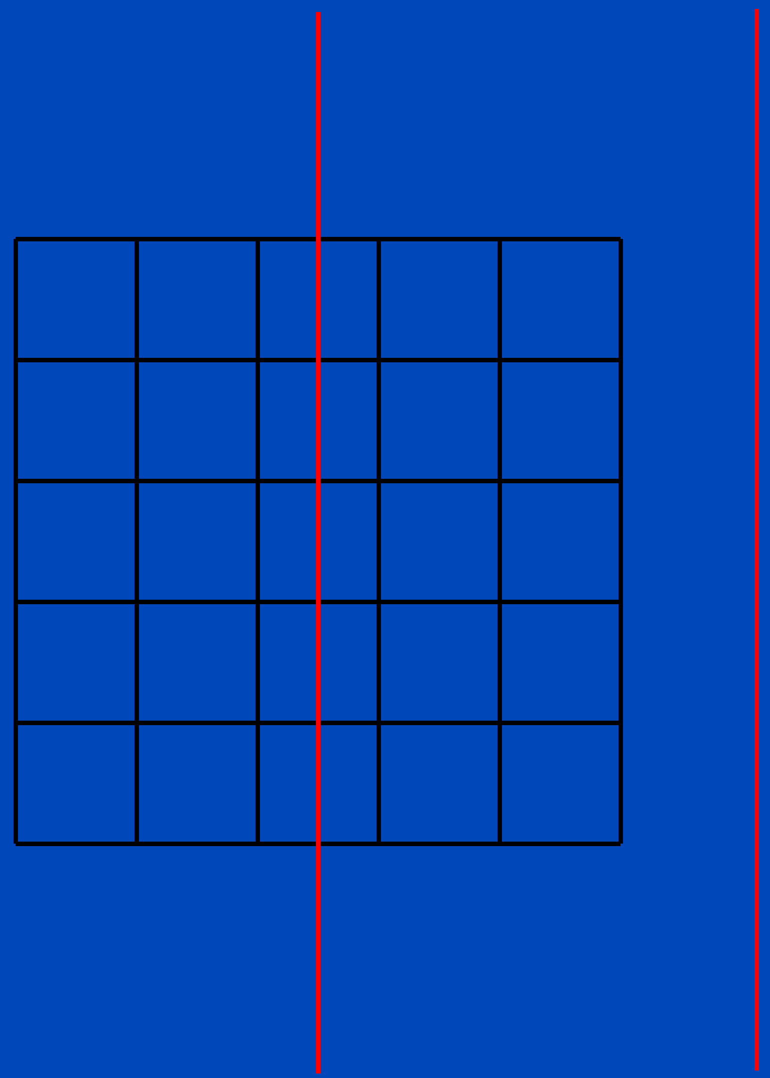

Forward Model: Beam Shape

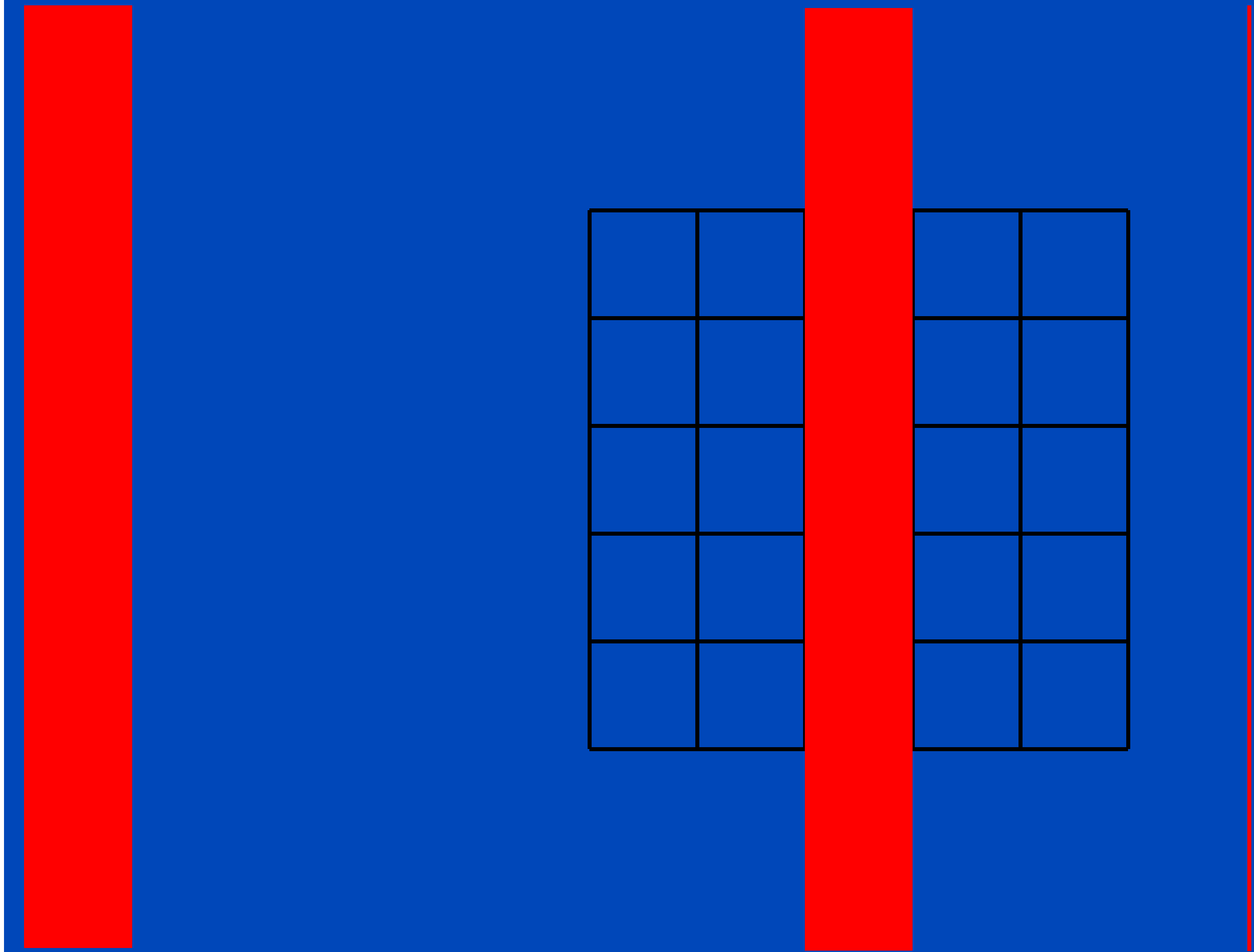

Forward Model: Beam Shape

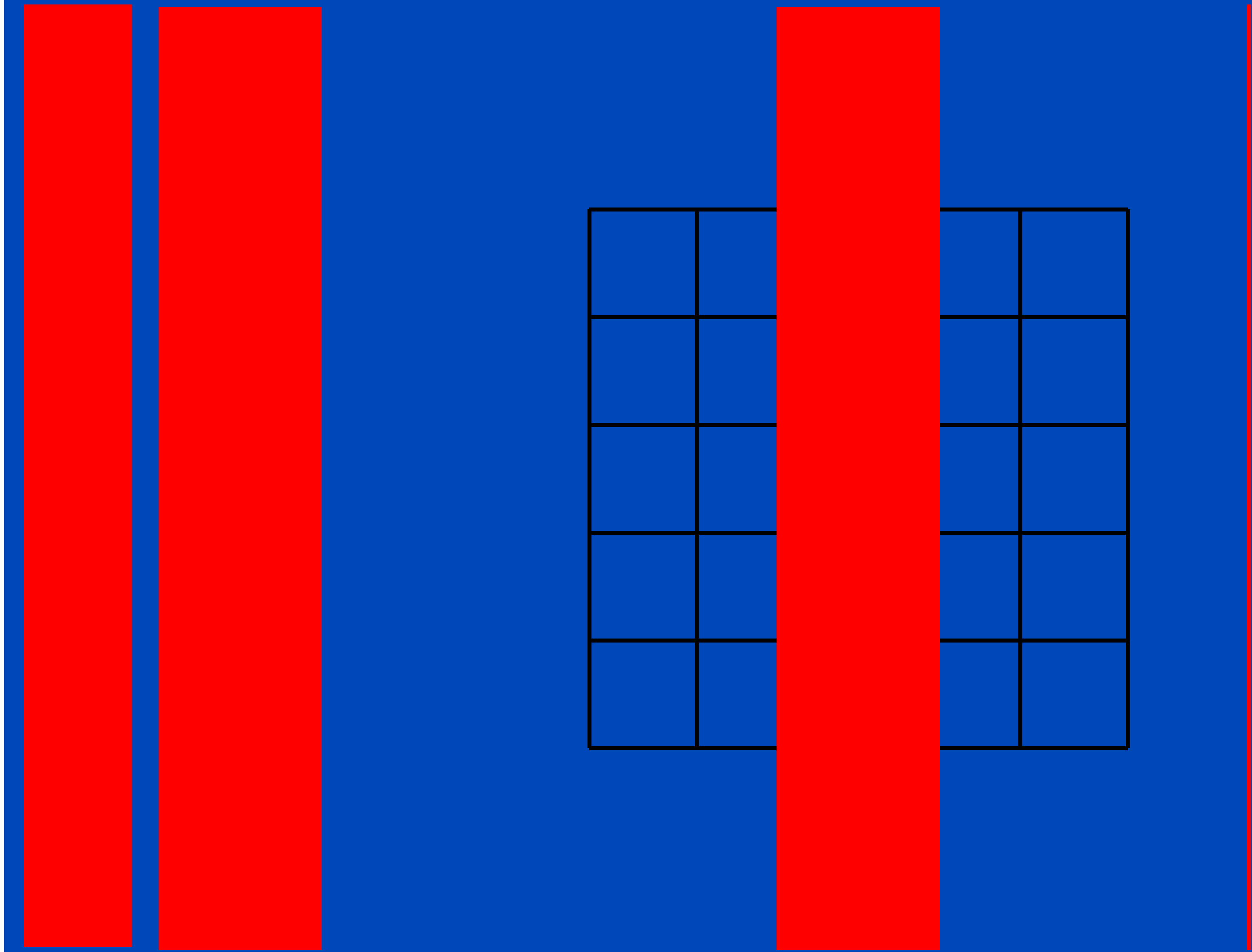

Forward Model: Beam Shape

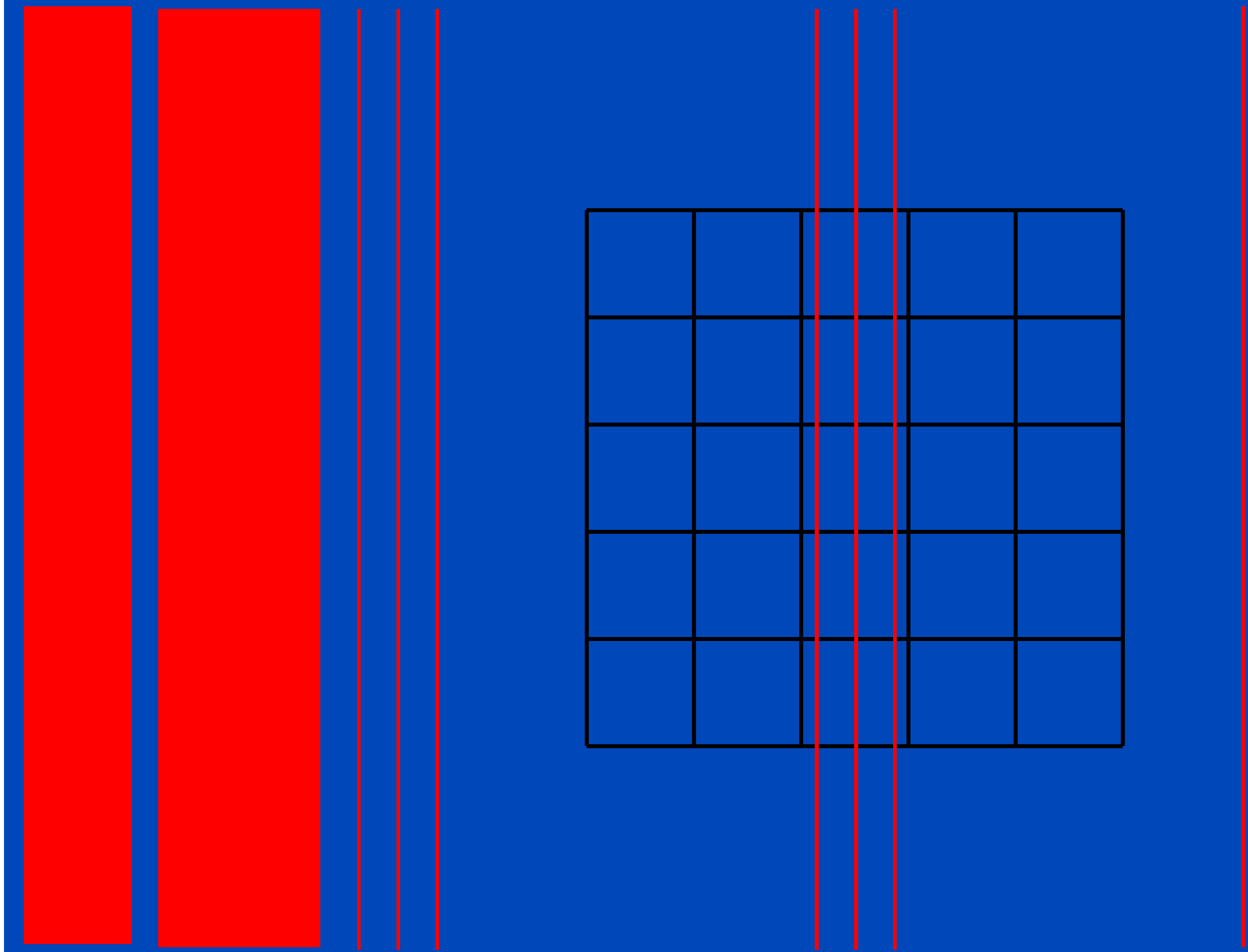

Forward Model: Beam Shape

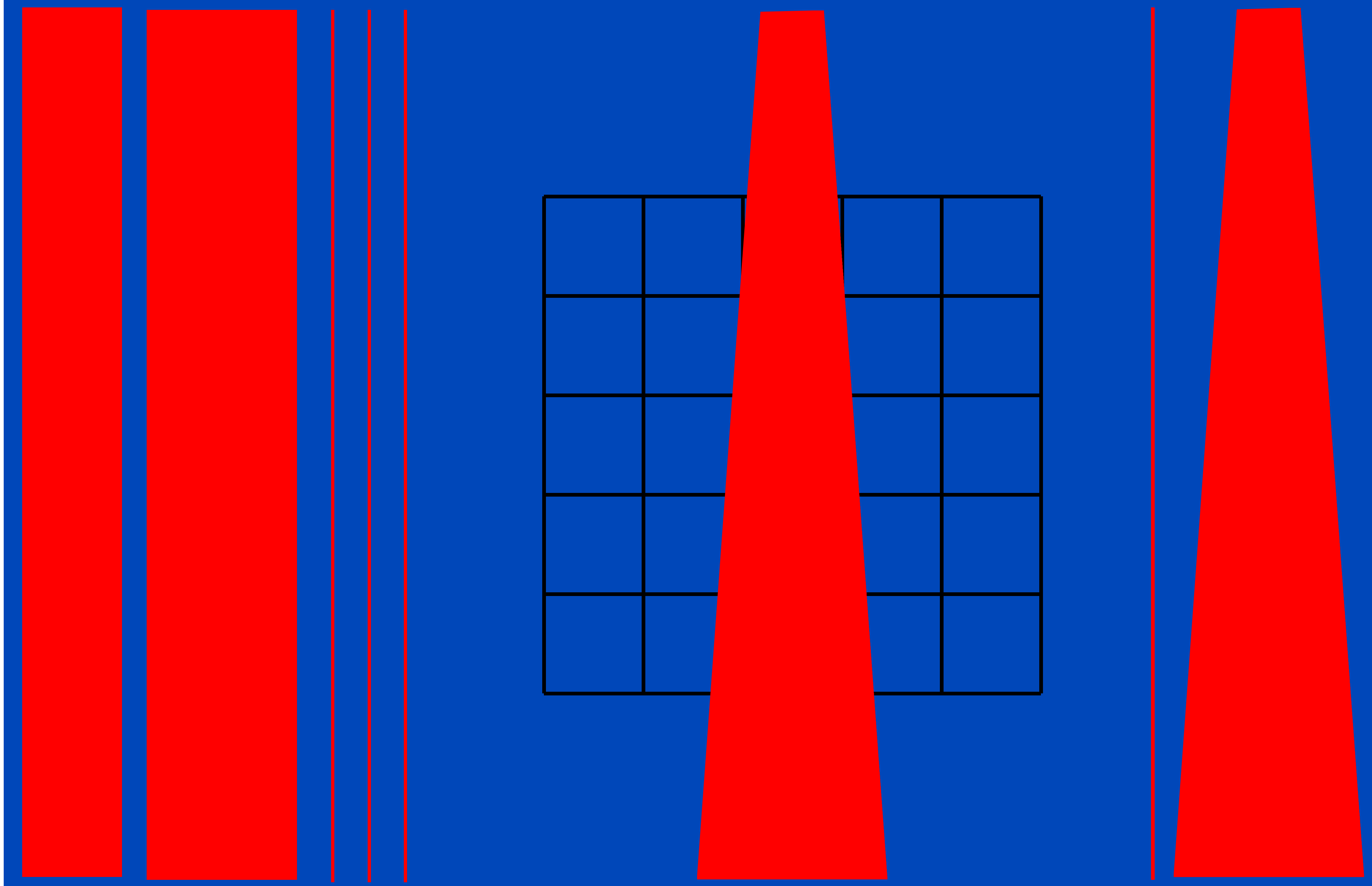

Forward Model: Beam Shape

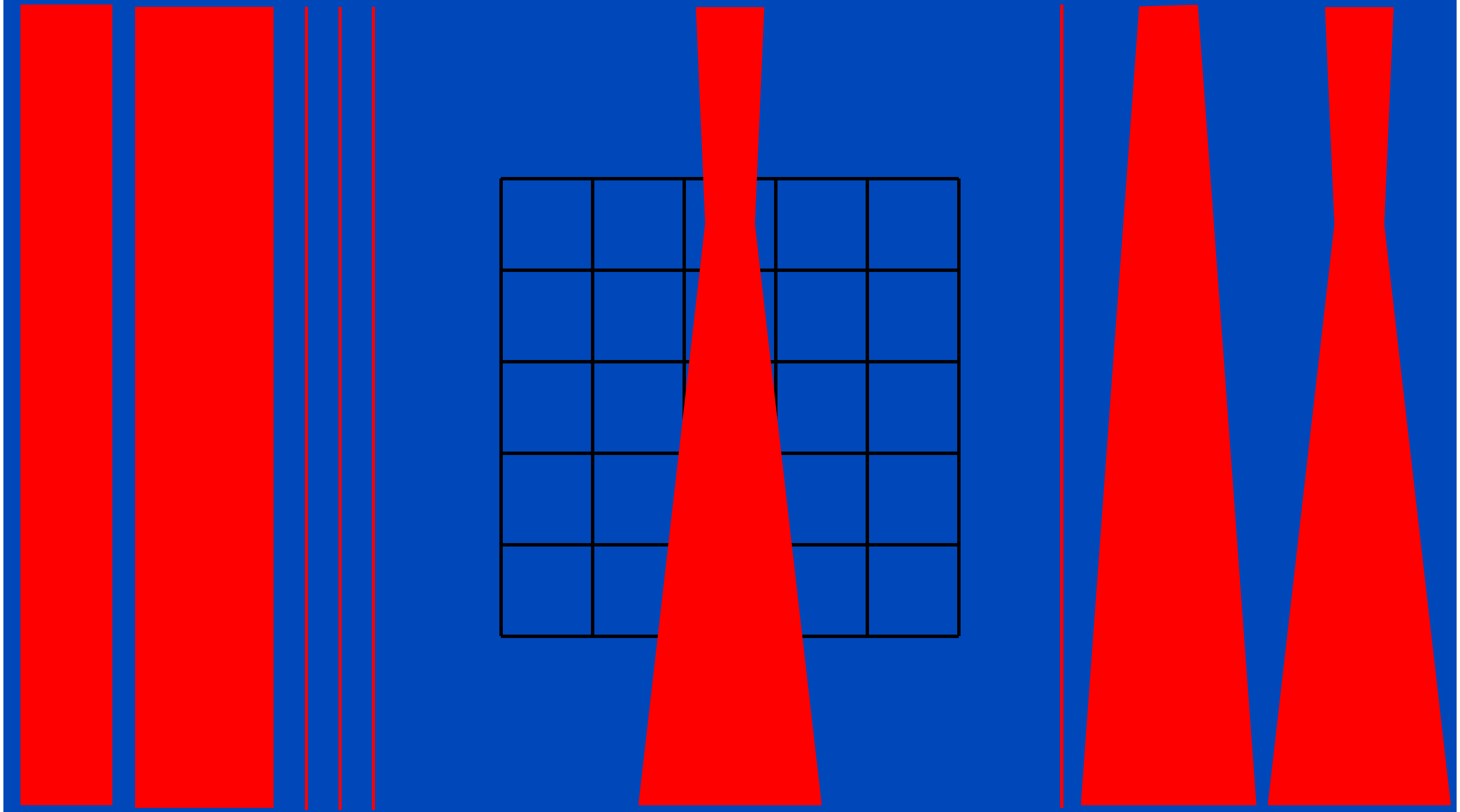

Image Representation and Forward Model are Linked!

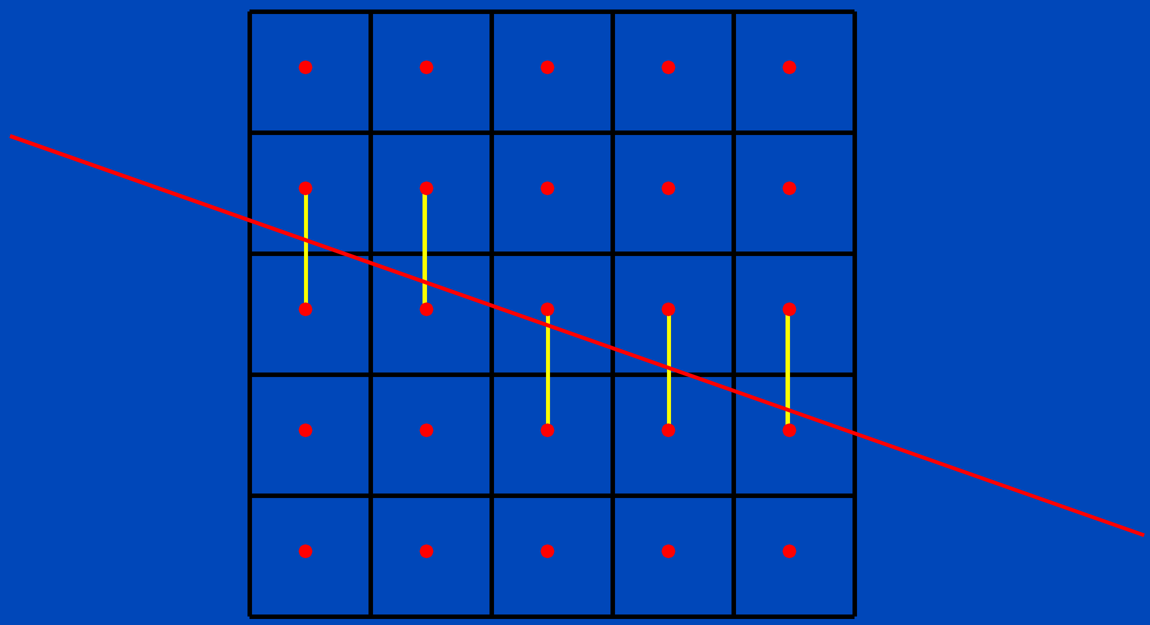

Joseph's forward projector

Objective Function: Gauß Model

- **Assume that the attenuation is Gaussian-distributed**

$$\mathcal{L}(A) = \mathcal{N}(\sigma, \boldsymbol{r} \cdot \boldsymbol{f})$$

i.e. $P(A = a) = \frac{1}{\sqrt{2\pi}\sigma} e^{-\frac{1}{2}(a-\mu)^2/\sigma^2}$ **with** $\mu = \boldsymbol{r} \cdot \boldsymbol{f}$ **.**

- **Consequently, the likelihood for all *N* measured signals is (** $\mu_n = \boldsymbol{r}_n \cdot \boldsymbol{f}$ **):**

$$P(\boldsymbol{A} = \boldsymbol{a}, \boldsymbol{f}) = \prod_n P(A_n = a_n)$$

- **Before maximizing take the log, penalize roughness,**

$$L(\boldsymbol{f}) = -\sum_n \left(\frac{a_n - \mu_n}{\sigma_n} \right)^2 - \beta R(\boldsymbol{f})$$

and then find the image *f* that maximizes *L*.

- **This leads us to minimizing**

$$(\boldsymbol{R}\cdot\boldsymbol{f}-\boldsymbol{a})^{\mathrm{T}}\cdot\boldsymbol{D}\cdot(\boldsymbol{R}\cdot\boldsymbol{f}-\boldsymbol{a})$$

  which means solving

$$\boldsymbol{R}^{\mathrm{T}}\cdot\boldsymbol{D}\cdot(\boldsymbol{R}\cdot\boldsymbol{f}-\boldsymbol{a})=\boldsymbol{0}$$

- **This must be done numerically (e.g. Jacobi method) and the solutions are often of type**

$$\boldsymbol{f}_{\nu+1}=\boldsymbol{f}_{\nu}+\mathrm{diag}(\boldsymbol{u})\cdot\boldsymbol{R}^{\mathrm{T}}\cdot\mathrm{diag}(\boldsymbol{v})\cdot(\boldsymbol{a}-\boldsymbol{R}\cdot\boldsymbol{f}_{\nu})$$

Update Equation: Gauß Model

- **ART** $$f_{\nu+1} = f_\nu + R^{\mathrm{T}} \cdot \frac{p - R \cdot f_\nu}{R^2 \cdot 1}$$
- **SART** $$f_{\nu+1} = f_\nu + \frac{1}{R^{\mathrm{T}} \cdot 1} R^{\mathrm{T}} \cdot \frac{p - R \cdot f_\nu}{R \cdot 1}$$
- **and many more …**

Objective Function: Poisson Model

- **Assume that the intensities are Poisson-distributed**

$$\mathcal{L}(I) = \mathcal{P}(I_0 e^{-\boldsymbol{r} \cdot \boldsymbol{f}})$$

which means $P(I = i) = \frac{\mu^i}{i!} e^{-\mu}$ **with** $\mu = I_0 e^{-\boldsymbol{r} \cdot \boldsymbol{f}}$ **.**

- **Consequently, the likelihood for all *N* measured signals is (** $\mu_n = I_0 e^{-\boldsymbol{r}_n \cdot \boldsymbol{f}}$ **):**

$$P(\boldsymbol{I} = \boldsymbol{i}, \boldsymbol{f}) = \prod_n P(I_n = i_n) = \prod_n \frac{\mu_n^{i_n}}{i_n!} e^{-\mu_n}$$

- **Before maximizing take the log, penalize roughness,**

$$L(\boldsymbol{f}) = \sum_n (i_n \ln \mu_n - \mu_n) - \beta R(\boldsymbol{f})$$

and then find the image *f* that maximizes *L*.

Update Equation: Poisson Model

- **MLEM** $$f_{\nu+1} = f_\nu \frac{\boldsymbol{R}^{\mathrm{T}} \cdot \left(e^{-\boldsymbol{R}\cdot\boldsymbol{f}_\nu}\right)}{\boldsymbol{R}^{\mathrm{T}} \cdot \left(e^{-\boldsymbol{p}}\right)}$$

- **OSC** $$f_{\nu+1} = f_\nu + f_\nu \frac{\boldsymbol{R}^{\mathrm{T}} \cdot \left(e^{-\boldsymbol{R}\cdot\boldsymbol{f}_\nu} - e^{-\boldsymbol{p}}\right)}{\boldsymbol{R}^{\mathrm{T}} \cdot \left(e^{-\boldsymbol{R}\cdot\boldsymbol{f}_\nu}\boldsymbol{R}\cdot\boldsymbol{f}_\nu\right)}$$

- **and many more …**

Native OSC Converges Slowly

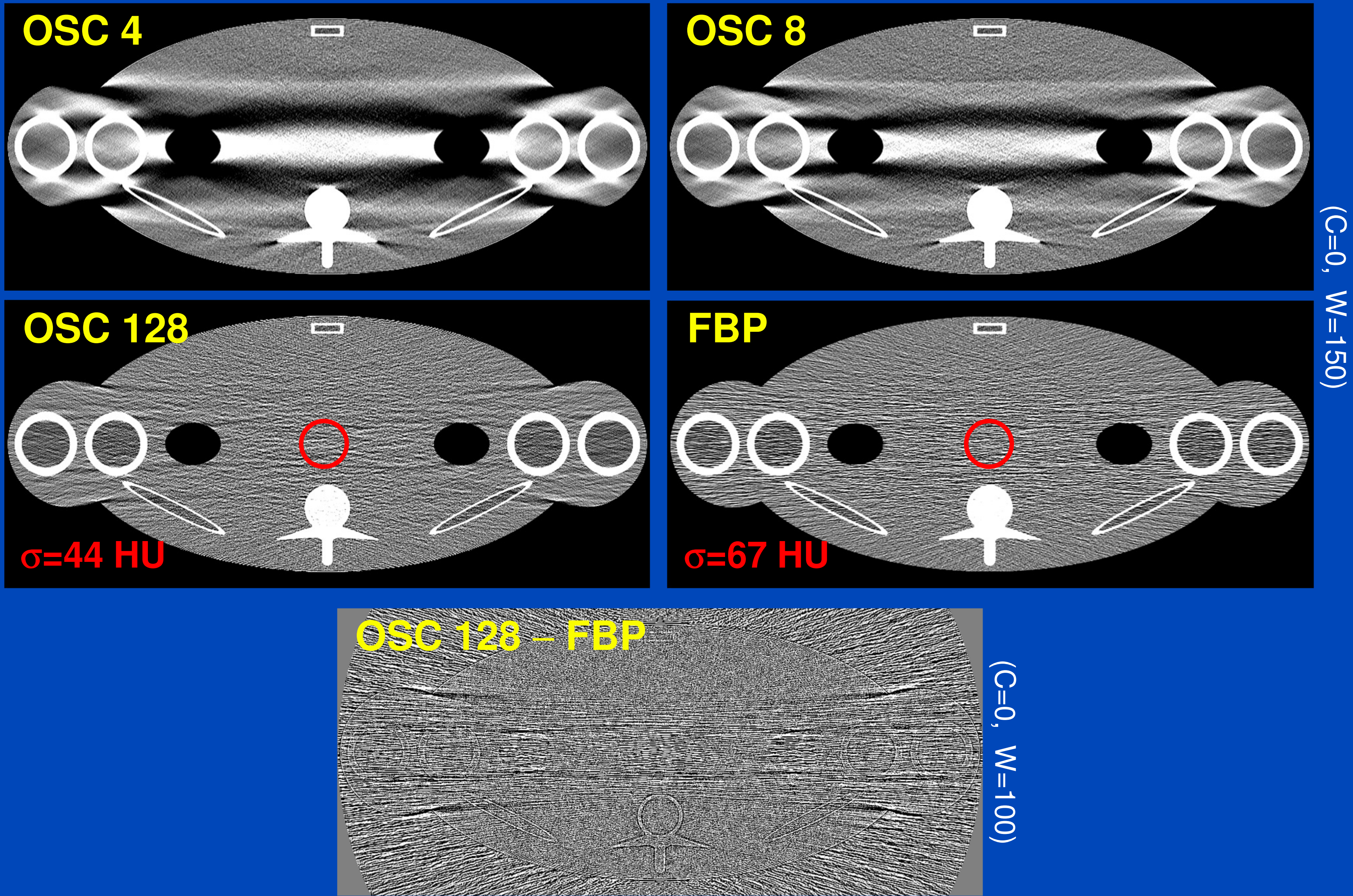

Proper Initialization Helps!

OSC 4, initialized with constant value	OSC 4, initialized with matched FBP	OSC 4, initialized with smooth FBP

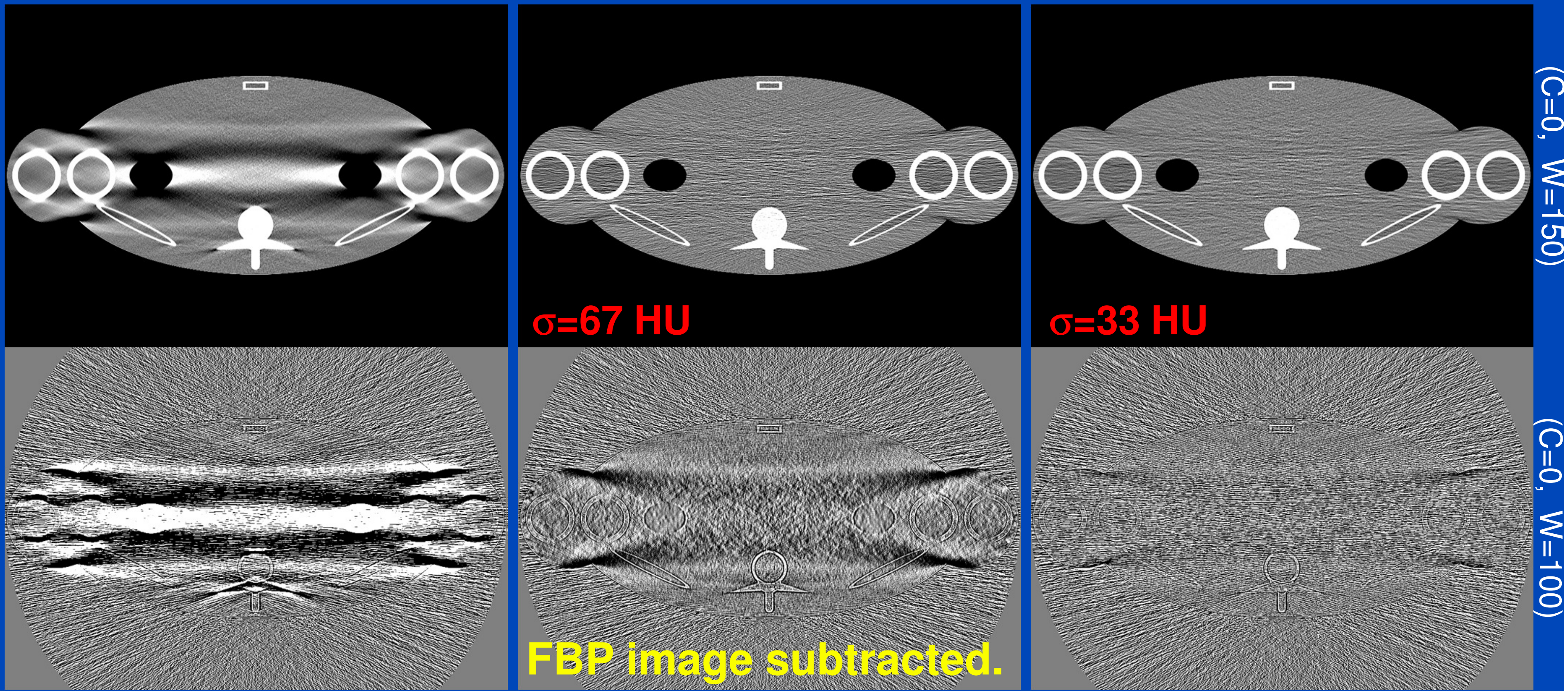

Insufficient image quality	Same noise as FBP	50% less noise than FBP

What Makes Iterative Recon Attractive?

- No need to come find an analytical solution
- Works for all geometries with only small adaptations
- Allows to model any effect
- Allows to incorporate prior knowledge
  - noise properties (quantum noise, electronic noise, noise texture, …)
  - prior scans (e.g. planning CT, full scan data, …)
  - image properties such as smoothness, edges (e.g. minimum TV)
  - …
- Handles missing data implicitly (but not necessarily better)

Phase-correlated Feldkamp

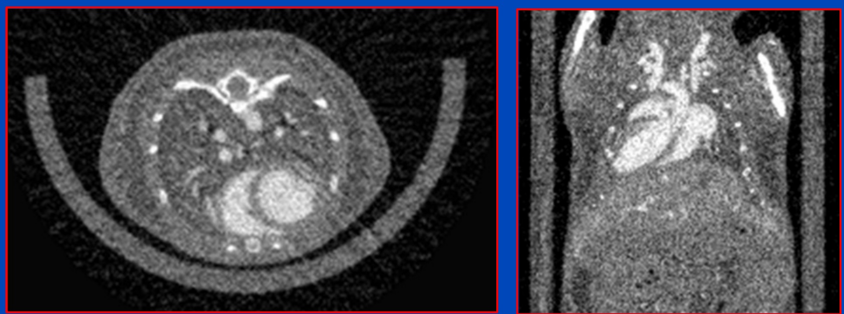

High dimensional TV minimization[1]

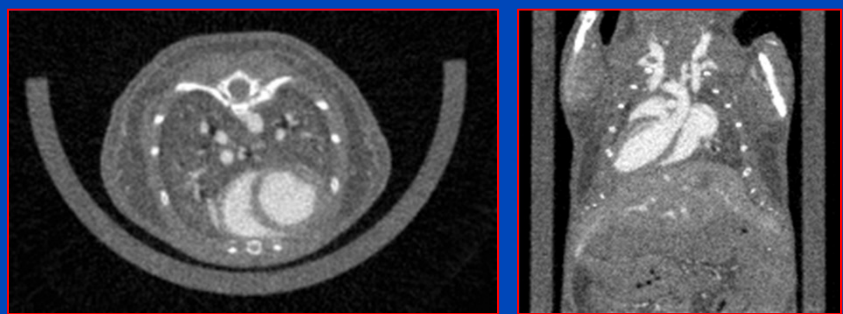

[1]L. Ritschl, S. Sawall, M. Knaup, A. Hess, and M. Kachelrieß, Phys. Med. Biol. 57, Jan. 2012

Downsides

- Classical iterative recon is slow!
- Classical iterative recon cannot do small FOVs.
- There are many open parameters.
- The reconstruction is non-linear.
- Can we trust the images?

Ordered Subsets

- Divide one iteration into *S* sub-iterations.
- Each of these *S* subsets covers *N*/*S* projections.
- During one iteration all subsets and therefore all projections are used exactly once.
- Per iteration the volume is updated *S* times (once per sub-iteration).
- An up to *S*-fold speed-up can be observed.

Ordered Subsets
Illustration for $N = 32$ Projections

Conventional procedure without subets ($S = 1$)

0 1 2 3 4 5 6 7 8 9 10 11 12 13 14 15 16 17 18 19 20 21 22 23 24 25 26 27 28 29 30 31

Ordered subsets with $S = 8$ sub-iterations

0 1 2 3 4 5 6 7 8 9 10 11 12 13 14 15 16 17 18 19 20 21 22 23 24 25 26 27 28 29 30 31

Ordered Subsets

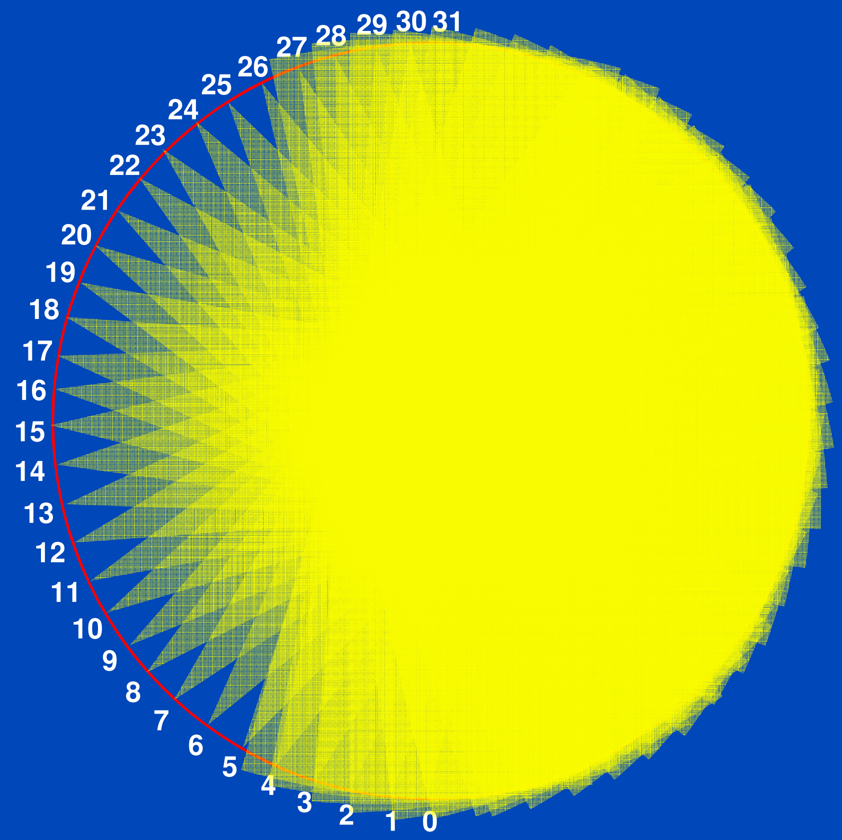

$N_{Projections} = 32$, Ordered Subsets: $N_{Subsets} = 8$

dkfz.

Sequence Can be Generated Using Simple Bit Reversal

0	->	0
1	->	16
2	->	8
3	->	24
4	->	4
5	->	20
6	->	12
7	->	28
8	->	2
9	->	18
10	->	10
11	->	26
12	->	6
13	->	22
14	->	14
15	->	30
16	->	1
17	->	17
18	->	9
19	->	25
20	->	5
21	->	21
22	->	13
23	->	29
24	->	3
25	->	19
26	->	11
27	->	27
28	->	7
29	->	23
30	->	15
31	->	31

Using Ordered Subsets Makes it Faster!

S = 1 (no subsets) | *S* = 32 (ordered subsets)

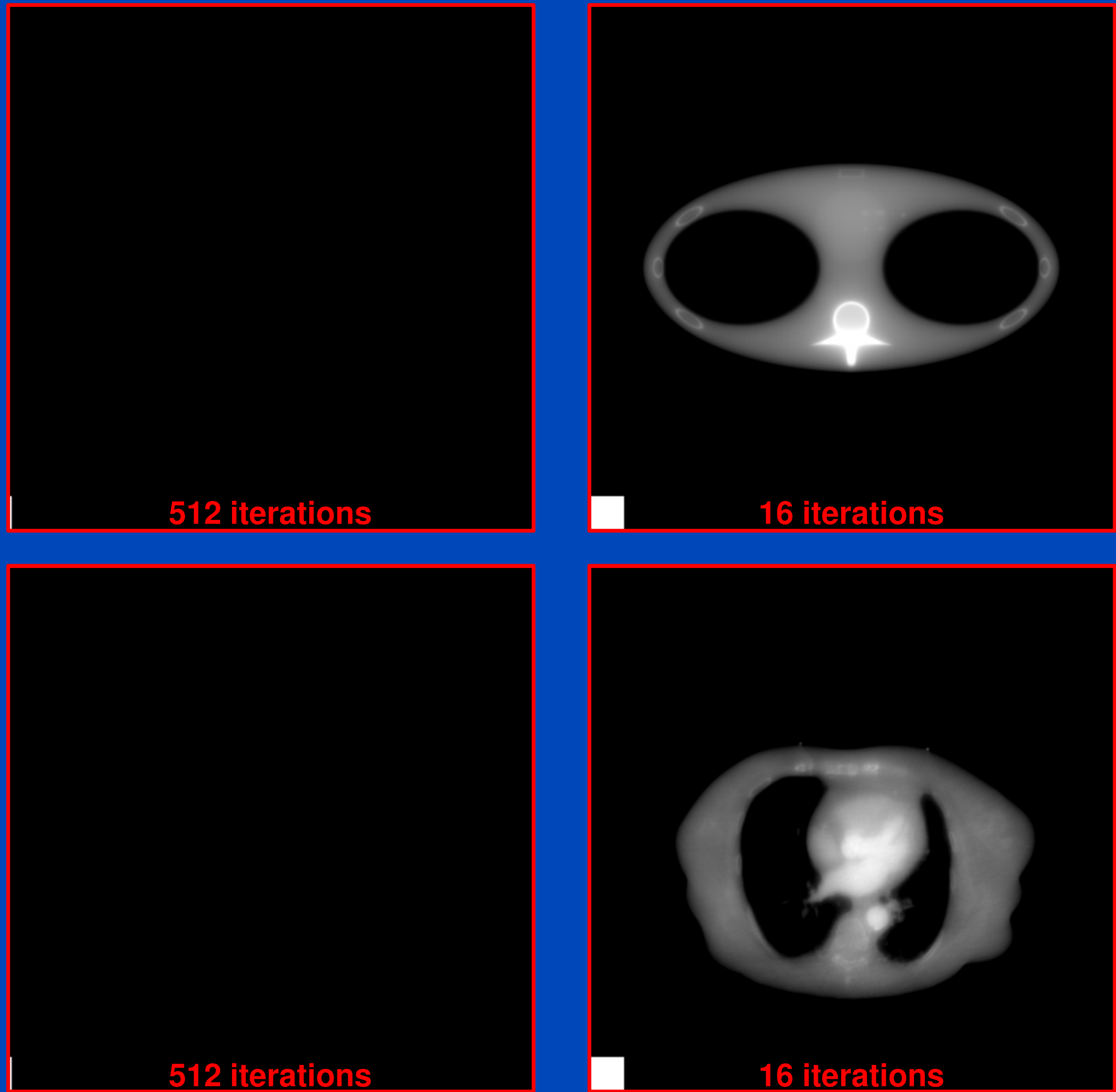

C = 0 HU, W = 1000 HU

Image Updates

S = 1 (no subsets) S = 32 (ordered subsets)

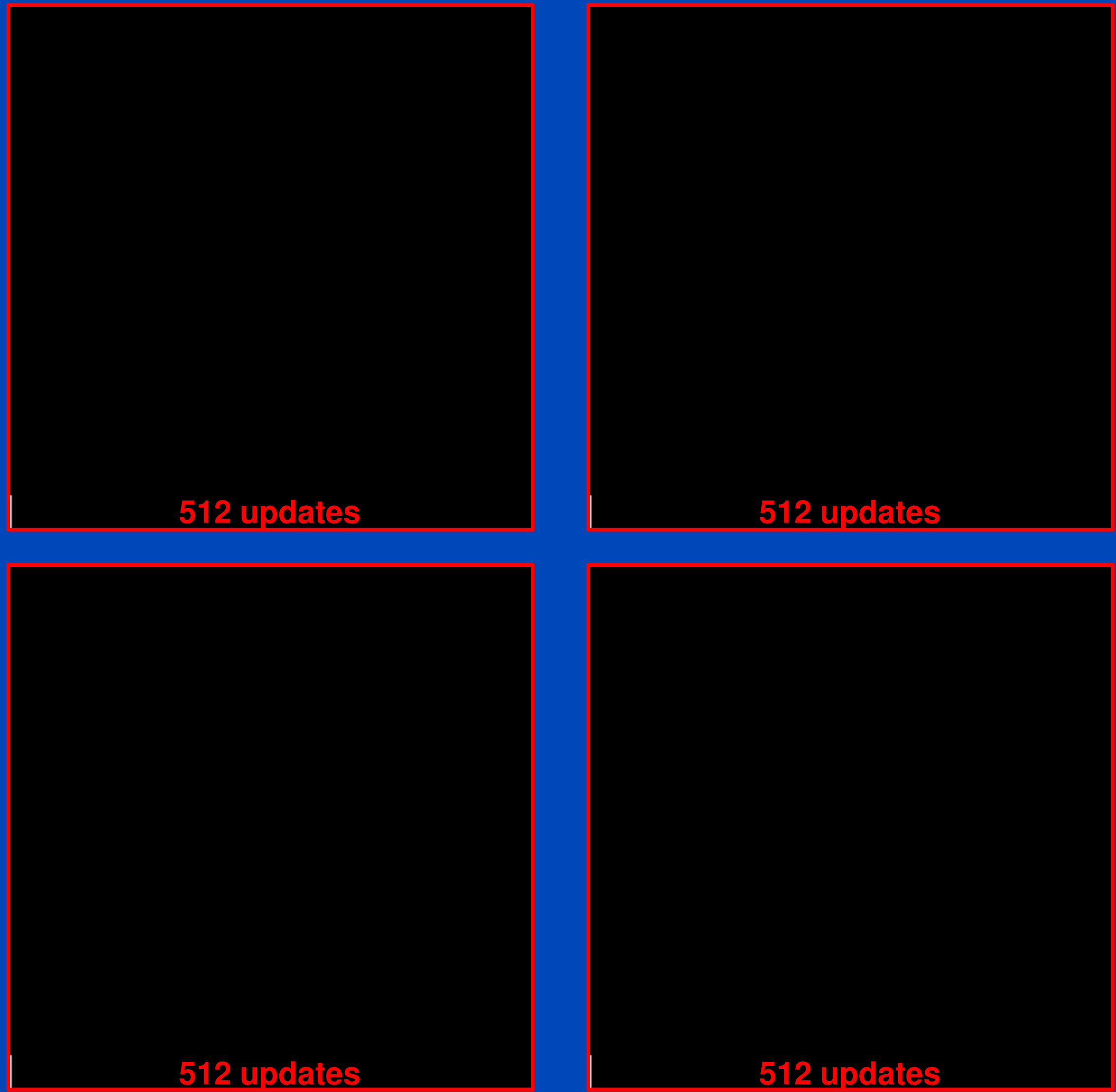

C = 0 HU, W = 1000 HU

Analytical Reconstruction

1. Problem

$$p(\vartheta,\xi) = \int dx dy\, f(x,y)\delta(x\cos\vartheta + y\sin\vartheta - \xi)$$

2. Solution

$$f(x,y) = \int_0^\pi d\vartheta\, p(\vartheta,\xi) * k(\xi)\Big|_{\xi = x\cos\vartheta + y\sin\vartheta}$$

3. Discretisation

$$\boldsymbol{f} = \boldsymbol{R}^{\mathrm{T}} \cdot \boldsymbol{K} \cdot \boldsymbol{p} = \boldsymbol{R}^{\mathrm{T}} \cdot (\boldsymbol{k} * \boldsymbol{p})$$

Classical Iterative Reconstruction

1. Problem

$$p(\vartheta,\xi) = \int dx dy\, f(x,y)\delta(x\cos\vartheta + y\sin\vartheta - \xi)$$

2. Discretisation

$$\boldsymbol{p} = \boldsymbol{R} \cdot \boldsymbol{f}$$

3. Update equation

$$\boldsymbol{f}_{\nu+1} = \boldsymbol{f}_\nu + \boldsymbol{R}^{\mathrm{T}} \cdot \frac{\boldsymbol{p} - \boldsymbol{R} \cdot \boldsymbol{f}_\nu}{\boldsymbol{R}^2 \cdot \boldsymbol{1}}$$

Iterative Image Reconstruction in CT

- Sinogram- and image restoration (not truly iterative)
- Fully iterative (GE‘s Veo/MBIR only, but very slow, now being replaced by ASIR-V)
- Hybrid technologies (only one or two full iterations, including preconditioning) are the way to go.
- Compressed sensing type image reconstruction is not used commercially.

Iterative != Iterative

- **In many cases artifact correction is iterative**
  - **Higher order beam hardening correction**
  - **Cone-beam artifact correction**
  - **Scatter correction**
- **Practical “iterative reconstruction” approaches**
  - **often use empirical solutions**
  - **combine iterative with analytical reconstruction**
  - **combine iterative or analytical reconstruction with image restoration**

Phase-correlated Feldkamp

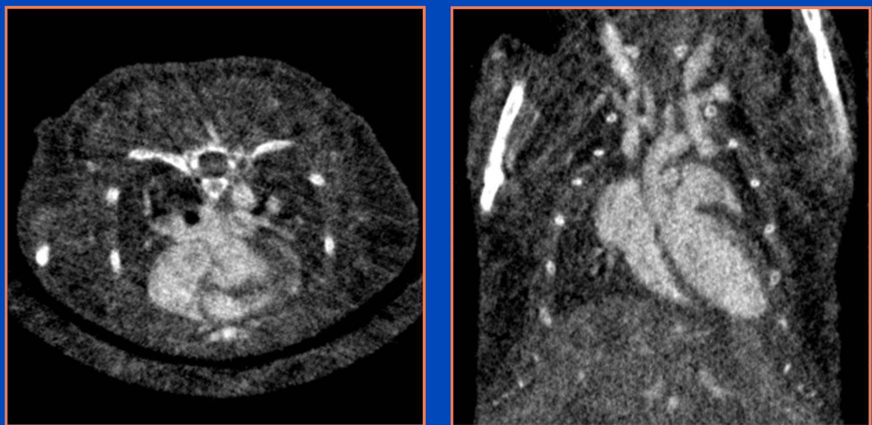

Low dose phase-correlated (LDPC) recon[1]

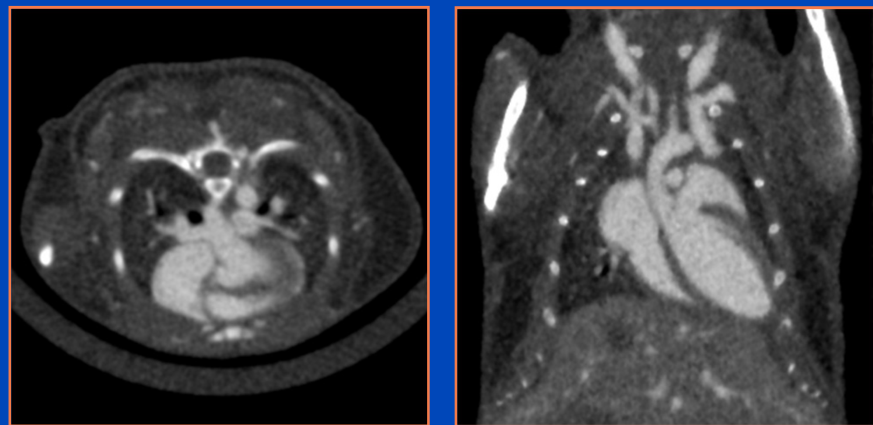

[1] S. Sawall, F. Bergner, R. Lapp, M. Mronz, A. Hess, and M. Kachelrieß, MedPhys 38(3), 2011

Iterative Reconstruction

- Aim: less artifacts, lower noise, lower dose
- Iterative reconstruction
  - Reconstruct an image.
  - Regularize the image.
  - Does the image correspond to the rawdata?
  - If not, reconstruct a correction image and continue.
- SPECT + PET are iterative for a long time!
- CT product implementations
  - AIDR (adaptive iterative dose reduction, Toshiba)
  - ASIR (adaptive statistical iterative reconstruction, GE)
  - iDose (Philips)
  - IMR (iterative model reconstruction, Philips)
  - IRIS (image reconstruction in image space, Siemens)
  - VEO, MBIR (model-based iterative reconstruction, GE)
  - SAFIRE, ADMIRE (advanced model-based iterative reconstruction, Siemens)

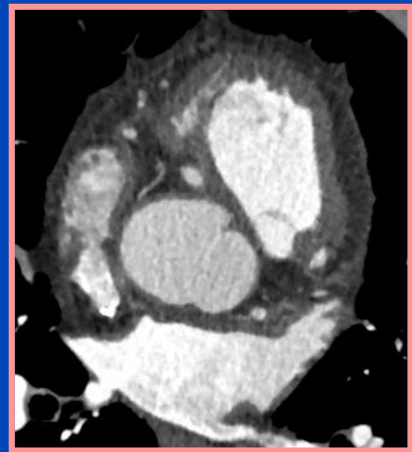

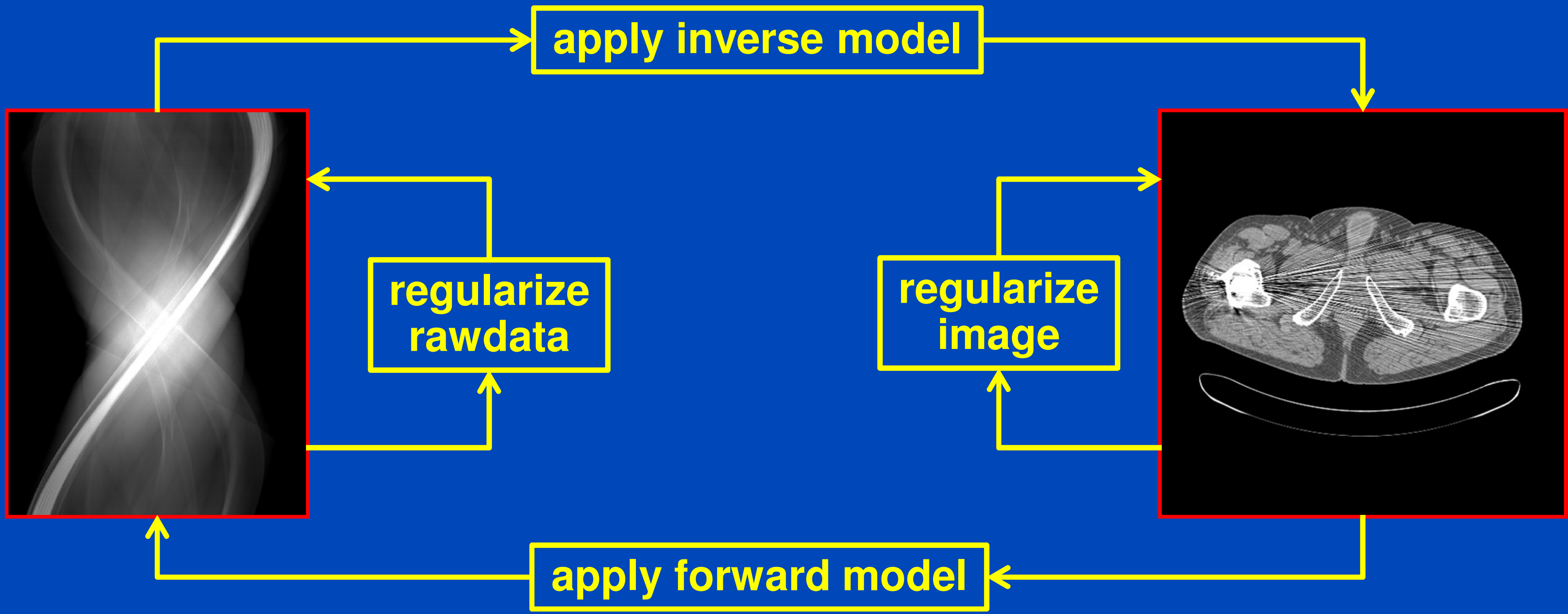

- Rawdata regularization: adaptive filtering[1], precorrections, filtering of update sinograms...
- Inverse model: backprojection (R^T) or filtered backprojection (R^{-1}). In clinical CT, where the data are of high fidelity and nearly complete, one would prefer filtered backprojection to increase convergence speed.
- Image regularization: edge-preserving filtering. It may model physical noise effects (amplitude, direction, correlations, …). It may reduce noise while preserving edges. It may include empirical corrections.
- Forward model (R_{phys}): Models physical effects. It can reduce beam hardening artifacts, scatter artifacts, cone-beam artifacts, noise, …

[1] M. Kachelrieß et al., Generalized Multi-Dimensional Adaptive Filtering, MedPhys 28(4), 2001

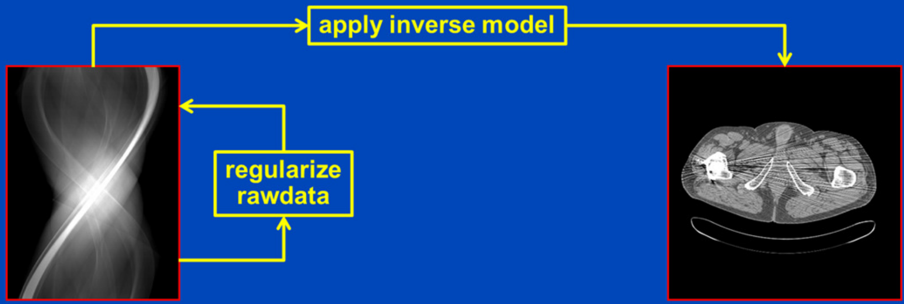

Conventional FBP with rawdata denoising (all vendors)

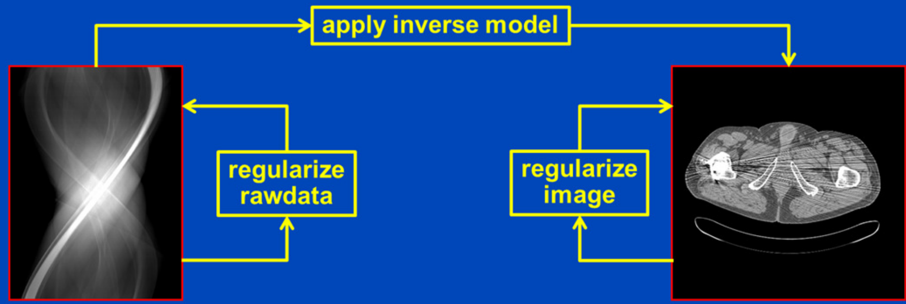

ASIR (Ge), AIDR3D (Toshiba), IRIS (Siemens), iDose (Philips)
SnapShot Freeze (GE), iTRIM (Siemens)

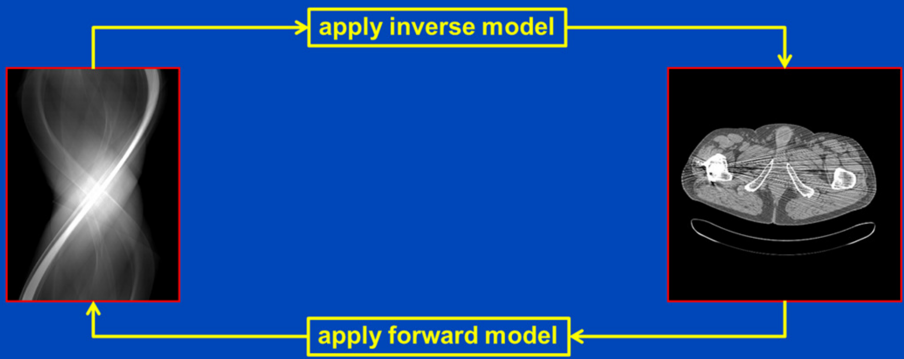

Veo/MBIR (Ge)

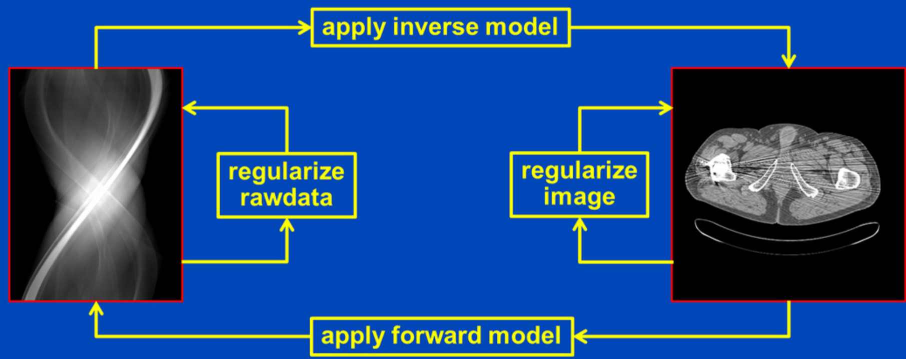

SAFIRE, ADMIRE (Siemens)

Plain FBP	Siemens Standard	IRIS VA34	SAFIRE VA40

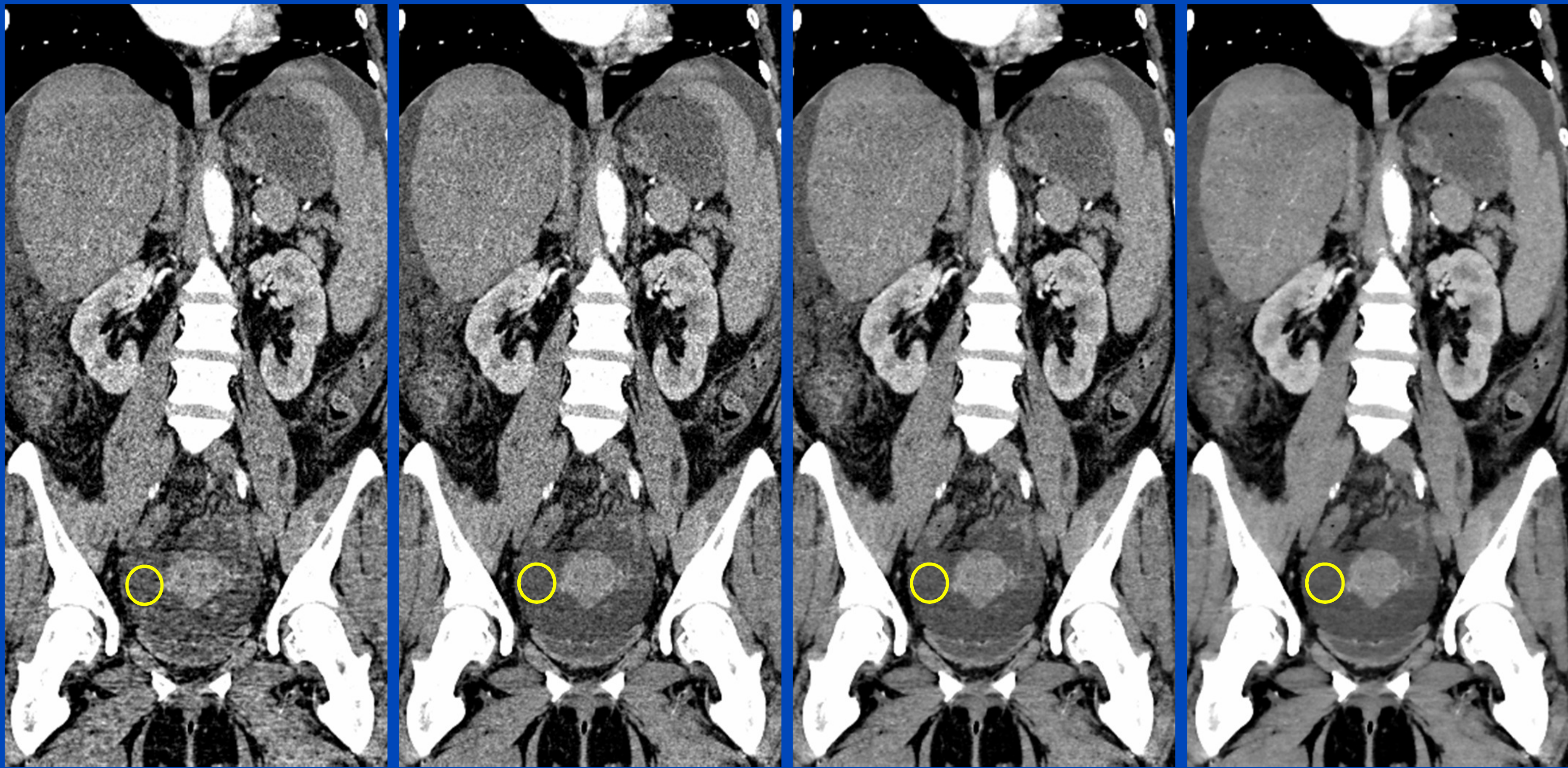

σ = 26.8 HU	σ = 17.6 HU	σ = 12.3 HU	σ = 7.8 HU

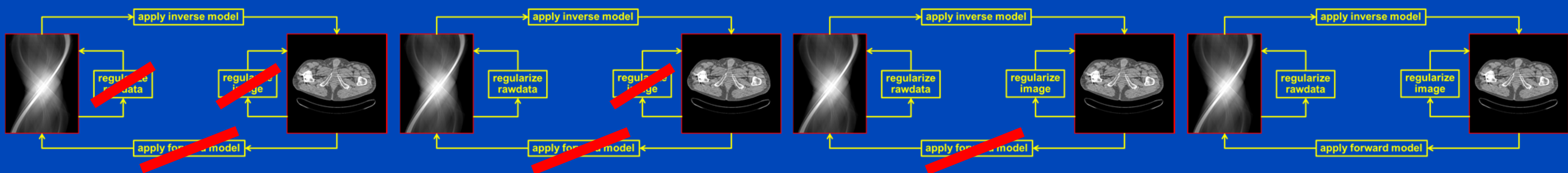

CT images provided by Siemens Healthcare, Forchheim, Germany

dkfz.

FBP ASIR Veo

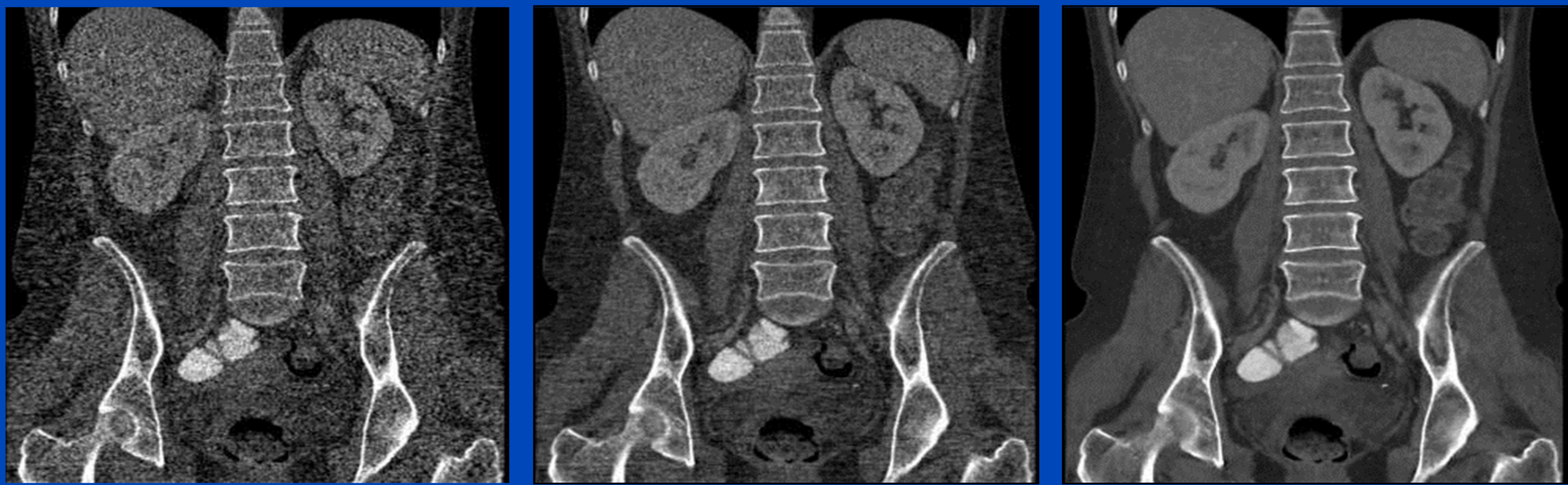

Courtesy of Dr. Jiang Hsieh, GE Healthcare Technologies, WI, USA.

Dose reduction values iterative compared to analytical image reconstruction claimed by clinical papers 2012 and earlier.

		GE		Philips		Siemens		Toshiba	
Type	Reference	ASIR	MBIR/Veo	iDose	IMR	IRIS	SAFIRE	AIDR	AIDR3D
Cardiac	[33]					38%*			
Cardiac	[36]						≥ 50%		
Cardiac	[37]						56%		
Cardiac	[29]			55%					
Cardiac	[25]	30%-45%*							
Cardiac	[20]	27%							
Cardiac	[38]						≥ 50%		
Cardiac	[34]					40%-51%			
Cardiac	[30]			52%*					
Cardiac	[35]					62%			
Cardiac	[45]							22%	
Cardiac	[39]						50%		
Cardiac	[46]								50%
Cardiac	[21]	23%	60%						
Cardiac	[22]	29%							
Cardiac	[23]	36%							
Cardiac	[28]			29%					
Abdominal/Chest	[79]	32%-65%							
Abdominal/Chest	[80]	15%*							
Abdominal/Chest	[81]			42%					
Abdominal/Chest	[82]	80%-90%							
Abdominal/Chest	[83]					36%*			
Abdominal/Chest	[77]	38%-46%							
Abdominal/Chest	[40]						≥ 50%		
Abdominal/Chest	[84]	≥30%							
Abdominal/Chest	[85]								64%
Abdominal/Chest	[86]	50%							
Abdominal/Chest	[87]							52%	
Abdominal/Chest	[88]	28%							
Abdominal/Chest	[24]	50%							
Abdominal/Chest	[89]					35%			
Abdominal/Chest	[90]			20%-80%*					
Abdominal/Chest	[91]	23%-66%							
Abdominal/Chest	[92]					40%			
Abdominal/Chest	[93]					50%			
Abdominal/Chest	[94]					50%			
Abdominal/Chest	[95]	34%							
Abdominal/Chest	[96]	41%							
Abdominal/Chest	[97]	25%							
Abdominal/Chest	[98]	38%							
Abdominal/Chest	[27]		75%						
Head	[99]					20%			
Head	[100]					60%			
Head	[101]	31%							
Head	[102]	26%							
REVIEW (Cardiac)	[17]	40%-50%	60%-70%				40%-50%		
REVIEW (General)	[16]	23%-76%		50%-76%		20%-60%	50%		52%
REVIEW (Cardiac)	[18]	40%		30%-40%					

M. Kachelrieß, Current Cardiovascular Imaging Reports 6:268–281, 2013.

Motion Management for IGRT

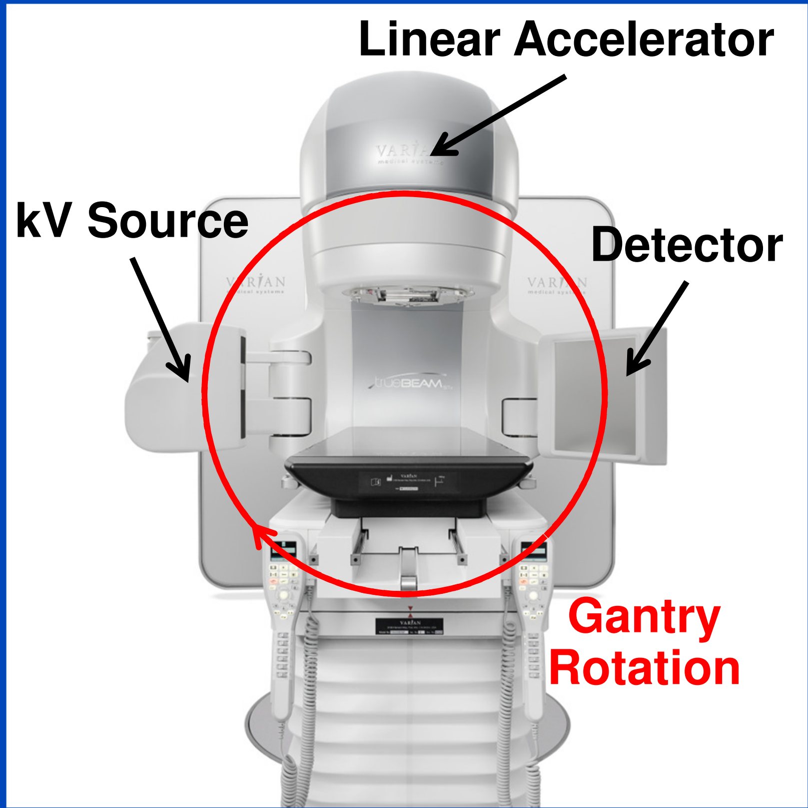

Retrospective Gating

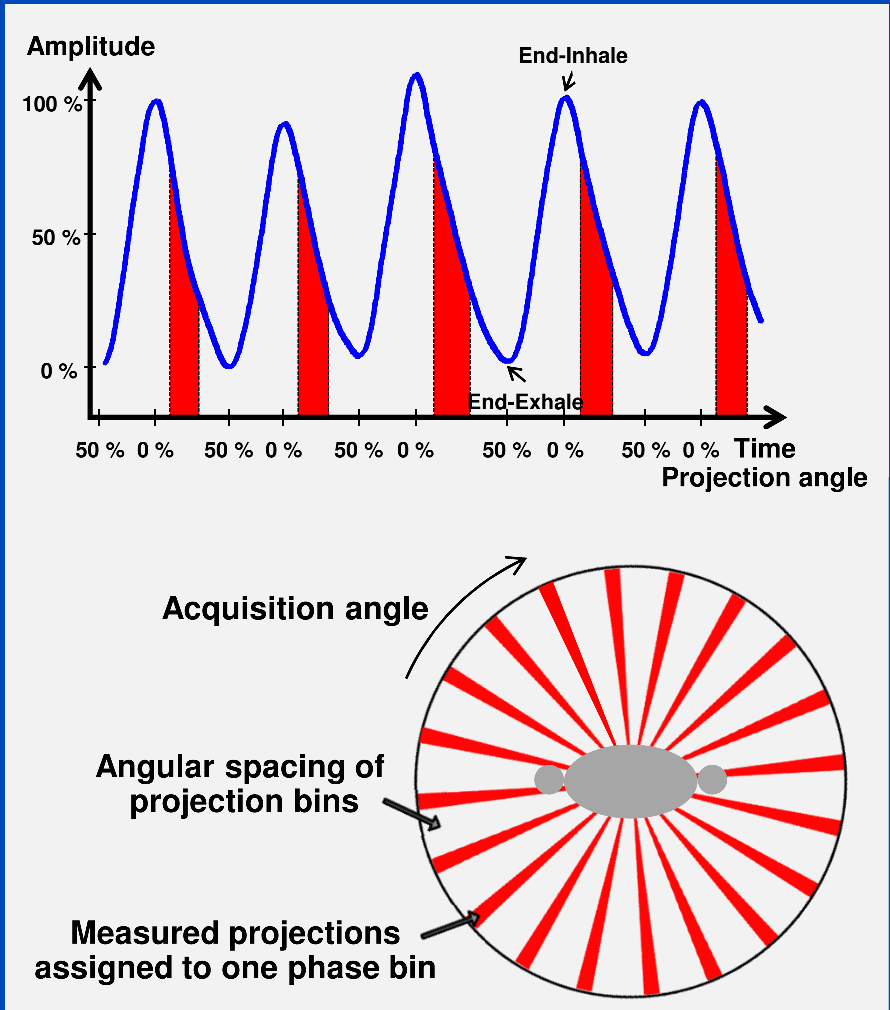

Without gating (3D): Motion artifacts

With gating (4D): Sparse-view artifacts

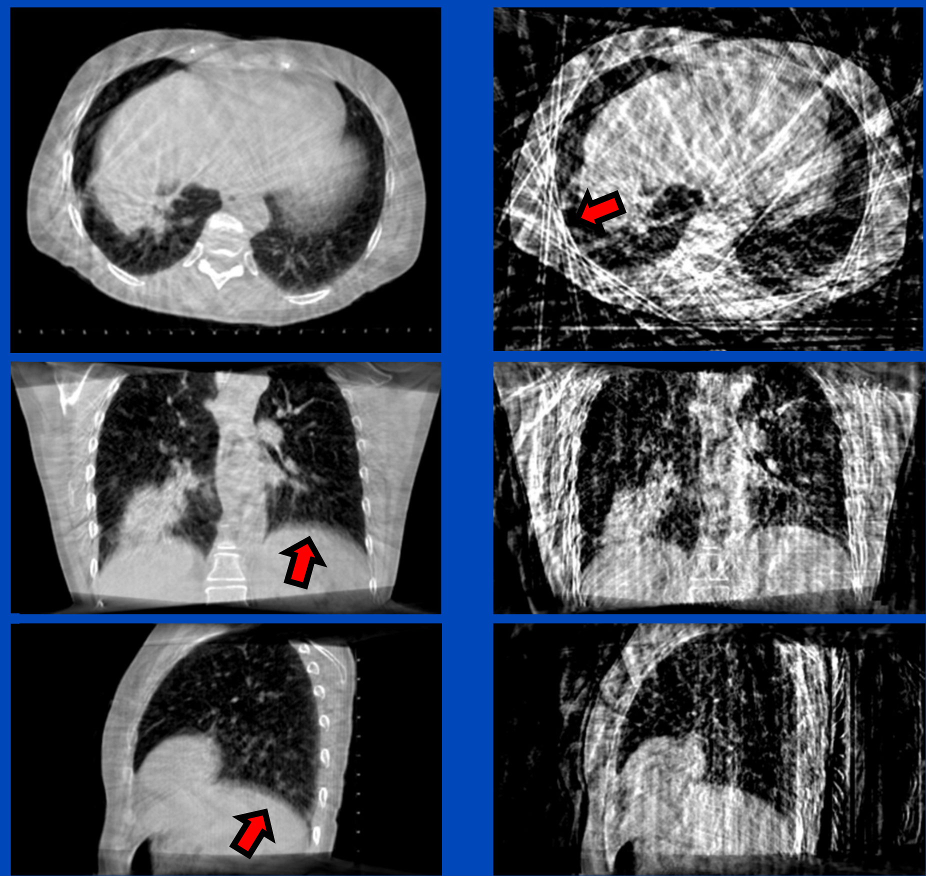

Image Registration

Target image

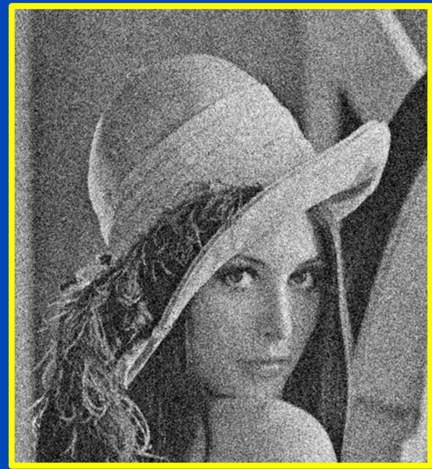

Image to be deformed

Image after registration

Image Registration

Image Registration

Motion Compensation (MoCo)

- **Use all projection data for each phase to be reconstructed**
  - Even those of other respiratory phase bins (100 % dose usage)
  - Compensate for motion applying motion vector fields (MVFs)
  - In our case MVFs are estimated from conventional gated reconstructions
- **Use MVFs during image reconstruction**
  - Backproject sparse data along straight lines, then warp with respect to the MVFs
  - Computational efficiency
    - » Corresponds to backprojection along deformed lines

Straight backprojection

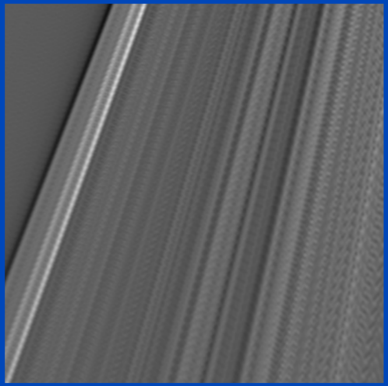

Warped backprojection

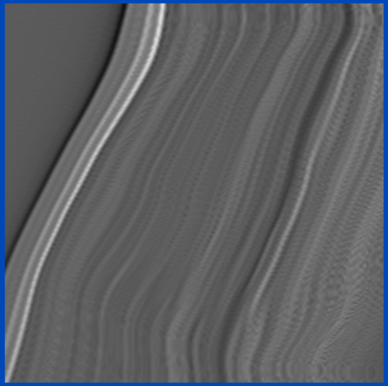

A Standard Motion Estimation and Compensation Approach (sMoCo)

- Motion estimation via standard 3D-3D registration

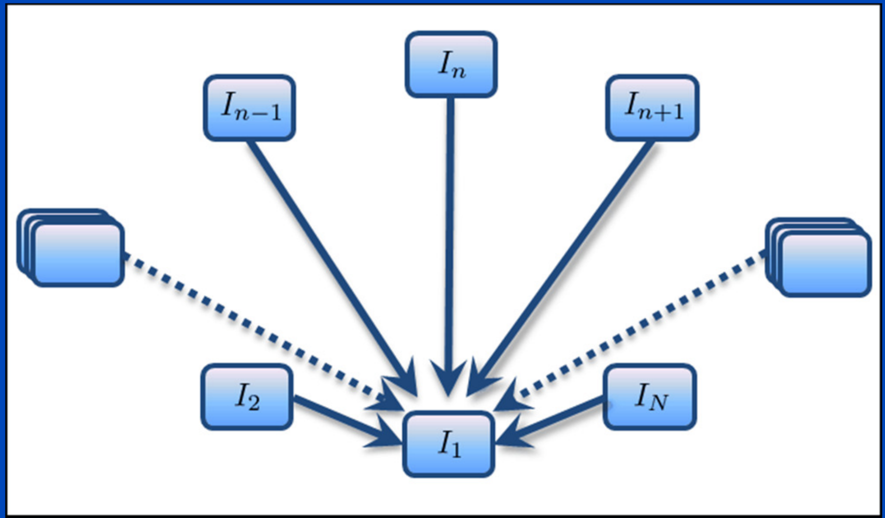

- Has to be repeated for each reconstructed phase

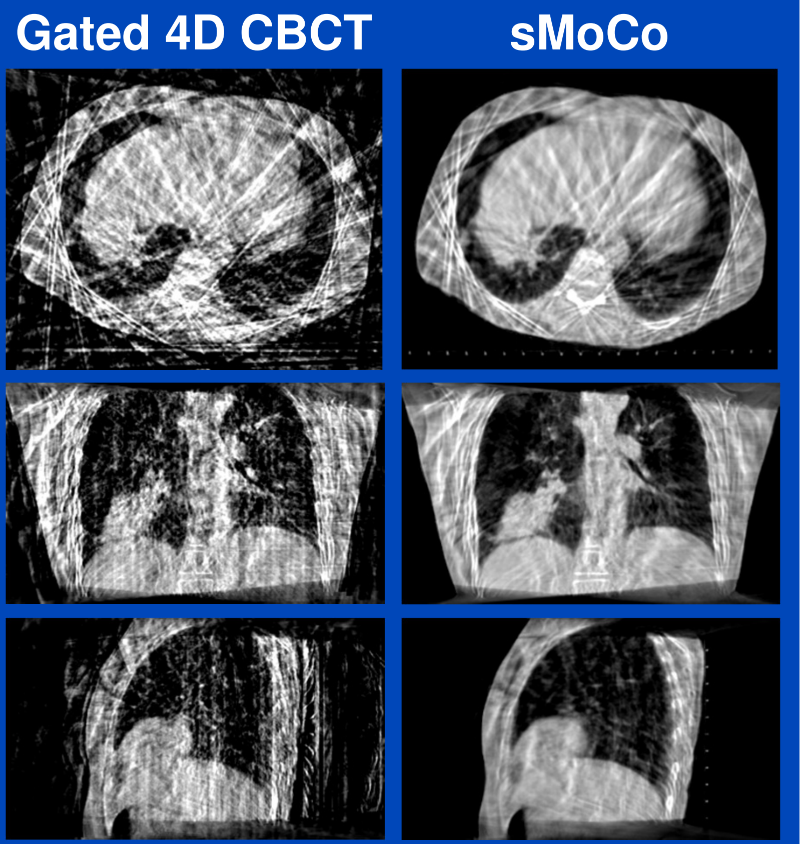

- Streak artifacts from gated reconstructions propagate into sMoCo results

Li, Koong, and Xing, "Enhanced 4D cone–beam CT with inter–phase motion model," Med. Phys. 51(9), 3688–3695 (2007).

A Cyclic Motion Estimation and Compensation Approach (cMoCo)

- Motion estimation only between adjacent phases
  - All other MVFs given by concatenation

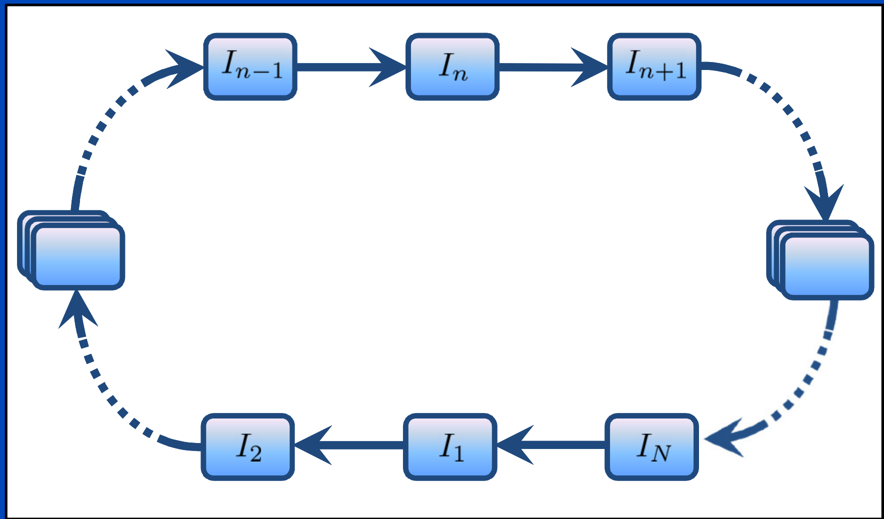

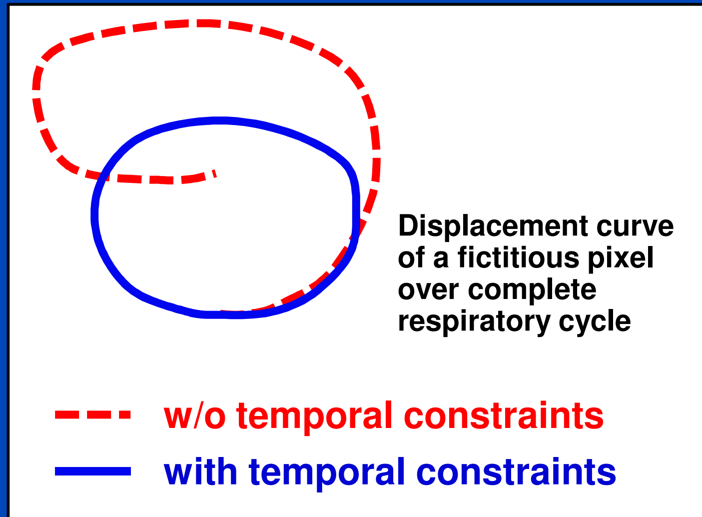

- Incorporate additional knowledge
  - A priori knowledge of quasi periodic breathing pattern
  - Non-cyclic motion is penalized
  - Error propagation due to concatenation is reduced

Brehm, Paysan, Oelhafen, Kunz, and Kachelrieß, "Self-adapting cyclic registration for motion-compensated cone-beam CT in image-guided radiation therapy," Med. Phys. 39(12), 7603-7618 (2012).

Artifact Model-Based MoCo (aMoCo)

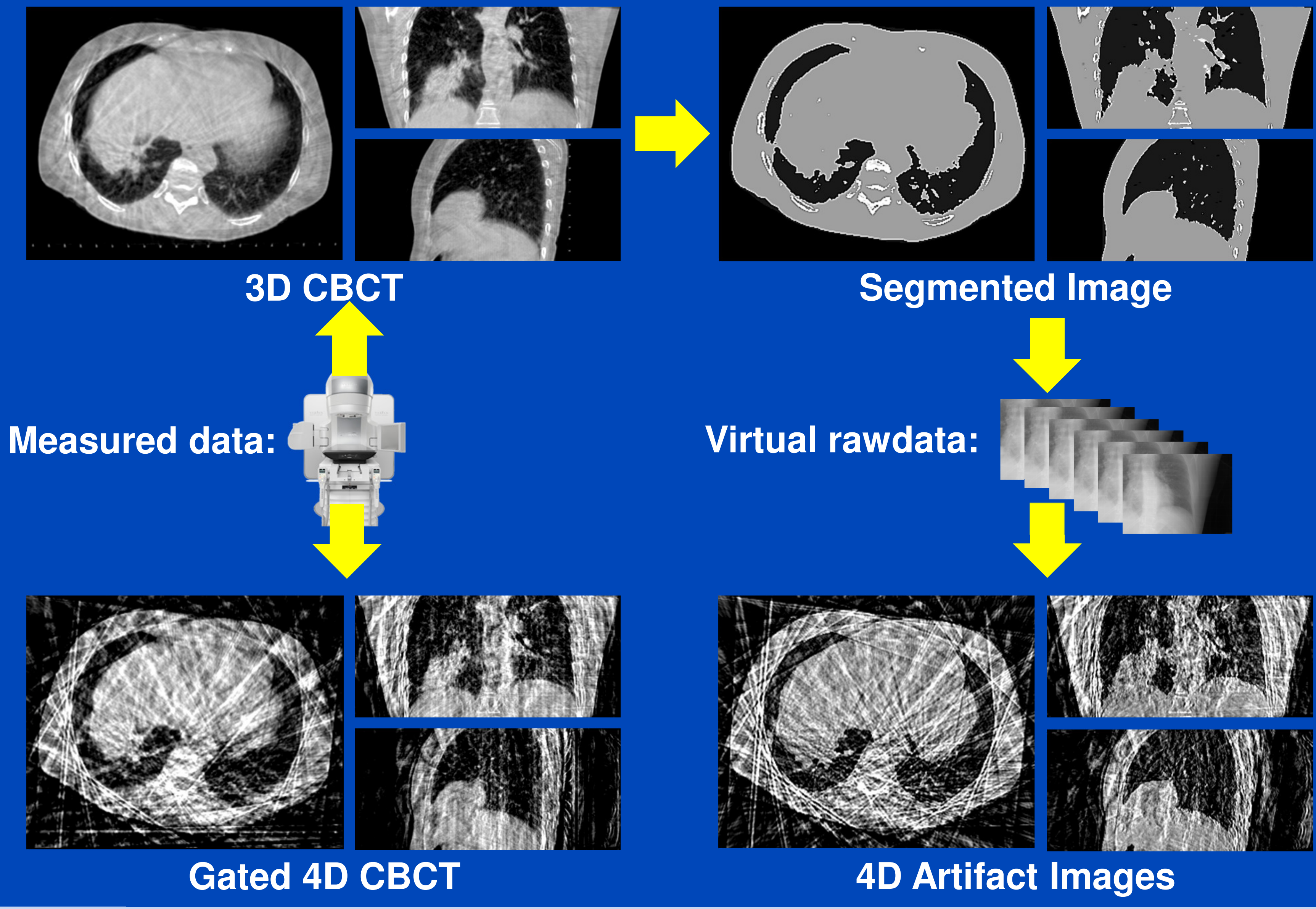

Propagation of Respiratory Motion

- Respiratory motion propagates into 3D reconstruction even if the image is stationary.
- Perform segmentation before forward projection.

$\mathrm{X}^{-1}p$ | $\mathrm{X}_{\mathrm{PC}}^{-1}p$ | $\mathrm{X}_{\mathrm{PC}}^{-1}\left(\mathrm{X}\left(\mathrm{X}^{-1}p\right)\right)$ | Artifact Image: $\mathrm{X}_{\mathrm{PC}}^{-1}(\mathrm{X}(\text{Segm. Im.}))$

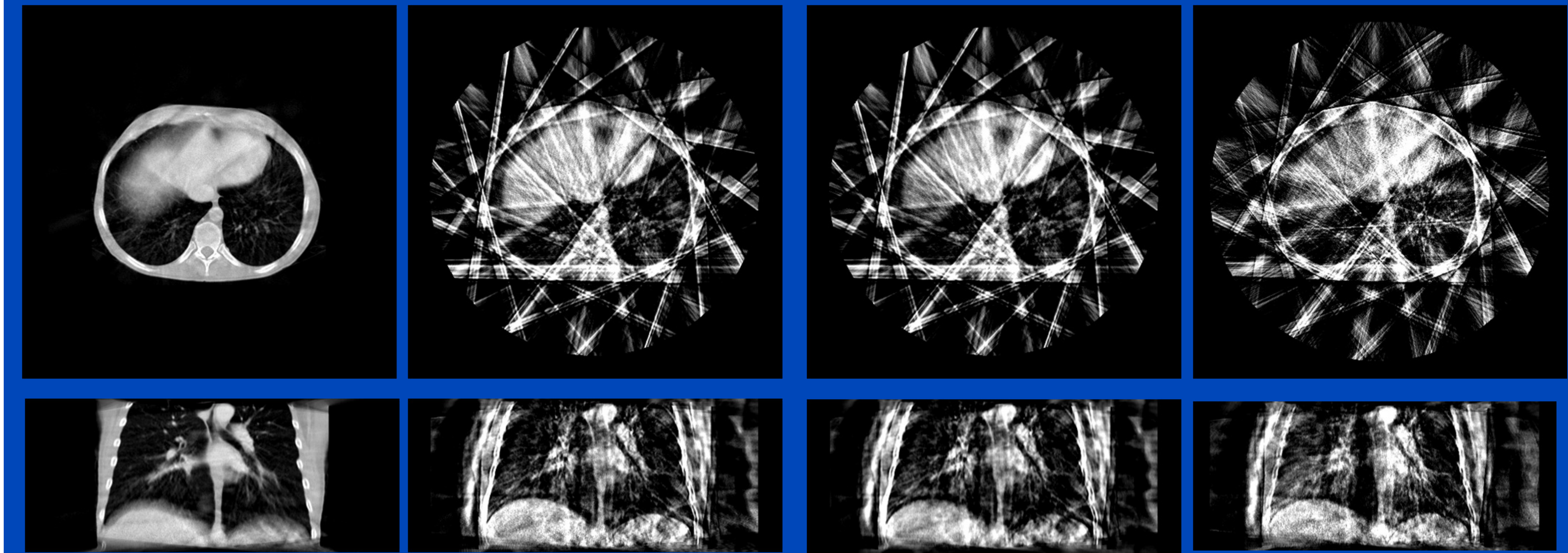

PC = phase-correlated reconstruction = gated reconstruction (CT or MR). *C* = -200 HU, *W* = 1400 HU

Motion Estimation using an Patient-Specific Artifact Model

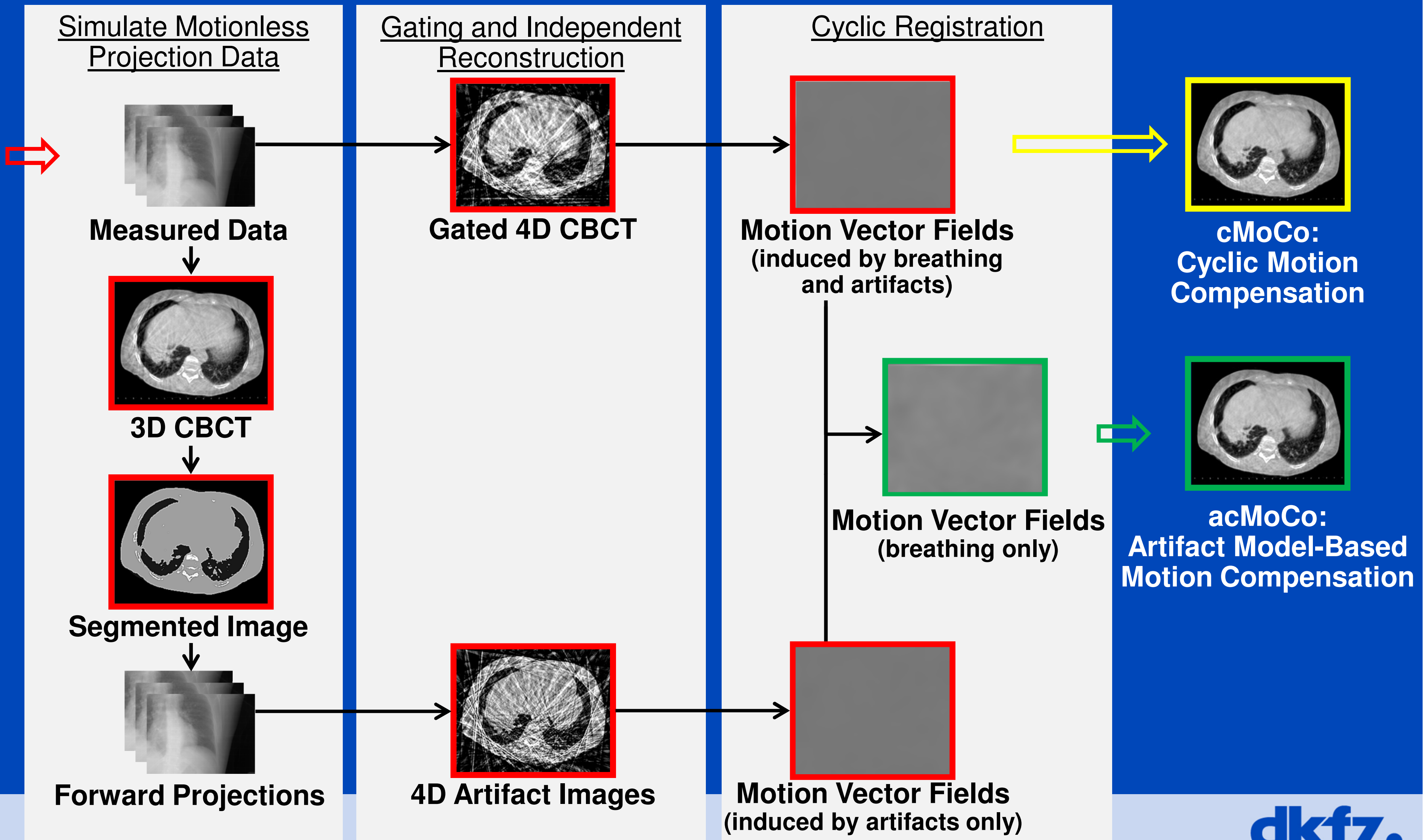

dkfz.

Patient Data – Results

3D CBCT	Gated 4D CBCT	sMoCo	acMoCo
Standard	Conventional Phase-Correlated	Standard Motion Compensation	Artifact Model-Based Motion Compensation

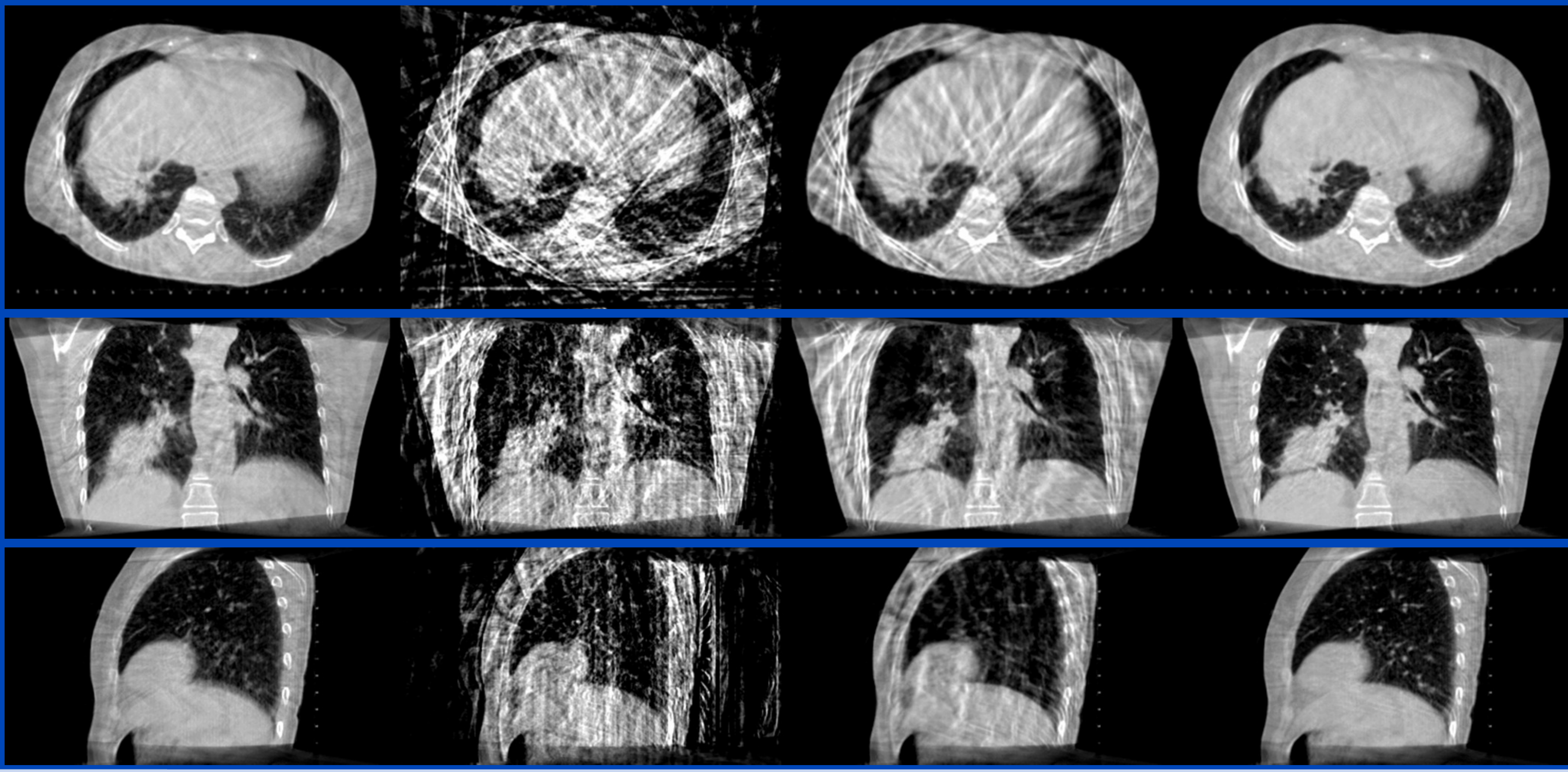

C = -200 HU, W = 1400 HU

Iterative Image Reconstruction in MR

- For cartesian k-space sampling, a simple inverse FFT usually suffices for image reconstruction.
- Therefore, iterative reconstruction methods are mainly needed for non-cartesian k-space sampling.
- Methods are similar to CT, but other difficulties arise, e.g. in parallel imaging with multiple coils, coil sensitivity profiles have to be considered, which are in general unknown and have to be estimated.
- Typically, cost functions consist of a rawdata fidelity term and regularization terms in a sparsity transformed space, such as TV, wavelets, …, which are optimized in an alternating manner.

MR
K-Space Sampling Scheme

Simulation	Measurement
160 radial spokes per slice	480 radial spokes per slice
3D encoded radial stack-of-stars sequence	
radial sampling in transversal plane	radial sampling in coronal or sagittal plane
acquisition time: 38 s	acquisition time: 57 – 69 s
data sorted retrospectively into 20 overlapping motion phases (10% width of respiratory cycle, 5% steps)	
reordered interleaved angle increment	interleaved Golden angle increment

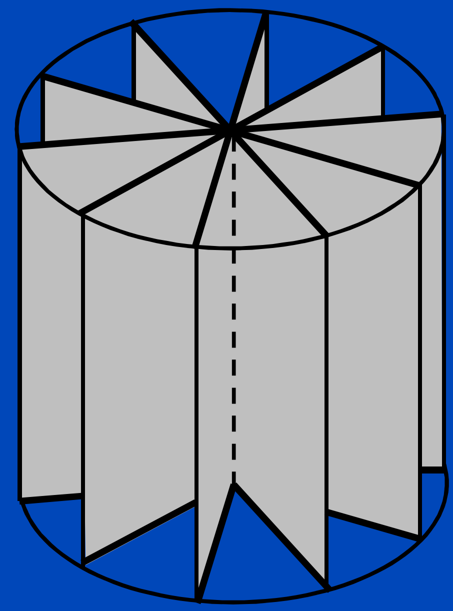

Motion Estimation Framework

MR rawdata

MR gated gridding

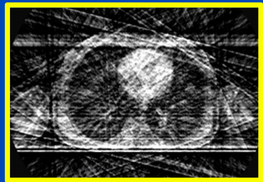

MR HDTV

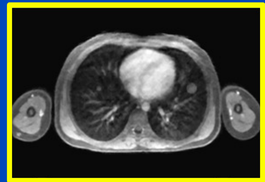

Demons artifact model-based registration[1,2] (acMoCo)

Demons cyclic registration[1] (cMoCo)

3D-2D cyclic registration[3] (3D-2D cMoCo)

RT tracking

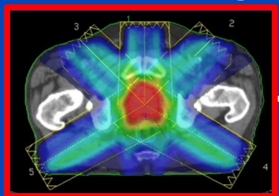

Motion Vector Fields (MVFs)

MR MoCo

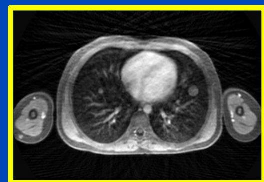

[1] Brehm, Paysan, Oelhafen, Kuntz, Kachelrieß. Self-adapting cyclic registration for motion-compensated cone-beam CT in image-guided radiation therapy. *Med. Phys.* 2012.
[2] Brehm, Paysan, Oelhafen, Kachelrieß. Artifact-resistant motion estimation with a patient-specific artifact model for motion-compensated cone-beam CT. *Med. Phys.* 2013.
[3] Flach, Brehm, Sawall, Kachelrieß. Deformable 3D-2D registration for CT and its application to low dose tomographic fluoroscopy. *Phys. Med. Biol.* 2014.

Deformable 3D-3D Registration (Demons Algorithm)

- Deform prior image $p(\boldsymbol{r})$ to match the target image $t(\boldsymbol{r})$.
- Calculate forces based on sum of squared differences in image domain:

$$\boldsymbol{v}^{(k)} = -\frac{\frac{1}{2}(t - p \circ (\mathrm{Id} + \boldsymbol{u}^{(k)}))(\nabla_{\boldsymbol{r}} t + \nabla_{\boldsymbol{r}}(p \circ (\mathrm{Id} + \boldsymbol{u}^{(k)})))}{\left\| \frac{1}{2}(\nabla_{\boldsymbol{r}} t + \nabla_{\boldsymbol{r}}(p \circ (\mathrm{Id} + \boldsymbol{u}^{(k)}))) \right\|^2 + \alpha(t - p \circ (\mathrm{Id} + \boldsymbol{u}^{(k)}))^2}$$

- Smooth velocity vector field $\boldsymbol{v}^{(k)}$ with a Gaussian kernel.
- Then update displacement vector field

$$\boldsymbol{u}^{(k+1)} = \boldsymbol{v}^{(k)} + \boldsymbol{u}^{(k)} \circ (\mathrm{Id} + \boldsymbol{v}^{(k)})$$

  and smooth with another Gaussian kernel.
- Do a few (about 10) iterations until convergence.

Thirion. Image matching as a diffusion process: An analogy with Maxwell's demons. Medical Image Analysis 2(3):243–260, 1998.

Deformable 3D-2D Registration

- **Deform prior image $p(\boldsymbol{r})$ to match the rawdata q:**
  - **Displacement vector field (DVF):** $\boldsymbol{u}(\boldsymbol{r}) = (u_1(\boldsymbol{r}), u_2(\boldsymbol{r}), u_3(\boldsymbol{r}))^{\mathrm{T}}$
  - **Deformed image:** $p_{\boldsymbol{u}}(\boldsymbol{r}) = p(\boldsymbol{r} + \boldsymbol{u}(\boldsymbol{r})) = (p \circ (\mathrm{Id} + \boldsymbol{u}))(\boldsymbol{r})$
  - **Matching criterion:** $S[\boldsymbol{u}] = \|\mathsf{X}p(\boldsymbol{r} + \boldsymbol{u}(\boldsymbol{r})) - q\|_2^2$ **(rawdata fidelity)**
  - **Velocity vector field:** $\boldsymbol{v}(\boldsymbol{r}) = (v_1(\boldsymbol{r}), v_2(\boldsymbol{r}), v_3(\boldsymbol{r}))^{\mathrm{T}} = \partial_t \boldsymbol{u}(\boldsymbol{r})$
  - **Smoothness of a vector field $\boldsymbol{w}(\boldsymbol{r}) = (w_1(\boldsymbol{r}), w_2(\boldsymbol{r}), w_3(\boldsymbol{r}))^{\mathrm{T}}$ achieved by minimizing**
    $$R[\boldsymbol{w}] = \sum_{d=1}^{3} \sum_{\boldsymbol{r}} \langle \boldsymbol{\nabla}_{\boldsymbol{r}} w_d(\boldsymbol{r}), \boldsymbol{\nabla}_{\boldsymbol{r}} w_d(\boldsymbol{r}) \rangle$$
  - **Diffusive regularization:** $R[\boldsymbol{u}]$
  - **Fluid regularization:** $R[\boldsymbol{v}] = R[\partial_t \boldsymbol{u}]$
- **Determine the DVF $\boldsymbol{u}$ by minimizing the following cost function:**

$$C[\boldsymbol{u}] = S[\boldsymbol{u}] + \beta R[\boldsymbol{u}] + \gamma R[\partial_t \boldsymbol{u}]$$

Flach, Brehm, Sawall, Kachelrieß. Deformable 3D-2D registration for CT and its application to low dose tomographic fluoroscopy. Phys. Med. Biol. 59:7865–7887, 2014.

MR
Artifact Model-Based Estimation of MVFs[2]

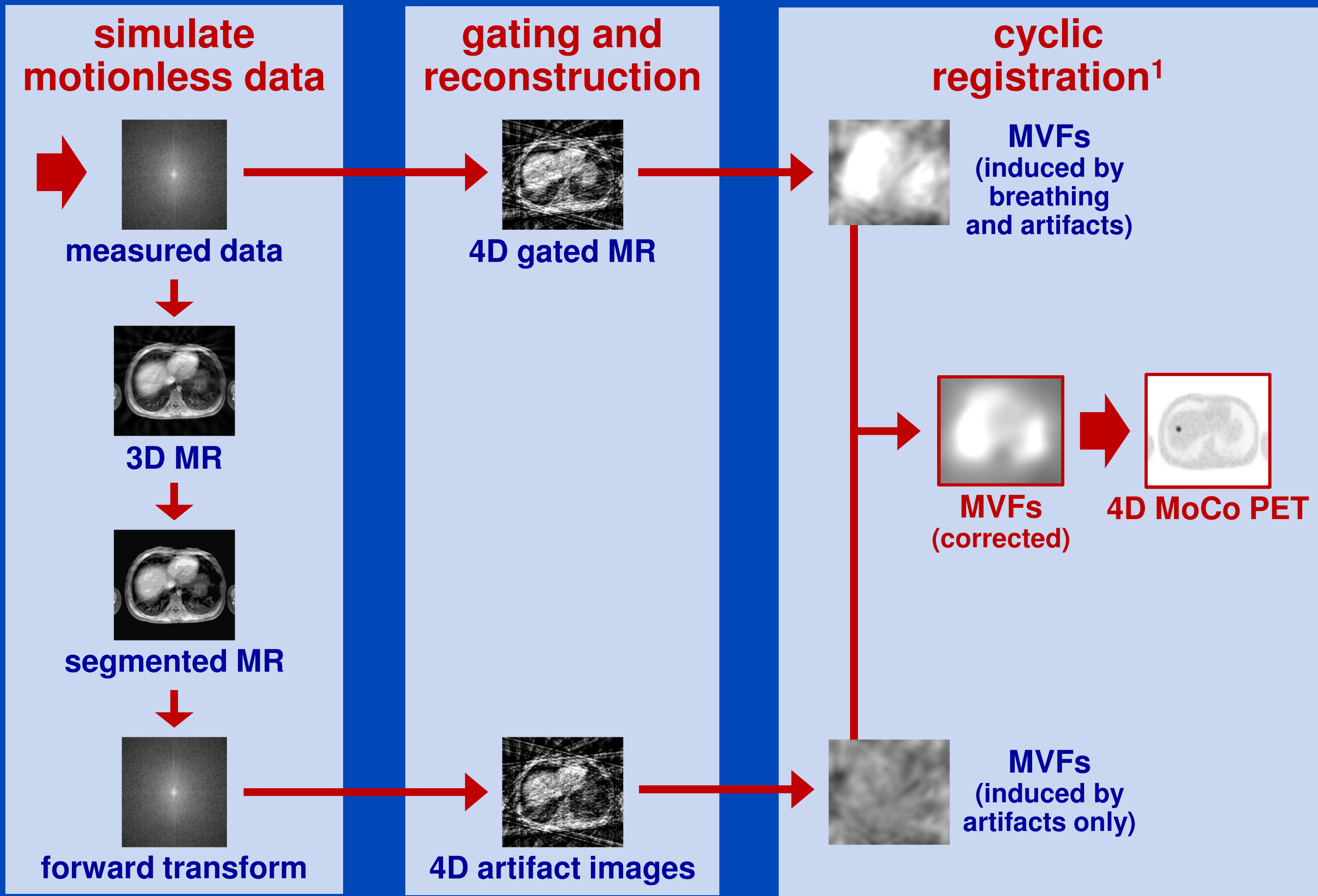

[1] Brehm, Paysan, Oelhafen, Kuntz, Kachelrieß. Self-adapting cyclic registration for motion-compensated cone-beam CT in image-guided radiation therapy. *Med. Phys.* 2012.
[2] Brehm, Paysan, Oelhafen, Kachelrieß. Artifact-resistant motion estimation with a patient-specific artifact model for motion-compensated cone-beam CT. *Med. Phys.* 2013.

Backproject-then-Warp MoCo

- **MVFs have to be calculated by one of the three options (acMoCo, cMoCo or 3D-2D cMoCo) in advance.**
- **A gated gridding reconstruction of the MR rawdata is performed.**
- **MoCo backproject-then-warp of gate *g*:**

$$f_g = \frac{1}{G}\sum_{g'} T^{\mathrm{T}}_{g'\mapsto g} f_{g'}$$

f_g:	image of gate g
g, g':	gate indices
G:	total number of gates
$T^{\mathrm{T}}_{g'\to g}$:	backward warping operation mapping gate g' to g

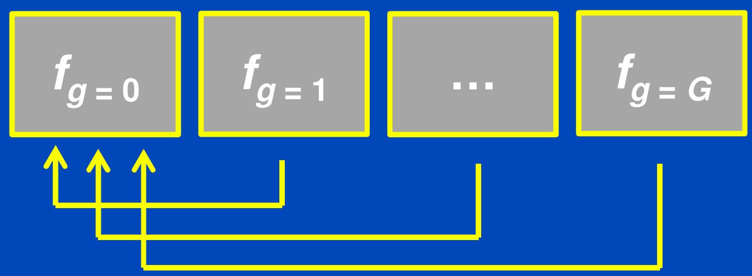

“warp” gated images

Iterative Reconstruction (HDTV)[1,2]

- **Cost function**

$$C = \|\mathsf{X}f - p\|_2^2 + \alpha\|f\|_{\mathrm{TV,\,xyzt}}$$

$$\underbrace{\|\mathsf{X}f - p\|_2^2}_{\text{rawdata fidelity}} + \alpha\underbrace{\|f\|_{\mathrm{TV,\,xyzt}}}_{\text{total variation}}$$

X:	Fourier transform
f:	image
p:	rawdata
α:	strength
$\|\cdot\|_{\mathrm{TV,\,xyzt}}$:	total variation

- **The rawdata fidelity and the spatial and temporal smoothness of the image are optimized in an alternating manner**
- **Instead of X^T we precondition and use X^{-1}, i.e. gridding followed by inverse Cartesian Fourier transform.**
- **The cost function is optimized for the complete 4D volume including all motion phases**

[1] Ritschl, Bergner, Fleischmann, Kachelrieß. Improved total variation-based CT image reconstruction applied to clinical data. *Phys. Med. Biol.* 2011.
[2] Ritschl, Sawall, Knaup, Hess, Kachelrieß. Iterative 4D cardiac micro-CT image reconstruction using an adaptive spatio-temporal sparsity prior. *Phys. Med. Biol.* 2012.

MoCo Iterative Reconstruction (MoCo HDTV)

- **MVFs have to be calculated by one of the three options (acMoCo, cMoCo or 3D-2D cMoCo) in advance**
- **The same cost function as for HDTV is optimized, but in the rawdata step, the image update u_g of gate g is calculated using backproject-then-warp**

$$u_g = \frac{1}{G} \sum_{g'} T^{\mathrm{T}}_{g' \mapsto g} u_{g'}$$

u_g:	image update of gate g
g, g':	gate indices
G:	total number of gates
$T^{\mathrm{T}}_{g' \to g}$:	backward warping operation mapping gate g' to g

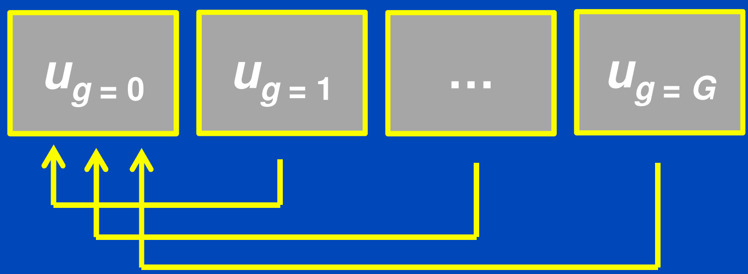

"warp" update images

Results of Simulated Data

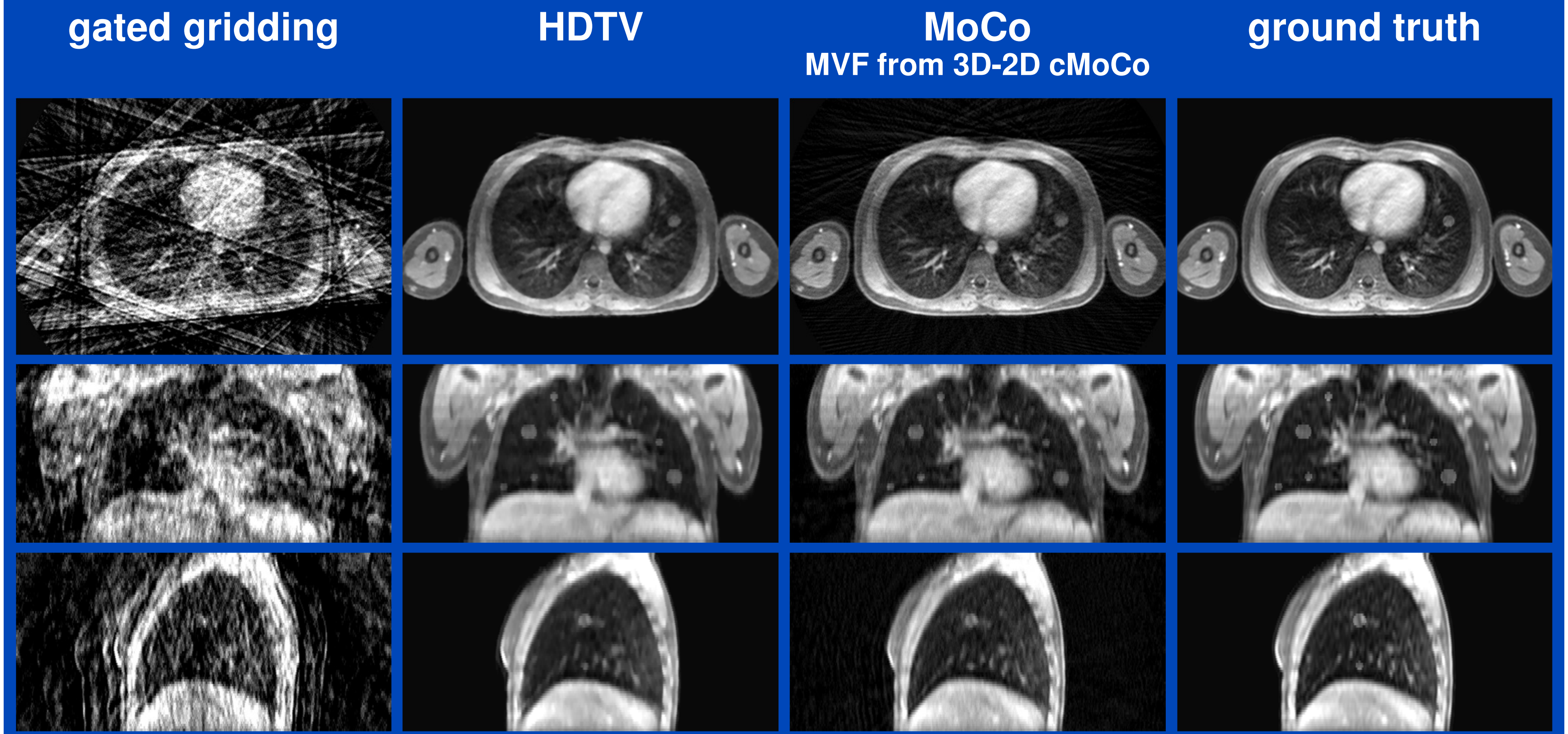

160 radial spokes per slice, 20 overlapping phases, acquisition time: 38 s

dkfz.

Results of Measured Data (Volunteer)

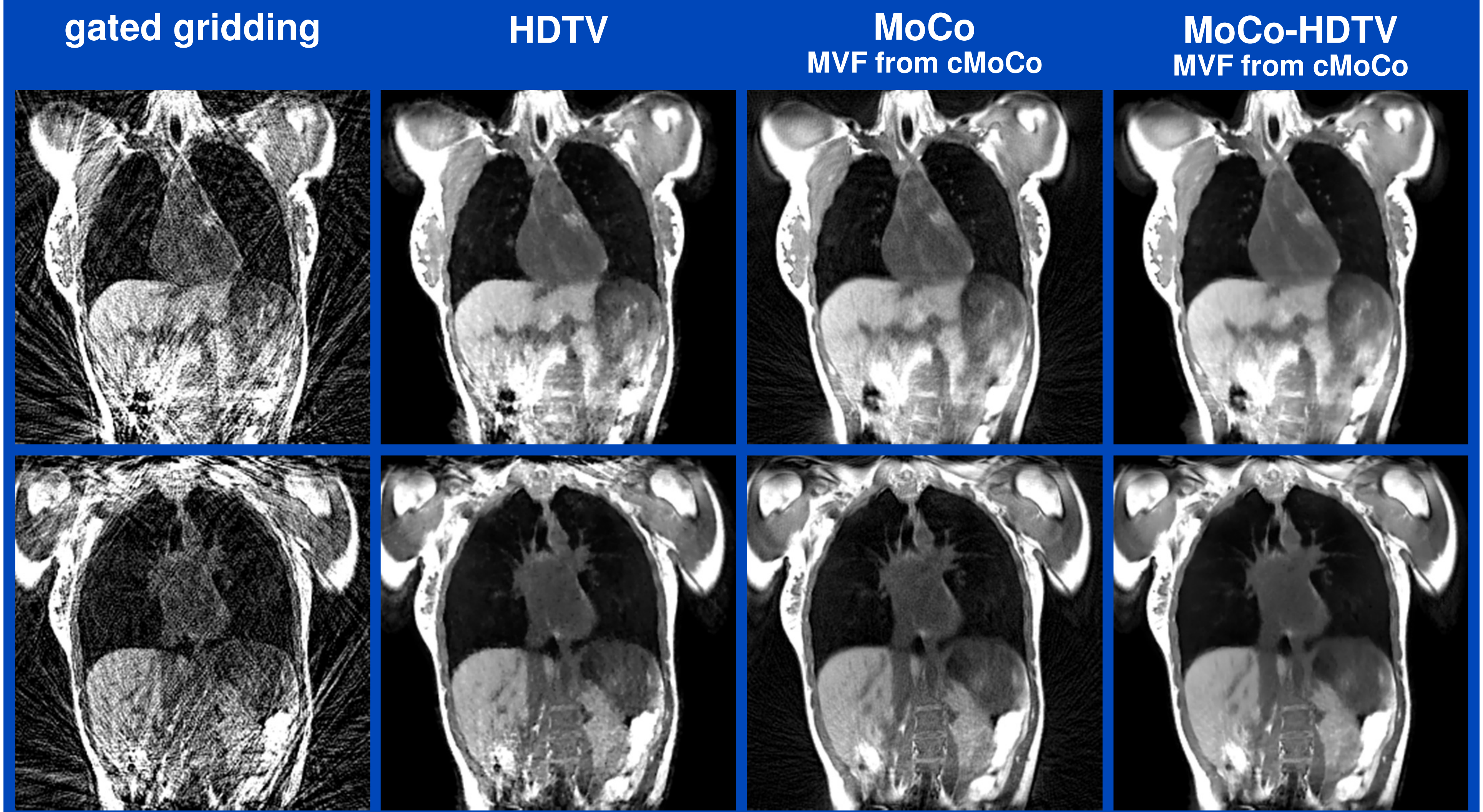

480 radial spokes per slice, 20 overlapping phases, acquisition time: 57 s

Results of Measured Data (Volunteer)

gated gridding (1925 spokes: 229 s)	HDTV	MoCo MVF from cMoCo	MoCo-HDTV MVF from cMoCo

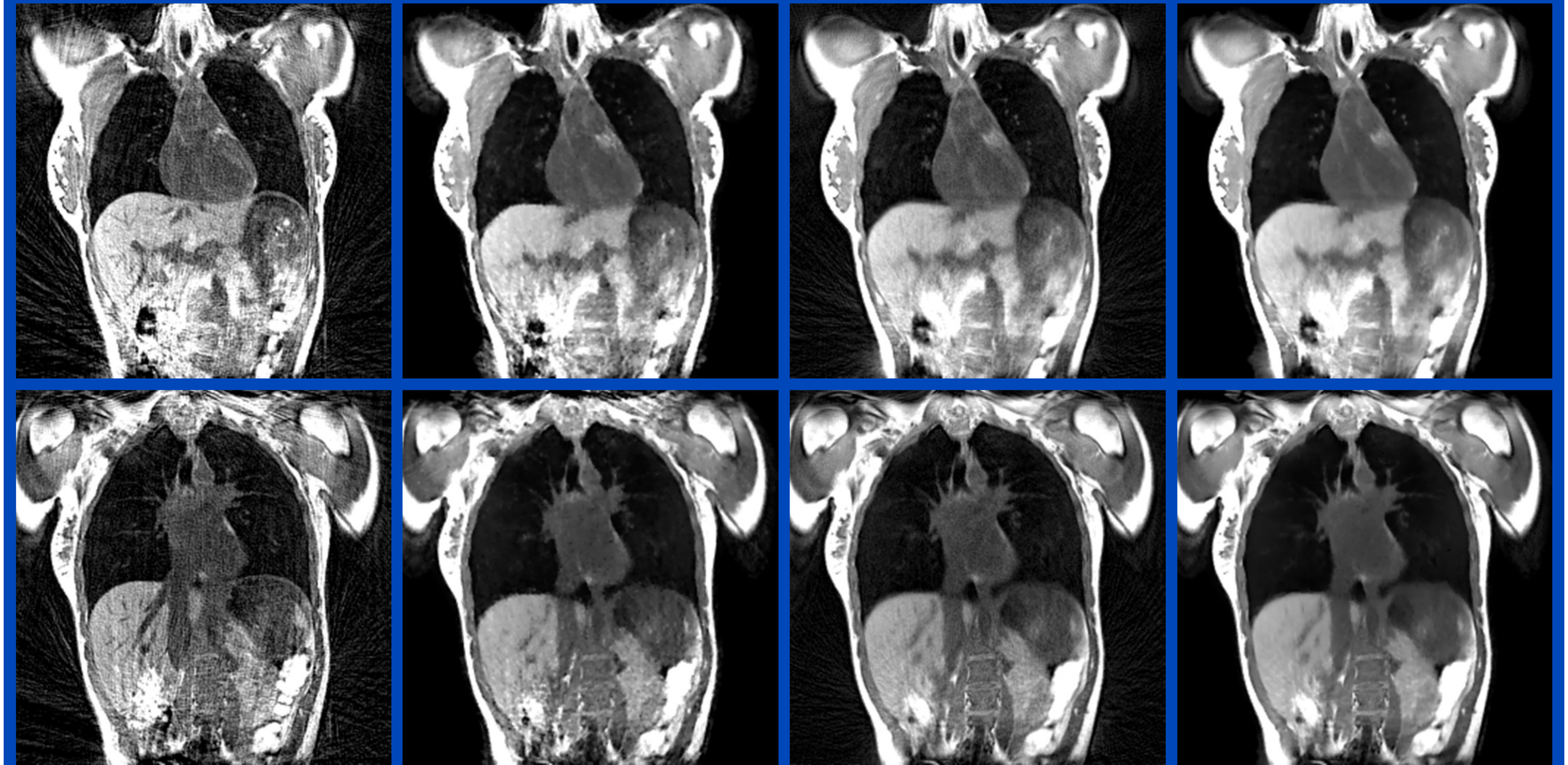

480 radial spokes per slice, 20 overlapping phases, acquisition time: 57 s

dkfz.

Results of Measured Data (Patient)

gated gridding	HDTV	MoCo MVF from cMoCo	MoCo-HDTV MVF from cMoCo

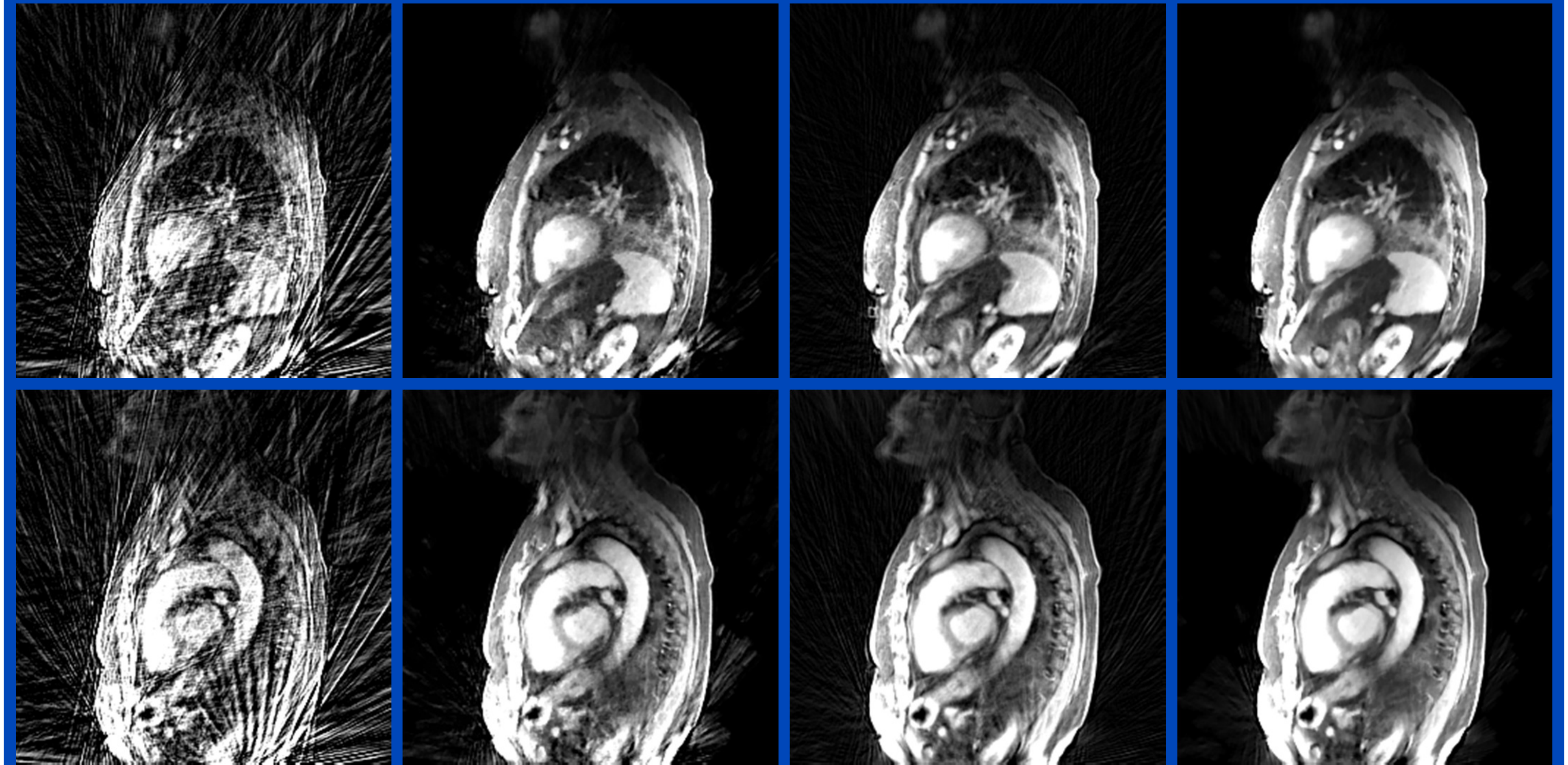

480 radial spokes per slice, 20 overlapping phases, acquisition time: 69 s

dkfz.

Results of Measured Data (Patient)

gated gridding (2035 spokes: 292 s)	iGRASP (2035 spokes: 292 s)	MoCo MVF from cMoCo	MoCo-HDTV MVF from cMoCo

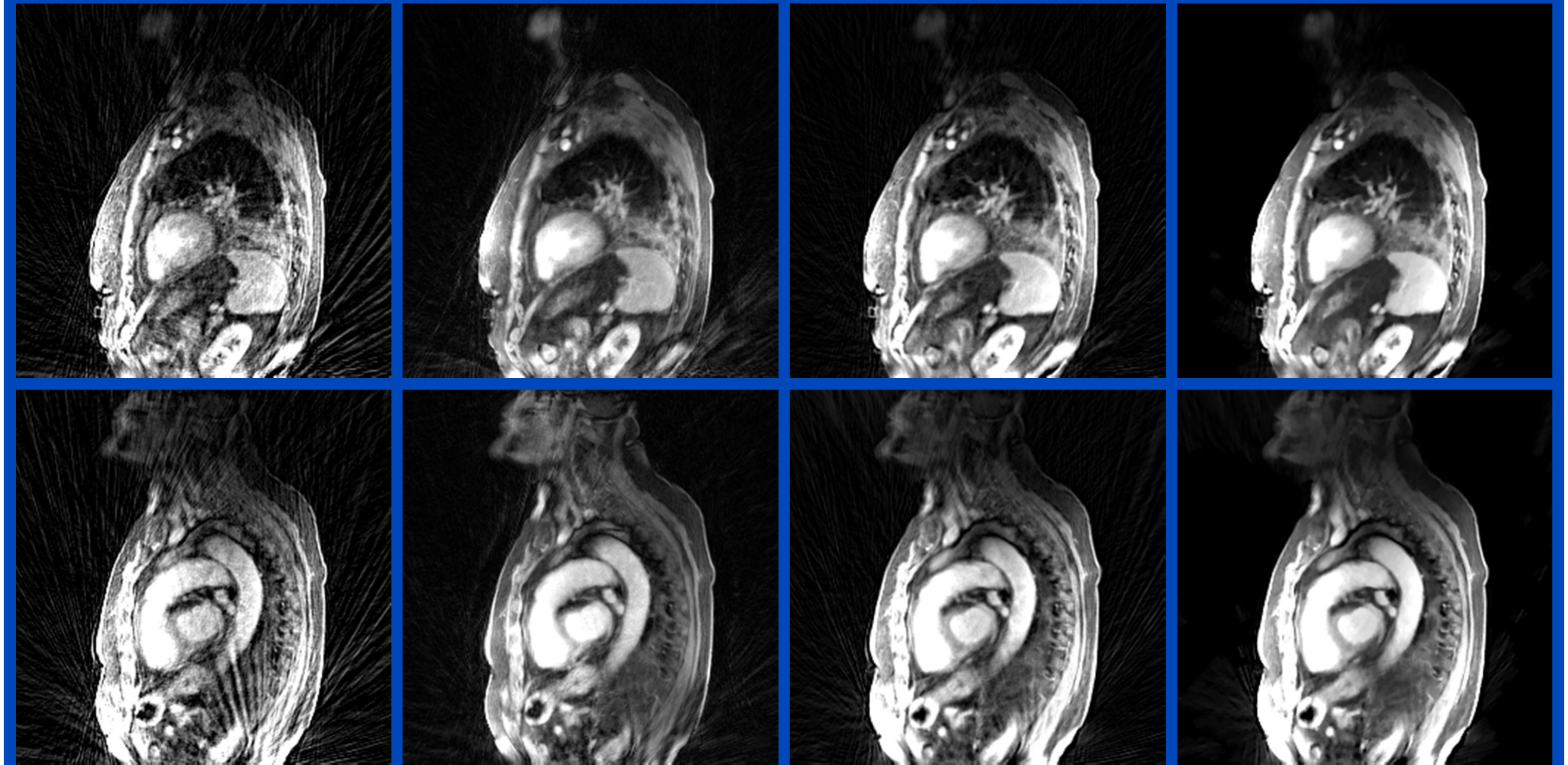

480 radial spokes per slice, 20 overlapping phases, acquisition time: 69 s

Iterative Image Reconstruction in PET

- Algebraic methods
  - Do not correctly account for noise in the measured data.
  - Example
    - » Algebraic reconstruction technique (ART).
- Statistical methods
  - Take into account the Poisson nature of the measured data.
  - Maximum-likelihood (ML) approach
    - » Maximum-likelihood expectation maximization (MLEM).
    - » Ordered subset expectation maximization (OSEM).
  - Maximum a posteriori (MAP) approach
    - » One-step-late (OSL) algorithm (= penalized MLEM).

Particle Decay

- Let M_{ij} denote the probability that a photon emitted from pixel i contributes to LOR j. M_{ij} is affected by
  - System geometry
  - Attenuation
  - Scatter
  - Detector inefficiencies
  - ...
- The probability p_{ij} for a photon emitted from pixel i within time interval $[t, t+\Delta t]$ contributes to LOR j is then given by

$$p_{ij} = M_{ij}(e^{-\mu t} - e^{-\mu(t+\Delta t)}) \approx M_{ij} e^{-\mu t} \mu \Delta t$$

with decay constant μ.

Poisson Statistics

- The number of decays K_{ij} resulting from n_i unstable particles in pixel *i* and contributing to LOR *j* is binomial distributed as

$$P(K_{ij} = k) = \binom{n_i}{k} p_{ij}^k (1 - p_{ij})^{n_i - k}$$

- For large n_i and small p_{ij}, the binomial distribution can be approximated by a Poisson distribution

$$P(K_{ij} = k) = e^{-\hat{k}_{ij}} \frac{\hat{k}_{ij}^k}{k!}$$

with mean value $\hat{k}_{ij} = n_i p_{ij} = n_i M_{ij} e^{-\mu t} \mu \Delta t$

$$= \lambda_i M_{ij}$$

and activity image $\lambda_i = n_i e^{-\mu t} \mu \Delta t$

Probability Density Function (PDF)

- **The measurement along each LOR *j* is the sum**

$$P_j = \sum_i K_{ij}$$

which also follows a Poisson distribution

$$P(P_j = p) = e^{-\hat{p}_j} \frac{\hat{p}_j^p}{p!} \qquad \hat{p}_j = \sum_i \hat{p}_{ij} = \sum_i \lambda_i M_{ij}$$

- **PDF and corresponding log- likelihood**

$$P(\boldsymbol{p}|\boldsymbol{\lambda}) = \prod_j P(P_j = p_j) = \prod_j e^{-\hat{p}_j} \frac{\hat{p}_j^{p_j}}{p_j!}$$

$$L(\boldsymbol{p}|\boldsymbol{\lambda}) = \sum_j \big(- \hat{p}_j + p_j \ln \hat{p}_j \big) + rest$$

Bayesian Approach

- Find **image $\boldsymbol{\lambda}$** maximizing the **probability** $P(\boldsymbol{\lambda}|\boldsymbol{p})$ given the **projection data** $\boldsymbol{p}$.
- Bayes rule:

$$P(\boldsymbol{\lambda}|\boldsymbol{p}) = \frac{P(\boldsymbol{p}|\boldsymbol{\lambda})\overbrace{P(\boldsymbol{\lambda})}^{\text{Prior term}}}{\underbrace{P(\boldsymbol{p})}_{\text{Constant}}}$$

- Maximum-a-posteriori (MAP) approach
  - Maximize the posterior $P(\boldsymbol{\lambda}|\boldsymbol{p})$
- Maximum-likelihood (ML) approach
  - Maximize the likelihood $P(\boldsymbol{p}|\boldsymbol{\lambda})$
  - Assumes $P(\boldsymbol{\lambda}) = const$, i.e., all images have equal probability

Maximum-Likelihood (ML) Approach

- **Bayes rule:** $P(\boldsymbol{\lambda}|\boldsymbol{p}) = \frac{P(\boldsymbol{p}|\boldsymbol{\lambda})P(\boldsymbol{\lambda})}{P(\boldsymbol{p})}$

- **Without prior, the problem reduces to maximizing**

$$P(\boldsymbol{p}|\boldsymbol{\lambda}) = \prod_j P(p_j|\boldsymbol{\lambda}) = \prod_j \frac{e^{-\hat{p}_j}\hat{p}_j^{\,p_j}}{p_j!} \longleftarrow \text{Poisson distribution}$$

with expected projection data $\hat{p}_j(\boldsymbol{\lambda}) = \sum_i \lambda_i M_{ij}$ **.**

- **Instead of the likelihood, it is more convenient to maximize the log-likelihood**

$$L(\boldsymbol{p}|\boldsymbol{\lambda}) = \ln P(\boldsymbol{p}|\boldsymbol{\lambda}) = \sum_j (-\hat{p}_j + p_j \ln \hat{p}_j) + rest$$

Maximum-Likelihood Expectation Maximization (MLEM)

- Maximization of the expectation value of the log-likelihood yields the update equation

$$\lambda_i^{(n+1)} = \lambda_i^{(n)} \frac{1}{\sum_j M_{ij}} \sum_j M_{ij} \frac{p_j}{\sum_k \lambda_k^{(n)} M_{kj}}$$

- Equivalent notation

$$\lambda^{(n+1)} = \lambda^{(n)} \frac{1}{\mathsf{M}^{\mathrm{T}} \mathbb{1}} \mathsf{M}^{\mathrm{T}} \frac{p}{\mathsf{M}\lambda}$$

$\lambda_i^{(n)}$ **Current image estimate in voxel *i***

M_{ij} **System matrix**

p_j **Measured projections in pixel *j***

Ordered Subset Expectation Maximization (OSEM)

- Accelerated version of MLEM sorting the LORs into subsets.
- Update equation

$$\lambda_i^{(n+1)} = \lambda_i^{(n)} \frac{1}{\sum_{j \in J} M_{ij}} \sum_{j \in J} M_{ij} \frac{p_j}{\sum_k \lambda_k^{(n)} M_{kj}}$$

p_j **Measured projections along LOR *j***

M_{ij} **System matrix**

$\lambda_i^{(n)}$ **Estimated activity in voxel *i* for iteration *n***

J **Subset**

dkfz.

Subsets

$NSub_{Tran} > 1$; $NSub_{Long} = 1$

- Each subset must cover entire FOV.
- Standard approach: Number of longitudinal subsets $NSub_{Long}$ is set to one.

Transversal

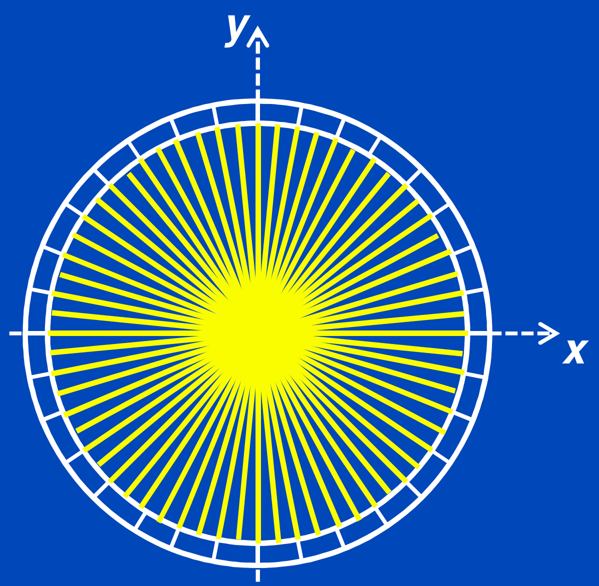

Only direction of LORs shown!

Longitudinal

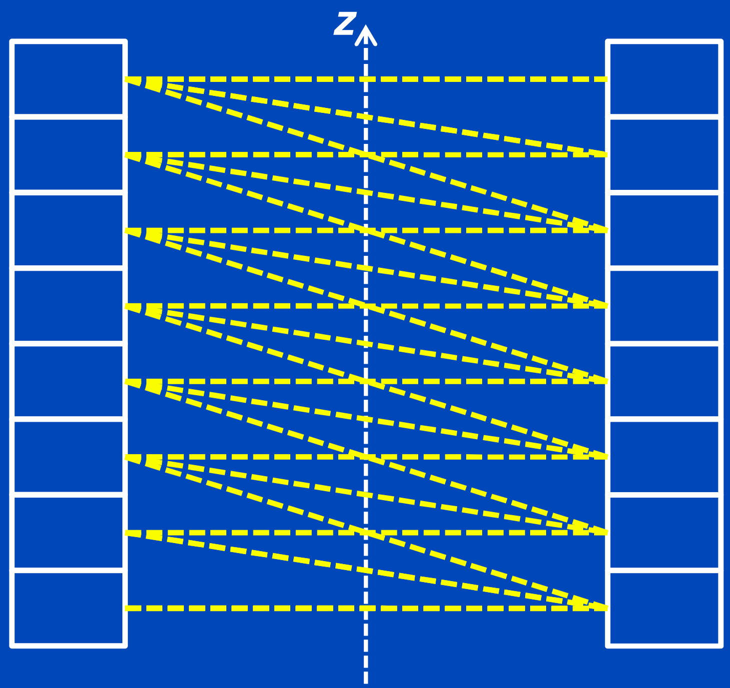

Oblique LORs shown only once!

Subsets

$NSub_{Tran} = 1; NSub_{Long} > 1$

- **Each subset must cover entire FOV.**
- **Alternative approach (I): subsets are defined in longitudinal direction only.**

Transversal

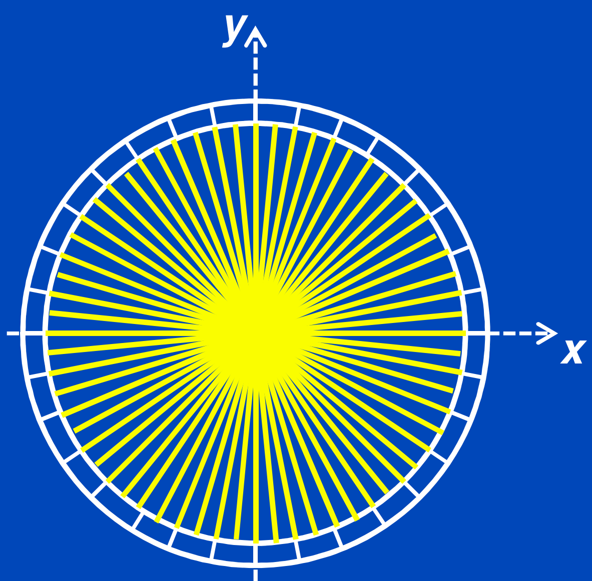

Only direction of LORs shown!

Longitudinal

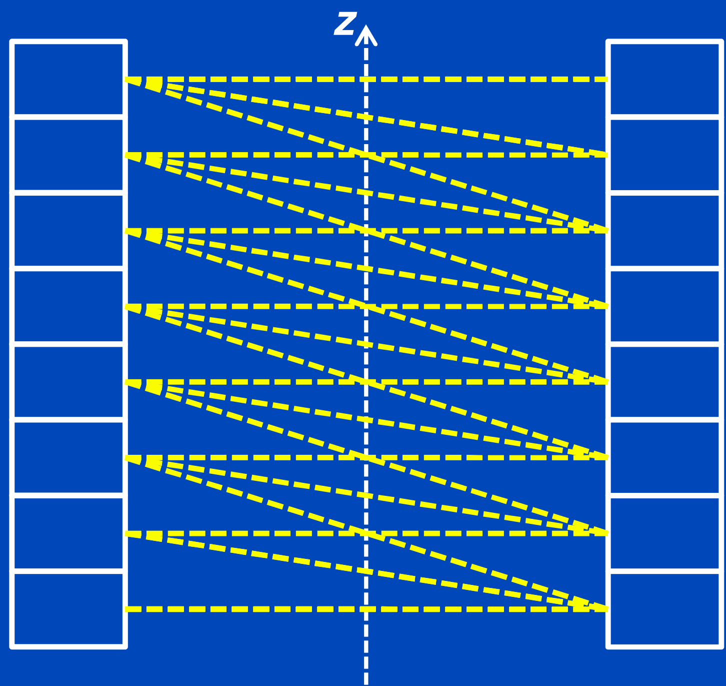

Oblique LORs shown only once!

Subsets

$NSub_{Tran} > 1$; $NSub_{Long} > 1$

- **Each subset must cover entire FOV.**
- **Alternative approach (II): subsets are defined in both directions.**

Transversal

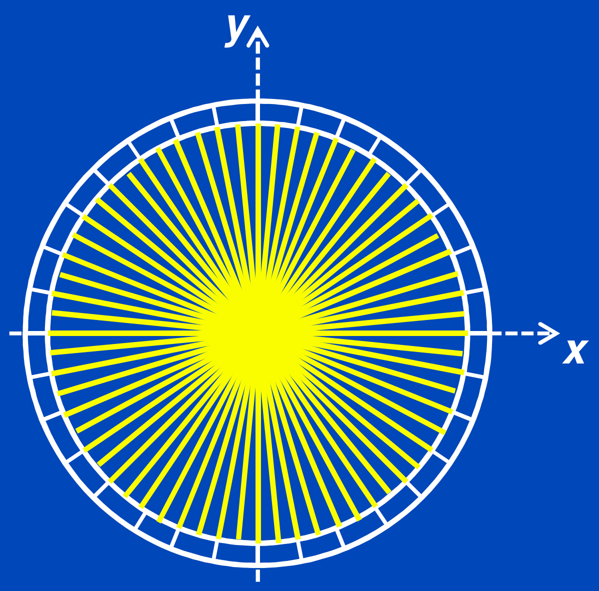

Only direction of LORs shown!

Longitudinal

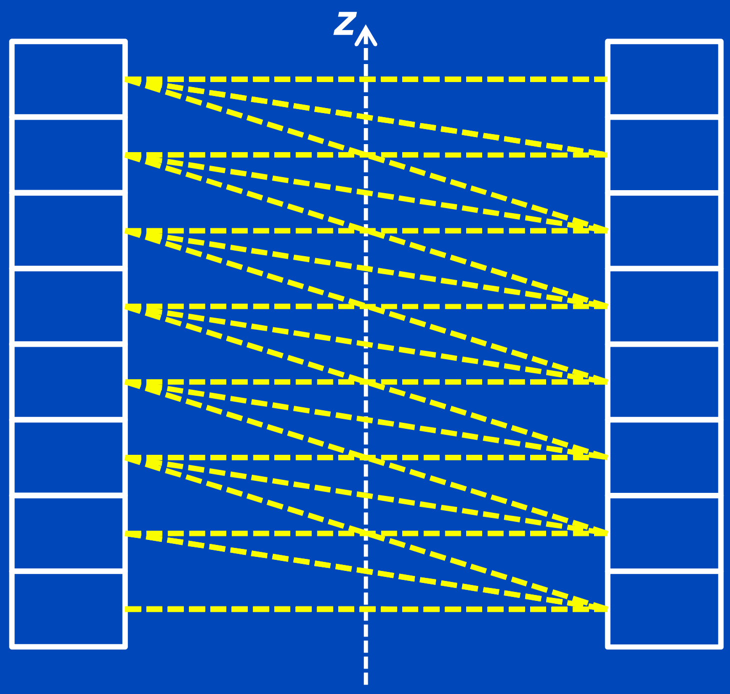

Oblique LORs shown only once!

FBP vs. MLEM

Simulation

FBP

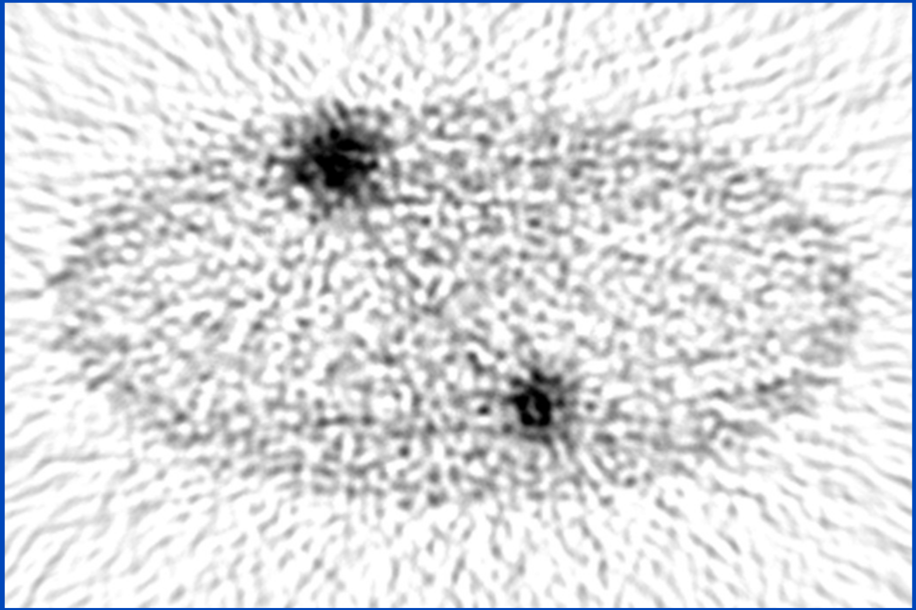

MLEM
10 Iterations

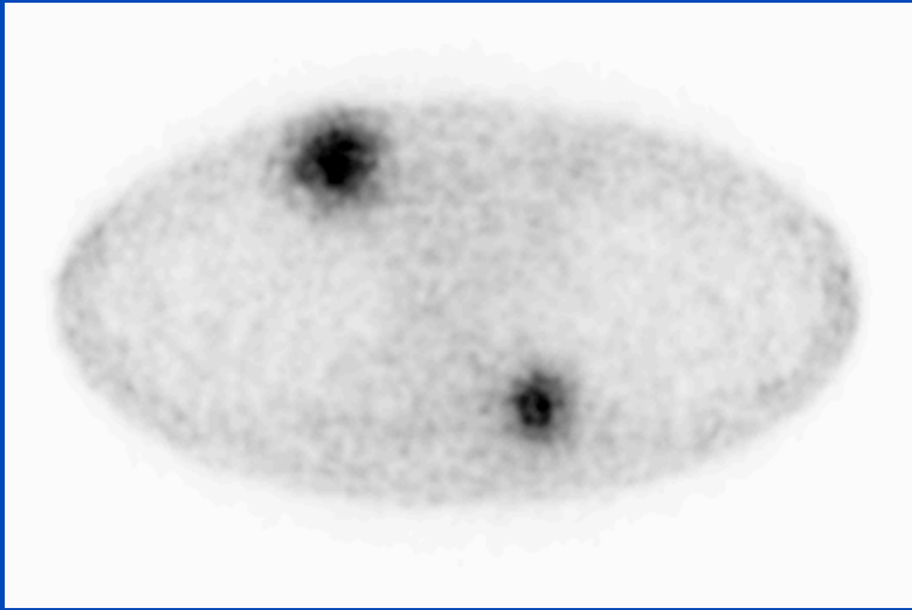

C = 15 kBq/mL, *W* = 30 kBq/mL

dkfz.

FBP vs. MLEM

Measurement

FBP

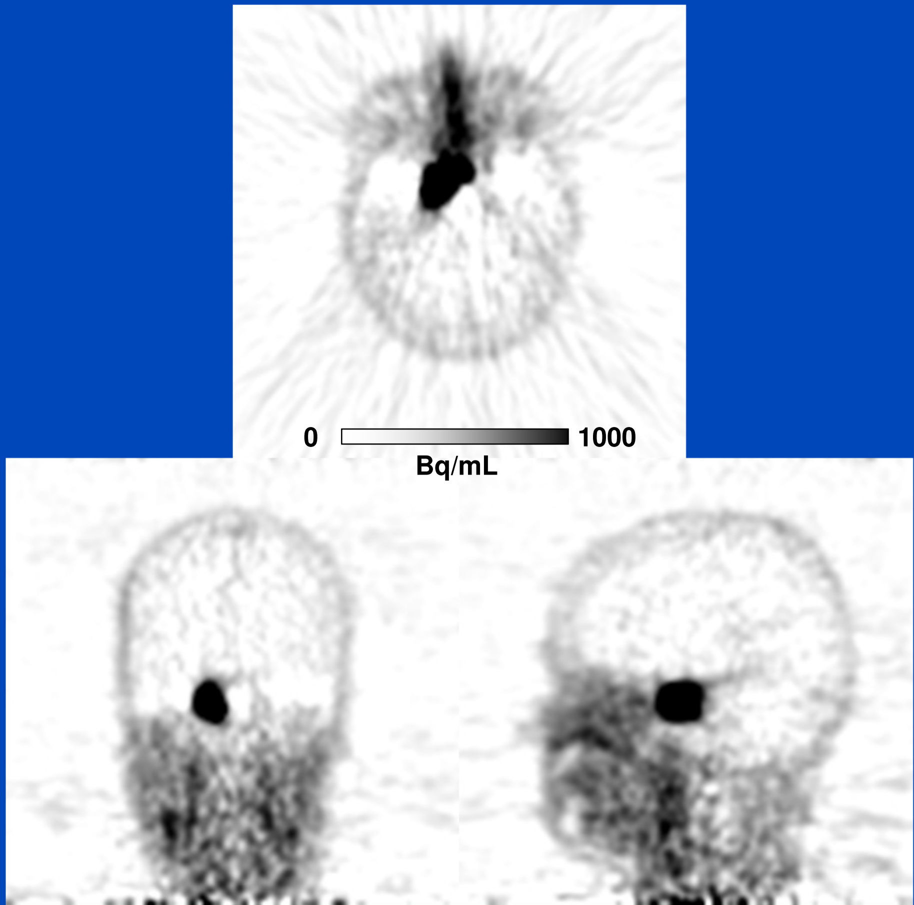

MLEM

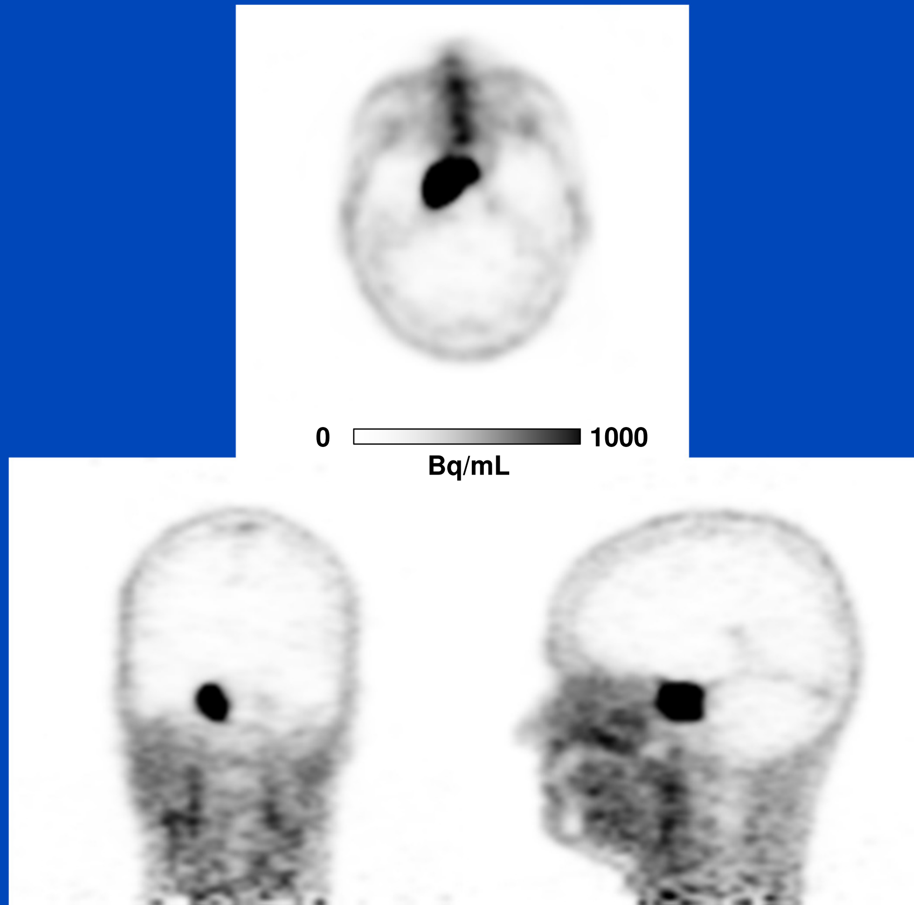

MLEM vs. OSEM

Simulation

MLEM
2 Iterations

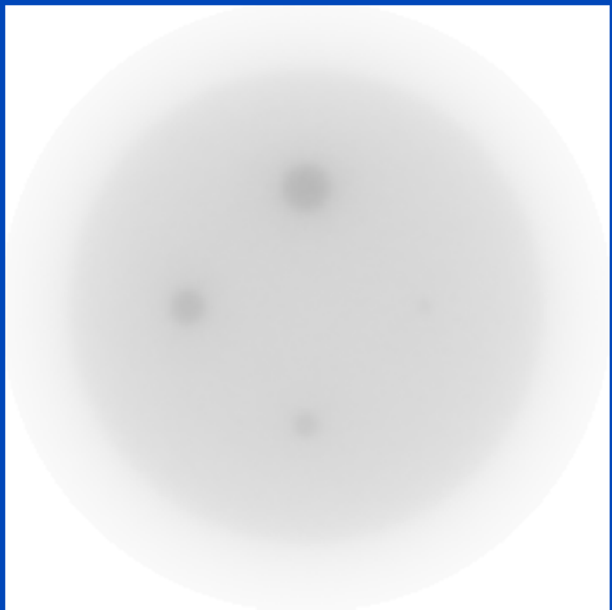

MLEM
28 Iterations

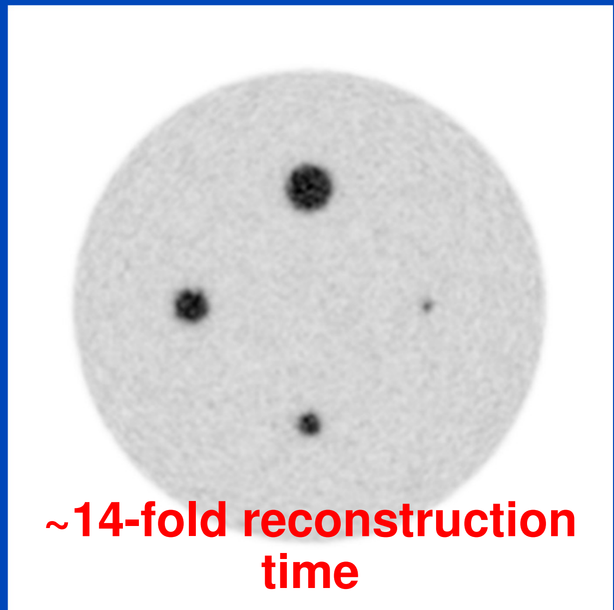

OSEM
2 Iterations; 14 Subsets

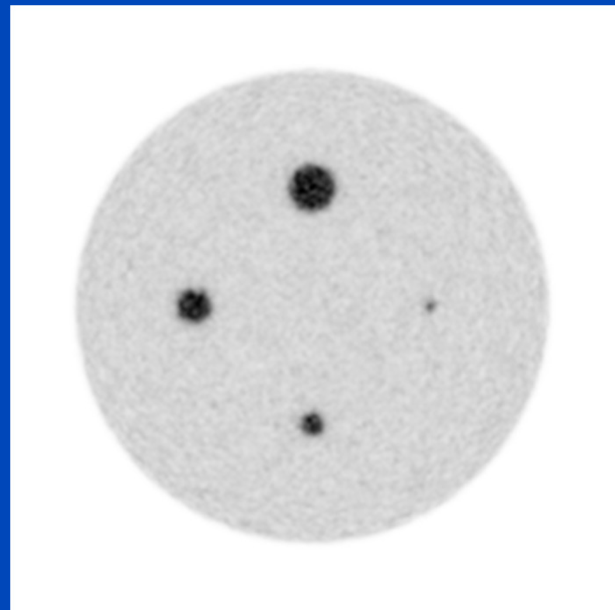

C = 15 kBq/mL, W = 30 kBq/mL

Ordinary-Poisson (OP) MLEM

- **Standard MLEM requires the projection data to be pre-corrected, e.g., for attenuation, randoms, scatter.**
- **However, pre-corrected projection data are not Poisson-distributed.**
- **To preserve Poisson statistics, the corrections can be included into the update equation:**

$$\lambda_i^{(n+1)} = \lambda_i^{(n)} \frac{1}{\sum_j M_{ij} a_j/N_j} \sum_j M_{ij} \frac{p_j}{\sum_k M_{kj} \lambda_{kj}^{(n)} + (r_j + s_j) N_j / a_j}$$

p_j **Measured projections along LOR *j***

$\lambda_i^{(n)}$ **Estimated activity in voxel *i* for iteration *n***

M_{ij} **System matrix**

$a_j = e^{-\sum_k \mu_k l_{kj}}$ **Attenuation along LOR *j***

N_j **Normaliziation**

r_j, s_j **Measured contribution of randoms and scatter along LOR *j***

Maximum-a-posteriori (MAP) Approach

- **Bayes rule:** $P(\boldsymbol{\lambda}|\boldsymbol{p}) = \frac{P(\boldsymbol{p}|\boldsymbol{\lambda})P(\boldsymbol{\lambda})}{P(\boldsymbol{p})}$

- **MAP objective funtion:**

$$\Phi(\boldsymbol{\lambda}|\boldsymbol{p}) = \ln P(\boldsymbol{\lambda}|\boldsymbol{p}) = L(\boldsymbol{p}|\boldsymbol{\lambda}) + \ln P(\boldsymbol{\lambda})$$
$$= L(\boldsymbol{p}|\boldsymbol{\lambda}) - \beta R(\boldsymbol{\lambda})$$

with the general Gibbs prior $P(\boldsymbol{\lambda}) = \frac{1}{Z}\exp(-\beta R(\boldsymbol{\lambda}))$
and dropping terms not dependent on *λ*

- **The regularization or penalty term *R*(*λ*) can be used to enforce desired image properties, such as, e.g.,**
  - **low noise.**
  - **preservation of edges.**
  - **structural similarity with anatomical prior information.**

One-step-late (OSL) Algorithm[1]

- Directly optimizing the MAP objective function is difficult.
- In the OSL approach, the partial derivatives of $R(\boldsymbol{\lambda})$ are evaluated for the current image estimate $\boldsymbol{\lambda}^{(n)}$ yielding the update equation

$$\lambda_i^{(n+1)} = \lambda_i^{(n)} \frac{1}{\sum_j M_{ij} + \beta \frac{\partial}{\partial \lambda_i} R(\boldsymbol{\lambda})_{|\boldsymbol{\lambda}=\boldsymbol{\lambda}^{(n)}}} \sum_j M_{ij} \frac{p_j}{\sum_k \lambda_k^{(n)} M_{kj}}$$

- Similar form as standard MLEM, but
  - OSL does not generally converge.
  - negative values may occur and need special handling.

[1] P. J. Green, “Bayesian Reconstructions From Emission Tomography Data Using a Modified EM Algorithm,” *IEEE Trans. Med. Imaging*, vol. 9, no. 1, pp. 84–93, 1990.

Time-of-flight (TOF)

- Measure the difference δt in the arrival times of two photons originating from the same annihilation event.

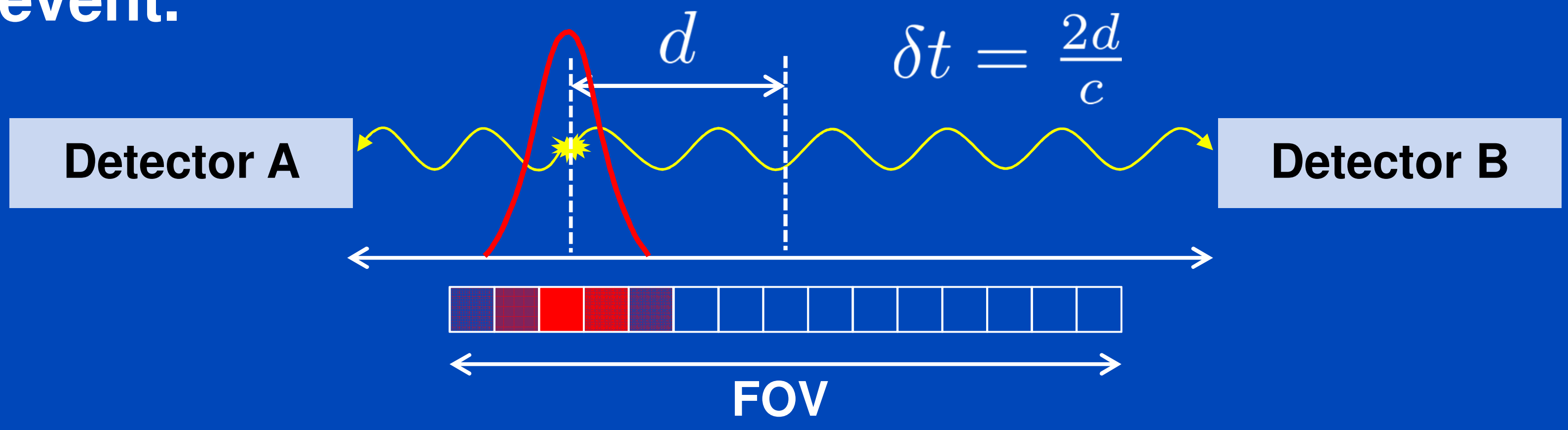

- 500 ps timing resoultion yields ≈ 7.5 cm spatial resolution.
- TOF can be used to increase SNR.

TOF Reconstruction

- **TOF information can be incorporated into the system matrix *M*.**

$$M_{ij} \rightarrow M_{ijt} = M_{ij} \frac{1}{\sqrt{2\pi\sigma_j}} e^{-\frac{1}{2}\left(\frac{t\Delta_t - \delta t}{\sigma_j}\right)^2}$$

δt **Measured time difference** Δ_t **Size of TOF bins**

$t = -N_t/2, \cdots, +N_t/2$ N_t **Number of TOF bins**

σ_j **Standard deviation, dependent on LOR *j* and system timing resolution**

- **The form of the update equation does not change.**

$$\lambda_i^{(n+1)} = \lambda_i^{(n)} \frac{1}{\sum_{j,t} M_{ijt}} \sum_{j,t} M_{ijt} \frac{p_{jt}}{\sum_{k,t} \lambda_k^{(n)} M_{kjt}}$$

Advanced AC Methods for PET/MR

- Segmentation-based methods
  - To include bone information, extend the standard MR-based method using
    - dedicated sequences, e.g., UTE.
    - additional low dose CT scans.
    - external transmission sources.
- Atlas-based methods
  - Co-register external CT data from a patient database (atlas) with the measured MR data to obtain a pseudo-CT of the investigated patient.
- Emission-based methods
  - Reconstruct activity distribution and attenuation map simultaneously using the PET emission data and additional constraints such as
    - Time-of-flight (TOF) information
    - MR-derived anatomical prior information

MR-MLAA

- Reconstruct attenuation and activity distributions simultaneously from PET emission data using MR prior information.
  - Optimize an objective function which is a combination of the log-likelihood and some MR-based prior information.
  - Initialize the simultaneous algorithm with an MR-based attenuation map.
- The presented algorithm is an extension of the maximum-likelihood reconstruction of attenuation and activity (MLAA)[1] for non-TOF PET/MR, called MR-MLAA.

[1] J. Nuyts, P. Dupont, S. Stroobants, R. Benninck, L. Mortelmans, and P. Suetens, "Simultaneous maximum a posteriori reconstruction of attenuation and activity distributions from emission sinograms.," IEEE Trans. Med. Imaging 18(5), 393–403 (1999).

Workflow

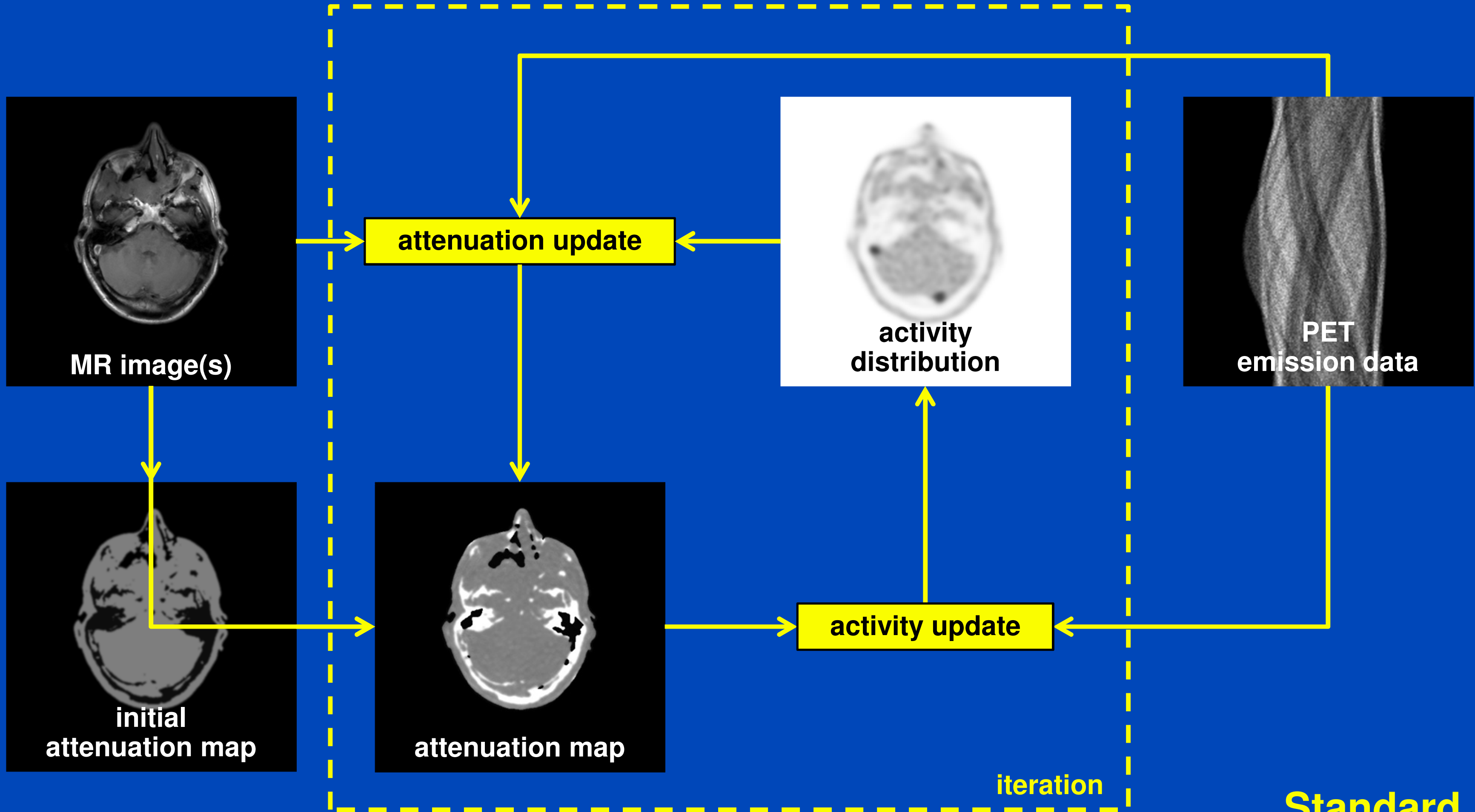

Standard
MR-based AC
MR-MLAA

Cost Function and Update Equations

- Simultaneous reconstruction of the **activity** λ and the **attenuation** μ from the **measured projections** p by optimizing the **cost function** C consisting of the **log-likelihood** L and the prior terms L_S and L_I.

$$C(\boldsymbol{\lambda}, \boldsymbol{\mu}) = L(\boldsymbol{\lambda}, \boldsymbol{\mu}) + L_{\mathrm{S}}(\boldsymbol{\mu}) + L_{\mathrm{I}}(\boldsymbol{\mu})$$

- Activity Update (AW-MLEM)

$$\lambda_i^{(n+1)} = \lambda_i^{(n)} \frac{1}{\sum_j M_{ij}\, a_j^{(n)}} \sum_j M_{ij} \frac{p_j}{b_j^{(n)}}$$

- Attenuation Update

$$\mu_j^{(n+1)} = \mu_j^{(n)} + \alpha \frac{\sum_j \left(M_{ij} \left(a_j^{(n)} b_j^{(n)} - p_j \right) \right) + \frac{\partial}{\partial \mu_i} (L_{\mathrm{S}} + L_{\mathrm{I}})}{\sum_j \left(M_{ij} a_j^{(n)} b_j^{(n)} \sum_i l_{ij} \right) - \frac{\partial^2}{\partial \mu_i^2} (L_{\mathrm{S}} + L_{\mathrm{I}})}$$

i	voxel index
j	LOR index
n	iteration number
M	system matrix
a	est. attenuation
b	est. projections
$\alpha > 0$	Relaxation para.

Prior Information

- When both the attenuation distribution μ and the activity distribution λ are unknown, optimizing the log-likelihood $L(\lambda, \mu)$ is an ill-conditioned problem.
- Prior information can help to drive the algorithm towards a 'meaningful' solution.
- Cost function: $C(\boldsymbol{\lambda}, \boldsymbol{\mu}) = L(\boldsymbol{\lambda}, \boldsymbol{\mu}) + L_{\mathrm{S}}(\boldsymbol{\mu}) + L_{\mathrm{I}}(\boldsymbol{\mu})$
- Smoothing prior L_S
  - Favors smooth attenuation map.
- Intensity prior L_I
  - Voxel-dependent Gaussian-like probability distribution of pre-defined attenuation coefficients, e.g., for soft tissue, air, bone, etc. Deviating values are penalized.

Intensity Prior

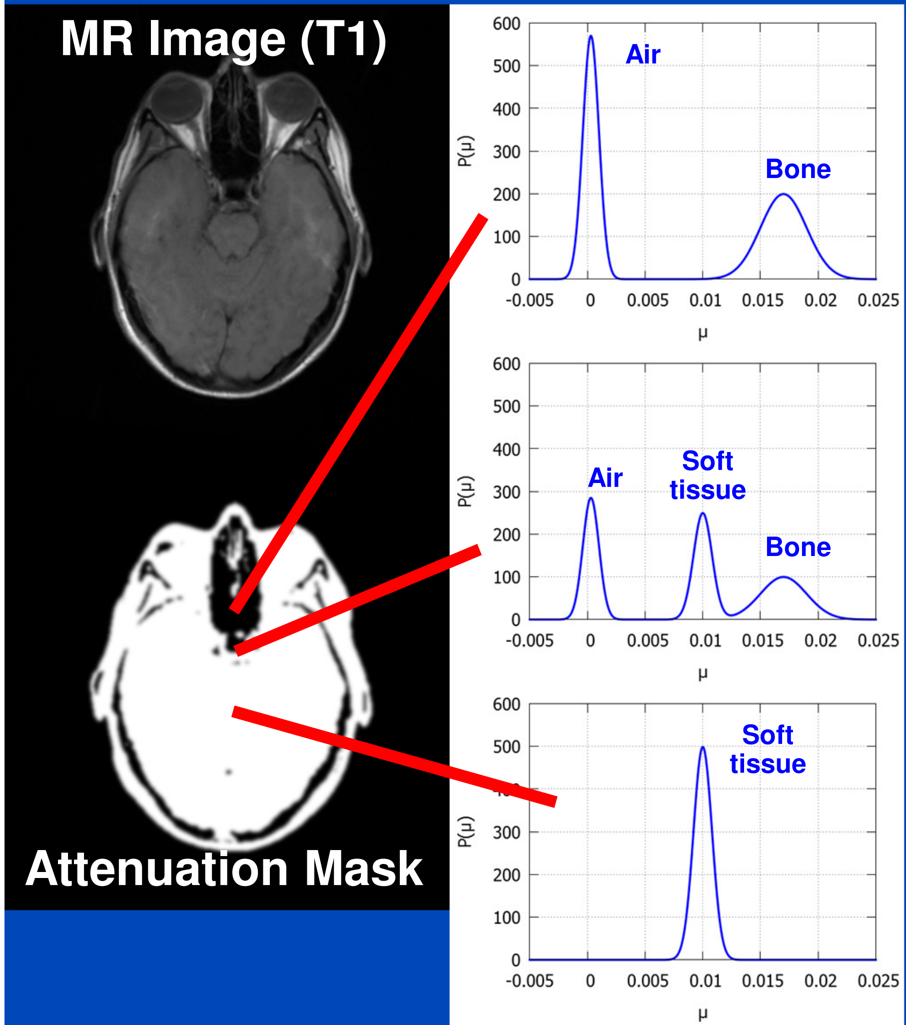

- **Use the MR image to create a mask defining air/bone and soft tissue.**
- **Smooth mask.**
- **Define logarithm of intensity prior L_I as linear combination of air/bone intensity prior L_{AB} and soft tissue intensity prior L_{ST}:**

$$L_{\mathrm{I}} = (1-\omega)\beta_{\mathrm{AB}} L_{\mathrm{AB}} + \omega \beta_{\mathrm{ST}} L_{\mathrm{ST}}$$

ω **Voxel-dependent weighting factor, based on attenuation mask**

$\beta_{\mathrm{AB}}, \beta_{\mathrm{ST}}$ **Global weighting factors**

Simulations

- Simulate PET emission data accounting for Poisson noise and attenuation (and scatter and randoms).
- Perform reconstruction using
  - the true attenuation for AC.
  - standard MR-based AC (MRAC).
  - MR-consistent reconstruction of attenuation and activity (MR-MLAA).
- Evaluation
  - Measure mean activity in ROIs corresponding to simulated lesions.
    - Lesion 1: A_1
    - Lesion 2: A_2
  - Present results relative to the true AC case.

Patient 1

Attenuation Mask Derived from MR

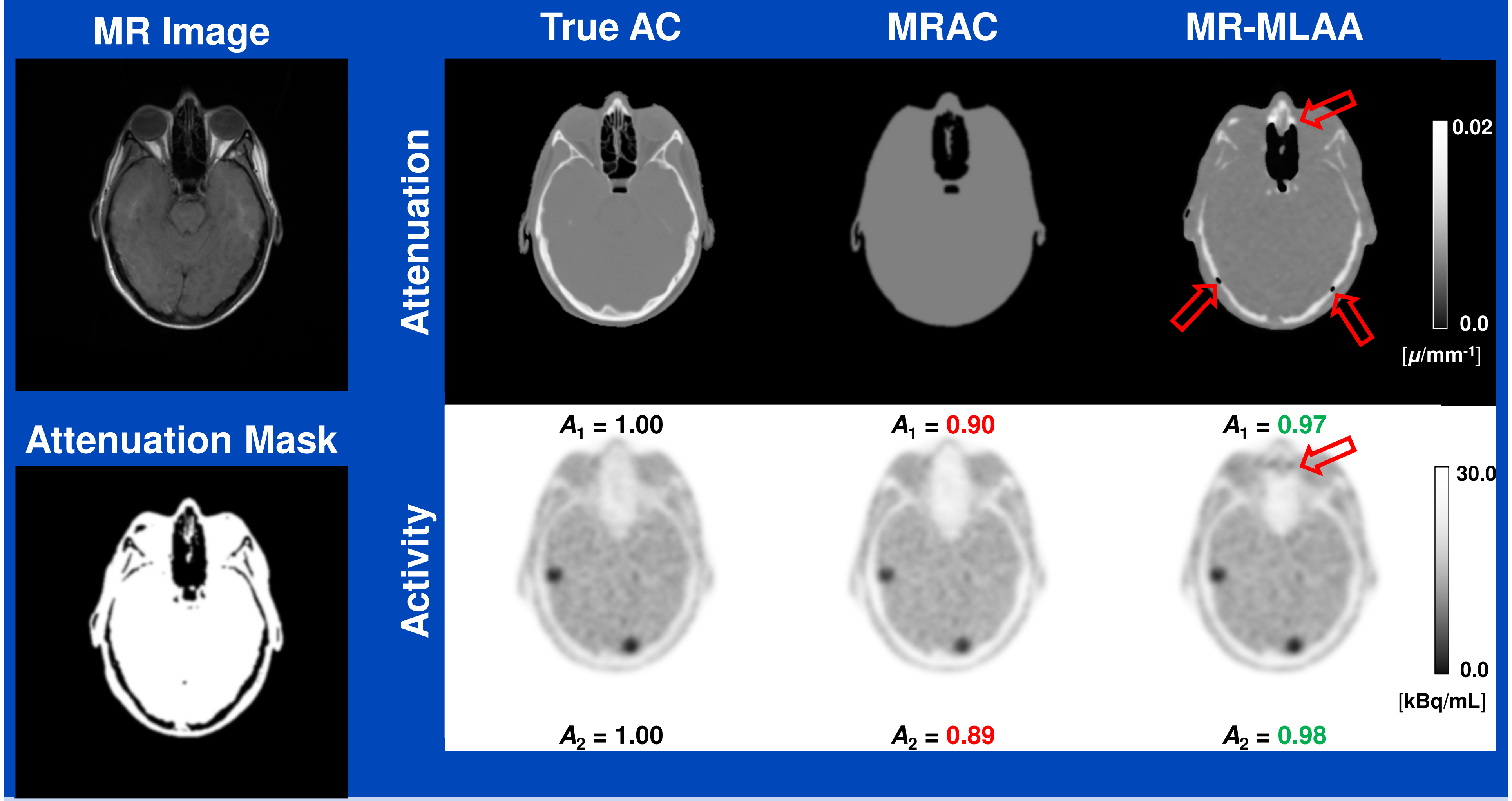

Patient 2

Attenuation Mask Derived from CT

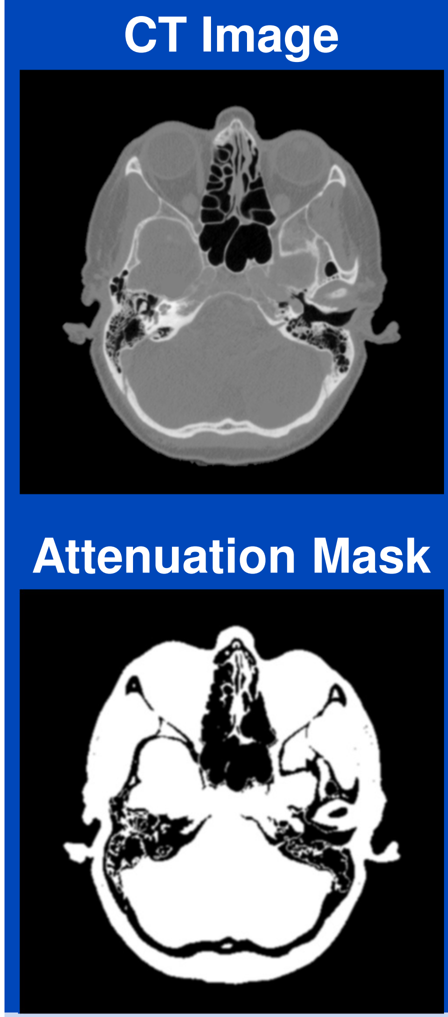

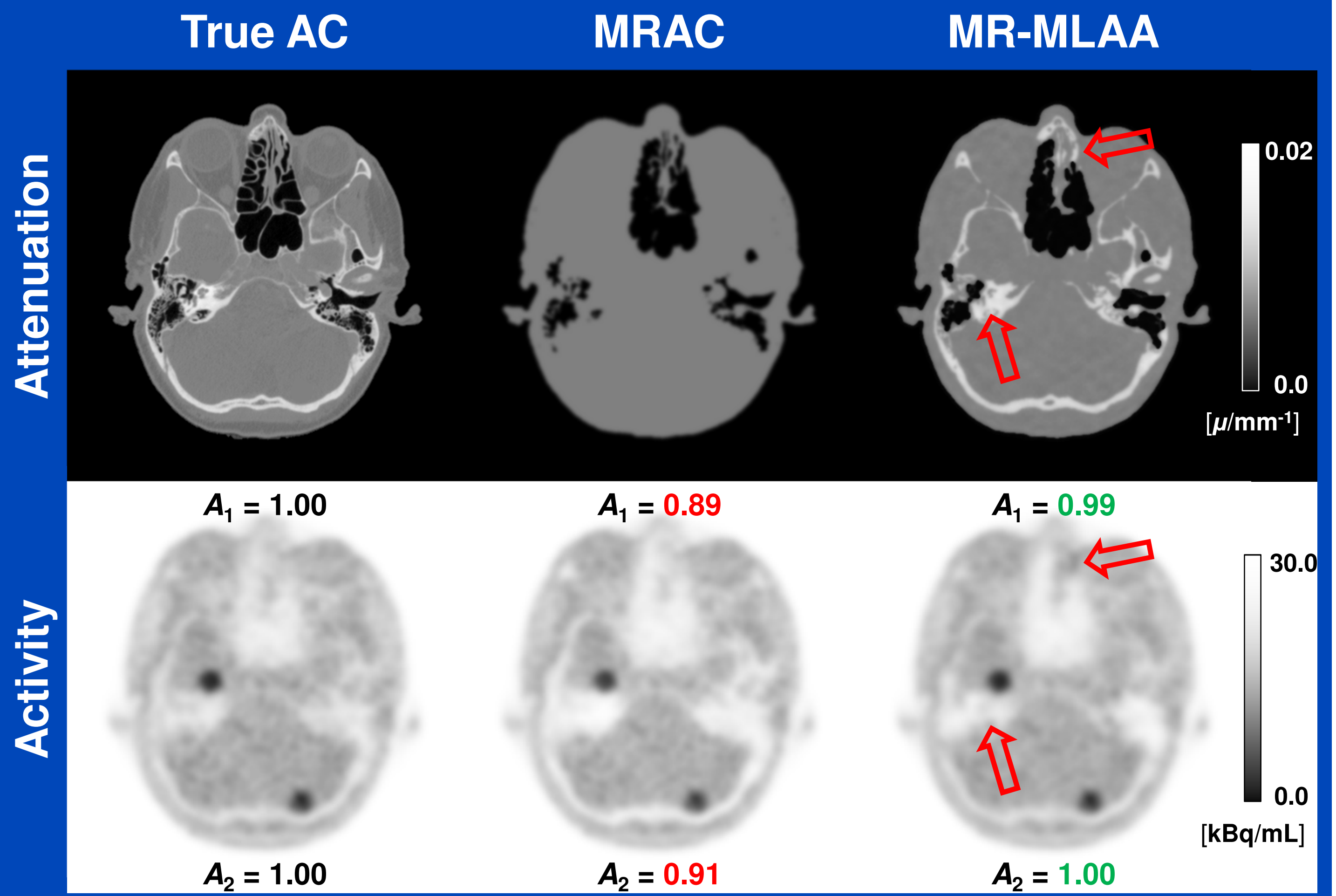

dkfz.

5D MoCo?

Illustration of Workflow

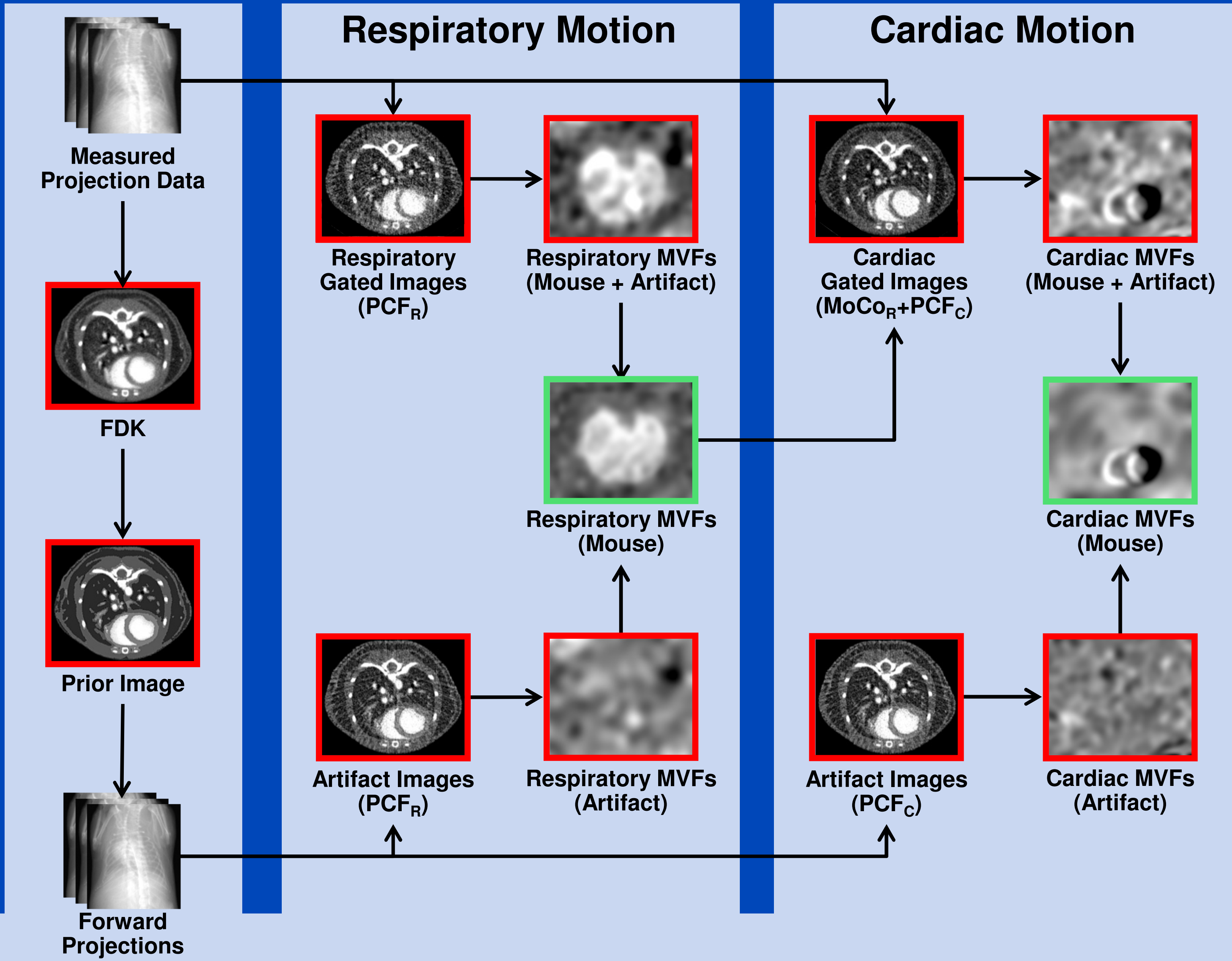

Respiratory–Gated Cardiac–Gated	Respiratory–Gated Only	Respiratory–Compensated Cardiac–Gated	Respiratory–Compensated Cardiac–Compensated
$\Delta r = 10\,\%,\ \Delta c = 20\,\%$	$\Delta r = 10\,\%,\ \Delta c = 100\,\%$	$\Delta r = 10\,\%,\ \Delta c = 20\,\%$	$\Delta r = 10\,\%,\ \Delta c = 20\,\%$

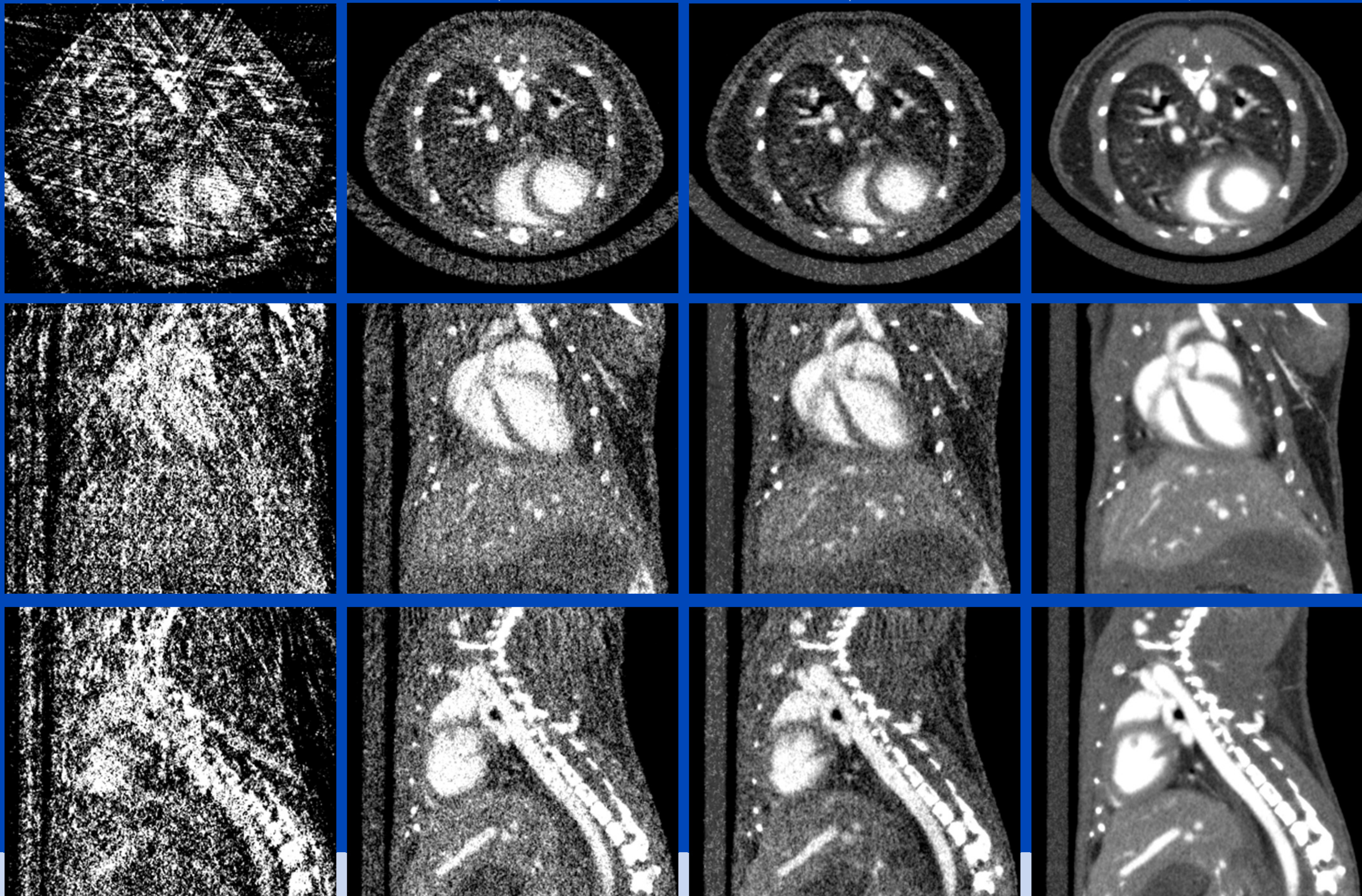

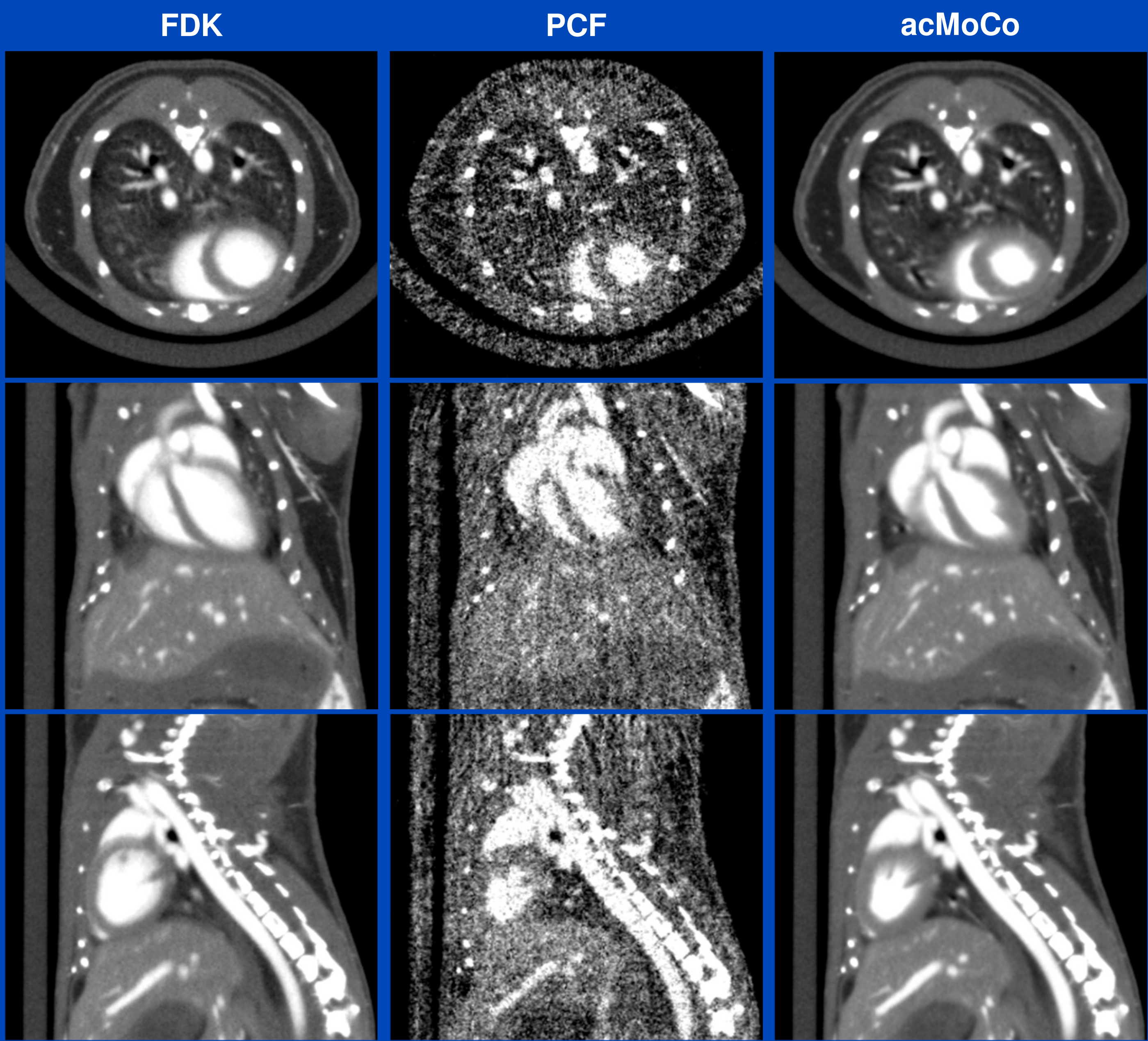

C = 200 HU, *W* = 1200 HU

Cardio-Respiratory Motion-Compensated Micro CT Imaging

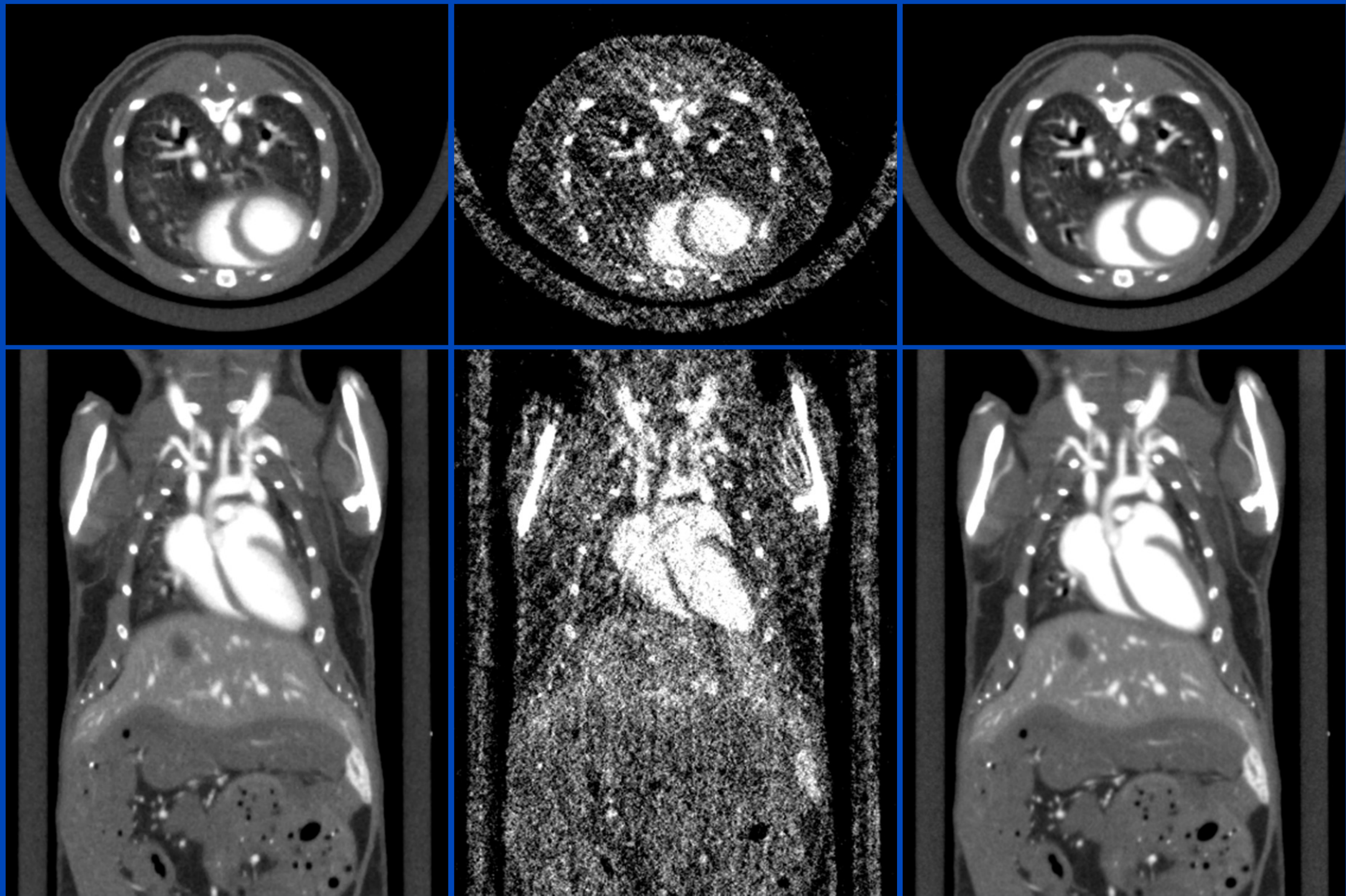

The cardiac motion is shown at a fixed respiratory phase.

Brehm, Sawall, Maier, and Kachelrieß, "Cardio-respiratory motion-compensated micro-CT image reconstruction using an artifact model-based motion estimation" Med. Phys. submitted (2015).

Thank You!

Thorsten Heußer and Christopher Rank have helped to prepare the presentation. This presentation will soon be available at www.dkfz.de/ct. Parts of the reconstruction software were provided by RayConStruct® GmbH, Nürnberg, Germany.